이학박사학위논문

기억력 개선 식물 소재 HX106N의 개발과 작용 원리 분석

Development of Botanical Formulation, HX106N, for Improving Memory Functions and Analysis of Underlying Mechanisms

2015년 2월

서울대학교 대학원

생명과학부

이 두 석

기억력 개선 식물 소재 HX106N의 개발과 작용 원리 분석

Development of Botanical Formulation, HX106N, for Improving Memory Functions and Analysis of Underlying Mechanisms

지도교수 김 선 영

이 논문을 이학박사 학위논문으로 제출함

2014년 12월

서울대학교 대학원

자연과학대학 생명과학부

이 두 석

이두석의 박사학위논문을 인준함

2014년 12월

위 원 장 _____ (인)

부 위 원 장 _____ (인)

위 원 _____ (인)

위 원 _____ (인)

위 원 _____ (인)

ABSTACT

Dementia is characterized by a decline in memory and other cognitive abilities enough to interfere with daily activities. The most common type of senile dementia is AD (Alzheimer's disease). With the rapid growth of the elderly population around the world, AD has emerged as one of the greatest social and financial problems. There are only 4 drugs approved by US FDA, but they are only symptom-relievers, providing no fundamental treatment. AD is believed to occur as a result of various pathogenic events, therefore, a single "magic bullet" cannot be expected to prevent or treat AD.

In this thesis study, I explored the possibility of developing evidence-based phytotherapeutics for senile dementia, including AD, from the perspectives of traditional Korean medicines (TKM), using their data and related information. "Chimae (痴呆)" described in ancient literatures of TKM is very close to AD. In the context of traditional Korean and Chinese medicines, "chimae" is classified into two categories; age-related degeneration or pathological conditions resulting from the accumulation of undesirable substances, called eohyul (瘀血) or dameum (痰飮) among others. I designed a botanical formulation, called HX106N, consisting of 4 plant sources, *Dimocarpus longan*, *Liriope platyphylla*, *Salvia miltiorrhiza* and *Gastrodia elata*. I found the initial batch of HX106N to contain biological activities that could improve memory functions in the animal model of AD-type amnesia. Because active compounds were not known at that initial stage, I needed to develop a method(s) to prepare reagents in a reproducible manner. To overcome this hurdle, the bioassay systems were developed using three markers; effects on NO (nitric oxide) in BV-2 cell line, cell death upon glutamate treatment in HT22 cell line and AChE (acetylcholinesterase) activity

using brain homogenates. Whenever new batches were made at different times, the bioassays were performed, and only those batches showing ± 20% of IC_{50} values of reference stock in all three markers were chosen for experiments

Oral treatment with HX106N markedly ameliorated memory deficits in both Y-maze alternation and passive avoidance tests in $A\beta_{25-35}$-injected mice, which coincided with a significant decrease in the level of TBARS (thiobarbituric acid-reactive substances), a maker for lipid peroxidation, in the hippocampus and cortex. The cholinergic amnesia induced by an injection of scopolamine, a muscarinic acetylcholine receptor antagonist, was also improved by treatment with HX106N. The level of AChE activity was significantly decreased in the hippocampus and cortex after HX106N administration. These data indicated that HX106N improved memory functions through the control of oxidative stress and activity of AChE.

In efforts to understand the underlying mechanism(s), effects of HX106N were investigated in cells of microglia and neuronal origins. In BV-2 cells, a murine microglia cell line, and primary microglia, HX106N controlled the production of NO at two levels, by suppressing the expression of iNOS at the post-transcriptional level, and also increasing HO-1 (heme oxygenase-1) expression and subsequently generating CO (carbon monoxide). In primary cortical neurons and HT22 cells, a murine hippocampal neuronal cell line, treatment with HX106N significantly decreased the level of glutamate-induced neuronal cell death and that of ROS production. These data indicated that HX106N control oxidative stress in several different ways.

The underlying mechanism by which HX106N regulates HO-1 expression was further investigated at molecular level. HX106N increased the RNA level of HO-1 by the activeation of Nrf2 (Nuclear factor E2-related factor 2) and NF-κB. Results from the experiments using chemical inhibitors for MAPKs (mitogen-activated protein kinases)

showed that both JNK (Janus N-terminal kinase) and p38 MAPK were involved in HO-1 induction by HX106N. These data indicated that multiple signaling pathways were involved in HX106N-mediated upregulation of HO-1.

Taken together, data presented in this thesis work strongly suggest that HX106N contains potent bioactivities which can improve memory functions and that it might be a useful starting point for developing a therapeutic agent for senile dementia, like AD.

Keywords: HX106N, traditional Korea medicine, dementia, Alzheimer's disease, neurodegenerative disease, amyloid β, scopolamine, oxidative stress, heme oxygenase-1

Student Number: 2008-20368

CONTENTS

LIST OF TABLES

LIST OF FIGURES

ABBREBIATIONS

ACh: acetylcholine

AChE: acetylcholinesterase

ActD: actinomycin D

AD: Alzheimer's disease

AP-1: activating protein-1

Aβ: amyloid β

CHX: cycloheximide

CO: carbon monoxide

CORM-3: carbon monoxide releasing molecule 3

DIV: day in vitro

DNZ: donepezil

GCLm: glutamate-cysteine ligase modifier subunit

GSH: glutathione

Hb: hemoglobin

HO-1: heme oxygenase-1

HPLC: high-performance liquid chromatography

IL-1β: interleukin-1β

iNOS: inducible nitric oxide synthase

LC-MS/MS: liquid chromatography-tandem mass spectrometry

LPS: lipopolyssacharide

MAPK: mitogen-activated protein kinases

NF-κB: nuclear factor kappa B

NO: nitric oxide

NQO1: NAD(P)H quinone oxidoreductase 1

Nrf2: Nuclear factor E2-related factor 2

ROS: reactive oxygen species

TBARS: thiobarbituric acid-reactive substances

TKM: traditional Korean medicines

TNF-α: tumor necrosis factor- α

ZnPP: protoporphyrin-IX

CHAPTER I

Introduction

1. Dementia from the perspectives of Western medicine and traditional Korean medicine

Korea is rapidly becoming an aging society. According to a report by the Korea Institute for Health and Society Affairs, the number of elderly persons was about 7 % of the total population of Korea in 2000, indicating that the country was entering the early stage of an aging society. This number is now expected to increase to 14 % in 2017, meaning that Korea will soon become an aged society.

Cognitive dysfunction is one of the major medical issues associated with the elderly population. An advanced state in which the decline in cognitive abilities is severe enough to interfere with daily activities is called dementia. Because dementia causes huge social and financial problems for both individual patients and society as a whole, it has become one of the greatest threats in the healthcare of the aged society.

The most common type of dementia is AD (Alzheimer's disease), currently affecting an estimated 0.2-0.5 million people in Korea and 5.4 million in the US (Assoc, 2011, Cho et al., 2011). The prevalence of AD has been reported to double approximately every five years after 65 years of age, and it approaches 50% at age 85-90 (Petersen, 2000, Tanzi, 2000). If no therapy intervenes, the number of patients with AD is estimated to reach as high as 2 and 13 million by 2050 in Korea and the US, respectively (Hebert et al., 2004, Kim et al., 2011). With the rapid growth of the aged population around the world, AD has become one of the leading causes of death.

AD is distinguished pathologically from other forms of dementia by, for example, the deposition of senile plaques and neurofibrilary tangles (NFTs) in the brain. Plaques are primarily composed of extracellular aggregates of amyloid β (Aβ) peptide,

Table 1. Types of dementia and their characteristics

Type of dementia	Characteristics
Alzheimer's disease	• Most common type of dementia (60-80% of all cases) • Slow onset, steady decline • The hallmark pathologies are amyloid plaque and neurofibrillary tangles
Vascular dementia	• Previously known as multi-infarct or post-stroke dementia • Associated with vascular risk factors (hypertension, diabetes, artery disease and smoking) • Many subtypes and etiologies (lacunar lesions, hemorrhagic lesions and mixed dementia)
Lewy Body dementia	• 15-25% of all dementias • Lewy bodies are composed of aggregated α-synuclein • Cognitive impairment fluctuates over time • Visual hallucinations, sleep disturbances and parkinsonian movement features are noteworthy
Frontotemporal dementia	• Originally called Pick's disease • Associated with frontal and temporal anterior lobe atrophy • Onset at a younger age (at about age 60) • Typical early symptoms are changes in personality and behavior and language problems • Visual-spatial and memory skill remain intact

Adopted and modified from reviews of (Thies et al., 2013, Grossman et al., 2006)

while NFTs are intracellular fibrils of the microtubule-associated protein tau which is abnormally hyperphosphorylated. Plaques and tangles are known to occur primarily in the brain regions responsible for learning and memory and emotion, such as the hippocampus, entorhinal cortex, basal forebrain and amygdala (Mattson, 2004). As a result of reduced synapse numbers and damaged neurites in these brain regions, AD patients lose their memory and cognitive abilities.

There are currently four FDA-approved drugs for AD. But all of these drugs are known to produce only symptomatic benefits through counterbalancing the neurotransmitter disturbance. Extensive researches are under way in all major countries to develop methods that can prevent, slow or even stop the progression of the disease, for example β-secretase inhibitors (LY2886721 and CTS-21166), γ-secretase inhibitors (Semagacestat and Tarenflurbil) and antibodies targeting Aβ (Bapineuzumab and Solanezumab). However, no drugs have shown a truly positive outcome in a large number of clinical trials, in spite of enormous investments of intellectual and financial resources. These disappointing results have led researchers to reconsider the problems from new perspectives (Korczyn, 2012). AD is not a specific disease with a single pathogenesis, and no single "magic bullet" can be expected to prevent or cure it. Therefore, various types of therapeutic strategies may have to be employed to deal with AD.

Original Korean medicines, which are now called traditional Korean medicine (TKM), originated from traditional Chinese medicines (TCM). Unlike in many other countries, TKM has been practiced as a part of a valid healthcare system in Korea. Various cognitive diseases have been described in ancient medical literature of TKM and TCM. For example, the term, "dementia" (痴呆), was first described in the medical book called *Jingyue Quanshu* (景岳全書), published around the 17th century, during

the Ming Dynasty, which described its pathogenesis and treatment methods in an elaborative manner (Liu et al., 2012). In various literatures of TKM and TCM, emotional and psychological problems, as well as the imbalance of body components, are described as an important etiology of dementia. A number of plants and other natural products have been suggested as medications for dementia, as an individual source or in the form of a mixture of various plants. Such a large body of literature, databases established over a thousand years, and know-hows accumulated during clinical practice provide a unique advantage of using TKM for developing innovative therapeutics for dementia, including AD, as opposed to the random screening method frequently employed during the search for active small molecules.

However, limitations of TKM are also apparent. Solid scientific data supporting their claimed activities are insufficient, and standardization of natural products is difficult due to its complex nature. Most importantly, the identity of active compounds is mostly elusive. For TKM to be positioned as a part of mainstream medicine, these limiting factors have to be overcome.

2. Molecular pathology of AD

Over the past few decades, large efforts have been made to understand potential genetic and environmental risk factors for AD and the detailed molecular pathogenic mechanisms leading to neuronal degeneration and cognitive dysfunction. Several hypotheses have been suggested to explain the cause of AD, and some have been experimentally proved. Nevertheless, the cause of a majority of AD cases, has not yet been clearly known, except for 1% to 5% of all AD cases in which genetic differences are known to play roles. Indeed, AD is believed to occur as a result of very complex

multiple pathogenic events.

2.1 Amyloid cascade hypothesis

In 1991, the amyloid cascade hypothesis was proposed by John Hardy and David Allsop (Hardy and Allsop, 1991). In this model, the accumulation of Aβ in the brain was proposed to play crucial roles in the pathogenesis of AD. Aβ peptides are derived from amyloidogenic processing the amyloid precursor protein (APP). Many studies have demonstrated that large amounts of Aβ peptide are neurotoxic, and its deleterious effects are mediated by distinct mechanisms, including the generation of reactive oxygen species, neuroinflammation and dysregulation of ionic homeostasis (Schubert et al., 1995, Akiyama et al., 2000, Mattson et al., 1992).

APP, a transmembrane protein highly expressed in the brain, is known to undergo two competing processing pathways. In the non-amyloidogenic pathway, APP is first cleaved by α-secretase to produce a soluble N-terminal fragment (sAPPα) and a C-terminal fragment (α-CTF), resulting in the destruction of the Aβ peptide sequence (Hooper and Turner, 2002). However, in the amyloidogenic pathway, β-secretase (BACE) act initially on APP instead of α-secretase, which generates an N-terminal, soluble APPβ (sAPPβ) fragment and an Aβ-containing C-terminal fragment (β-CTF). β-CTF is further processed by γ-secretase, leading to the production of Aβ peptide (Sinha and Lieberburg, 1999). Several genetic mutations found in familial Alzheimer's disease, have been reported to promote the amyloidogenic processing of APP (Hardy, 1997, Haass et al., 1995).

2.2 Tau hypothesis

NFTs in the brain of AD patients are known to be formed by hyperphosphorylated tau

proteins. The tau protein, as a microtubule associated protein, plays an essential role in the modulation of axonal microtubule stability. However, when tau proteins undergo hyperphosphorylation at specific residues, they aggregate in an insoluble form called paired helical filaments (PHF). As a result, the microtubules become unstable and the transport system of neurons collapses, eventually leading to neuronal death (Mandelkow et al., 2003).

Recent studies have suggested that the amyloid β and tau pathologies may be linked. In the pathogenesis of AD, deposition of Aβ peptides is reported to occur typically before the formation of NFTs, and can promote the hyperphosphorylation and aggregation of tau (Busciglio et al., 1995, Calhoun et al., 1998).

2.3 Cholinergic hypothesis

A variety of studies have consistently found abnormalities in the central cholinergic system of the brain of AD patients, which appeared to correlate with the loss of cognitive function (Francis et al., 1999, Terry and Buccafusco, 2003). These findings, together with the emerging role of acetylcholine as an important neurotransmitter for learning and memory, led to the cholinergic hypothesis of AD. This hypothesis gave rise to therapeutic strategies aimed to compensate for cholinergic deficits, resulting in the commercial development of acetylcholinesterase (AChE) inhibitors as the first approved drug for dementia symptoms.

2.4 Inflammation and oxidative stress

There is growing evidence supporting that inflammation and oxidative stress play a crucial role in the progression of AD (Markesbery, 1999, Wyss-Coray and Rogers, 2012). Although a variety of cellular and molecular factors are involved in these

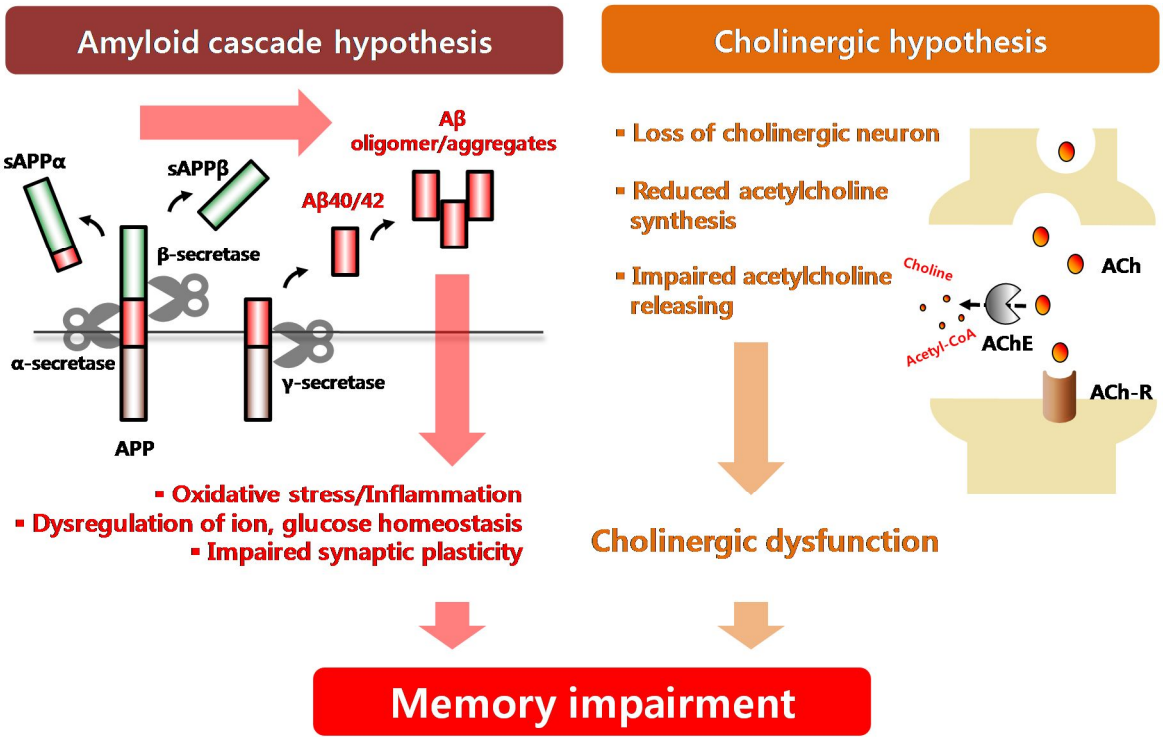

Figure 1. Major pathologies associated with memory deficits in AD. Aβ is derived from the sequential cleavage of APP by β-secretase and γ-secretase, and spontaneously aggregates into soluble oligomers and insoluble fibrils. Aβ causes memory impairment through various neurotoxic mechanisms, including oxidative stress, inflammation, dysregulation of ionic and glucose homeostasis and synaptic dysfunction. Cholinergic dysfunction, such as reduced choline uptake, ACh synthesis and loss of cholinergic neurons, in central nervous system has also been known to correlate with loss of cognitive function in AD. Adopted and modified from reviews of (Mattson, 2004, Francis et al., 1999, Terry and Buccafusco, 2003)

Figure 2. Schematic diagram for Aβ-induced neurotoxicity in AD. Aβ generates hydrogen peroxide by interacting with metal ions, such as Fe^{2+} and Cu^{+}. Some of the membrane transporters (ion-motive ATPases, glucose and glutamate transporters) and ion channels (NMDA receptor) are known to be oxidatively modified and impaired by Aβ-induced lipid peroxidation. Disturbing cellular ion homeostasis and energy metabolism makes neurons vulnerable to glutamate toxicity and apoptosis. Aβ can also cause mitochondrial dysfunctions, leading to generation of free radicals and ATP depletion. Increased phosphorylation and oxidative modification of tau by Aβ can promote the formation of neurofibrillary tangles. Microglia also plays a critical role in Aβ-induced neurotoxicity. In microglia, Aβ activates NADPH oxidase to generate superoxide anion and induced the production of inflammatory mediators, such as TNF-α, IL-1β and NO. Adopted and modified from a review of (Mattson, 2004)

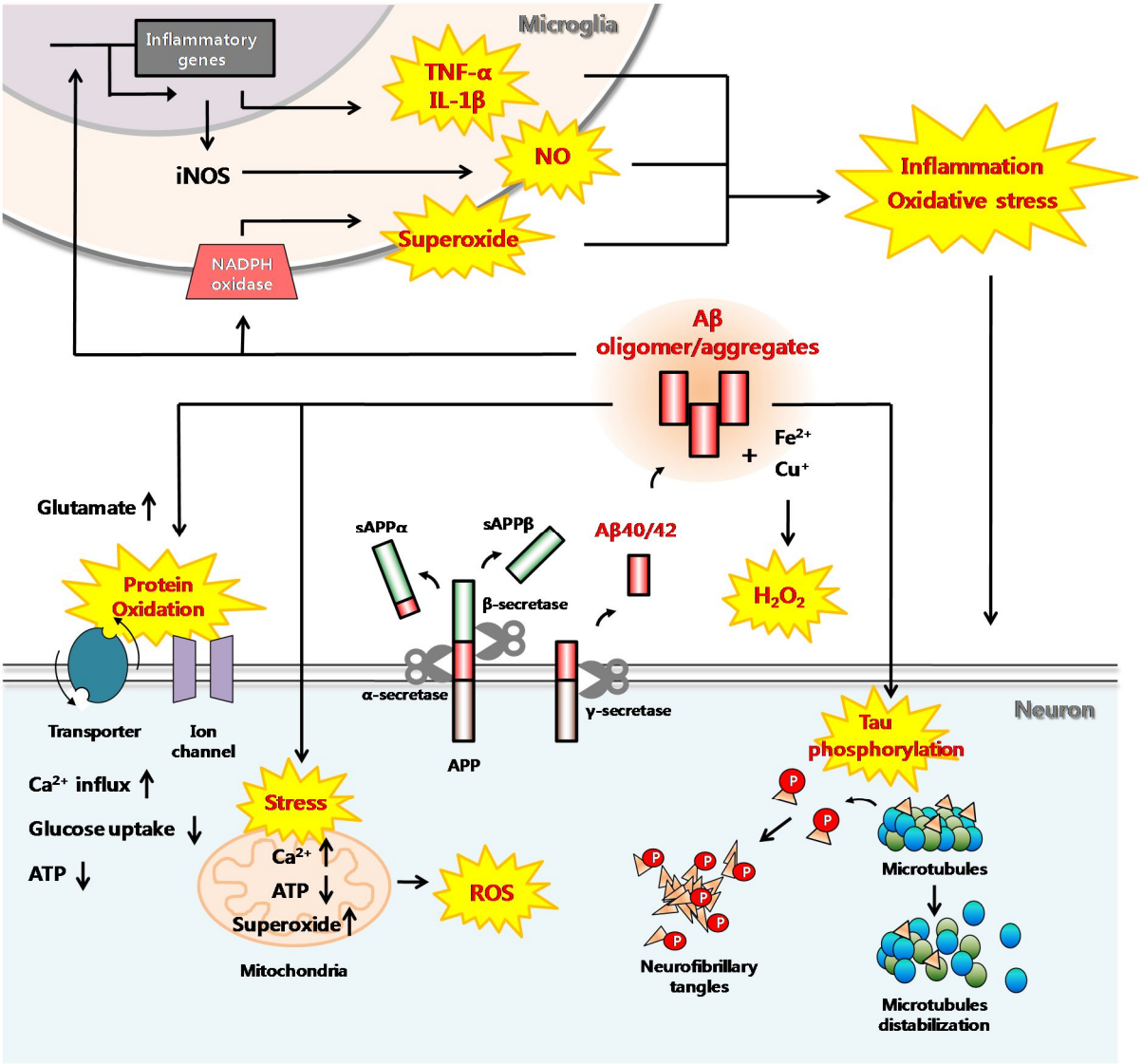
Microglia
Inflammatory genes
TNF-α
IL-1β
NO
iNOS
Superoxide
NADPH oxidase
Inflammation
Oxidative stress
Aβ
oligomer/aggregates
Fe2+
Cu+
Glutamate
Protein Oxidation
sAPPα
sAPPβ
Aβ40/42
β-secretase
α-secretase
γ-secretase
APP
H2O2
Transporter
Ion channel
Neuron
Tau phosphorylation
Ca2+ influx
Glucose uptake
ATP
Stress
Ca2+
ATP
Superoxide
ROS
Mitochondria
Microtubules
Neurofibrillary tangles
Microtubules distabilization

pathologies, microglia, a resident immune cell of the central nervous system, were suggested as a key player in the induction of inflammation and oxidative stress (Liu and Hong, 2003). Reactive microglia colocalize with senile plaques in the cortical region of AD brains (Rogers et al., 1988) and produce neurotoxic factors, including proinflammatory cytokines such as tumor necrosis factor-α (TNF-α) and interleukin-1β (IL-1 β), and free radical species such as nitric oxide (NO) and superoxides.

Glutamate has also been implicated as a direct neurotoxin in various neurodegenerative diseases involving AD (Butterfield and Pocernich, 2003). It acts normally as a main excitatory neurotransmitter in the brain, but excessive quantities of glutamate have been known to cause neuronal death through excitotoxicity and oxidative damage (Sattler and Tymianski, 2001, Schubert and Piasecki, 2001, Murphy et al., 1990).

2.5 Glucose metabolism

It has been demonstrated that glucose metabolism is impaired in the brain of AD patients (Costantini et al., 2008). Glucose, as an exclusive source of energy in the brain, is essential for maintaining neuronal functions, including the synaptic plasticity required for learning and memory. Therefore, altered glucose metabolism can cause neuronal dysfunctions, and indeed, studies, involving FDG-PET (18-fluoro-deoxyglucose positron emission tomography), have confirmed that low glucose metabolic rates correlate with lower cognitive scores (Landau et al., 2011).

3. Current therapeutics

3.1 AChE inhibitors

Based on the cholinergic hypothesis, many AChE inhibitors have been developed to enhance the cholinergic transmission by inhibiting the degradation of acetylcholine between the synaptic clefts. To date, three AChE inhibitors have been approved by the FDA for AD: donepezil (Pfizer, USA), rivastigmine (Novartis, Switzerland) and galantamine (Janssen, Belgium), which have been shown to improve cognitive functions of AD patients (Rogers et al., 1998, Rosler et al., 1999, Tariot et al., 2000). These drugs have been used as the first-line treatment for AD. Tacrine (First Horizon Pharmaceuticals, USA) was the first approved AChE inhibitor in 1993, but is no longer used due to hepatotoxicity (Alfirevic et al., 2007). Recent studies have shown that AChE inhibitors also produce effective neuroprotection by acting as the agonists of nicotinic receptors and sigma receptors (Kihara et al., 1997, Zamani et al., 1997, Meunier et al., 2006)

3.2 N-methyl-D-aspartate (NMDA) receptor antagonist

Memantine (Lundbeck, Denmark) is the first novel class of AD medications and approved in 2004 by the FDA to treat moderate to severe AD. It is a moderate-affinity, uncompetitive NMDA receptor antagonist believed to protect neurons from glutamate excitotoxicity. Several clinical trials have demonstrated that Memantine improved cognitive functions in patients with moderate to severe AD (McShane et al., 2006, Reisberg et al., 2003). However, despite the theoretical rationale for its neuroprotective effect, treatment of Memantine has shown to provide only symptomatic benefits, and not disease-modifying effects.

3.3 Drugs in development

Although various underlying mechanisms of AD pathology, such as tau deposition,

Table 2. FDA-approved drugs for Alzheimer's disease

Drugs	Class Indication	Mechanism of action	Adverse effects
Donepezil (Aricept)	AChE inhibitor Mild-to-moderate and moderate-to-sever AD	Prevent ACh breakdown	Nausea, vomiting, diarrhea
Galantamine (Razadyne)	AChE inhibitor Mild-to-moderate AD	Prevent ACh breakdown	Nausea, vomiting, diarrhea, loss of appetite, weight loss
Rivastigmine (Exelon)	AChE inhibitor Mild-to-moderate AD	Prevent ACh breakdown	Nausea, vomiting, diarrhea, loss of appetite, weight loss, muscle weakness
Memantine (Namenda)	NMDA antagonist Moderate-to-sever AD	Prevent glutamate excitotoxicity	Dizziness, headache, constipation, confusion

Adopted and modified from a review of (Yiannopoulou and Papageorgiou, 2013)

Table 3. Current status of drug development for AD

Drugs	Mechanism of action	Current status	Outcome in clinical trials
LY2886721	β-secretase inhibitor	Discontinued	Negative (Phase II)
CTS-21166	β-secretase inhibitor	Completed (Phase I)	Positive (Phase I)
Semagacestat	γ-secretase inhibitor	Discontinued	Negative (Phase III)
Tarenflurbil	γ-secretase inhibitor	Discontinued	Negative (Phase III)
Gammagard	Purified IgG	Discontinued	Negative (Phase III)
Bapineuzumab	Humanized anti-Aβ mAb	Discontinued	Negative (Phase III)
Solanezumab	Humanized anti-Aβ mAb	Ongoing (Phase III)	Negative (Phase III)
Crenezumab	Humanized anti-Aβ mAb	Ongoing (Phase II)	Positive (Phase I)
Gantenerumab	Human anti-Aβ mAb	Ongoing (Phase II/III)	Positive (Phase I)
Latrepirdine	Mitochondrial protection	Discontinued	Negative (Phase III)
Rosiglitazone	PPARγ agonist	Discontinued	Negative (Phase III)

Adopted and modified from reviews of (Yiannopoulou and Papageorgiou, 2013, Schneider et al., 2014)

inflammation and oxidative stress, have been researched as potential therapeutic targets, a majority of drugs currently under development are based on the amyloid cascade hypothesis.

According to this hypothesis, extensive investigations have been carried out with an aim of reducing the level of Aβ in the brain or preventing Aβ toxicity for the treatment of AD. To inhibit the production of Aβ peptide, for example, both β- and γ-secretase were suggested as a promising target. Only a few drugs targeting β-secretase have entered clinical trials to date, because of difficulty in making the appropriate compounds capable of inhibiting enzyme activity and crossing the blood-brain barrier (Yiannopoulou and Papageorgiou, 2013). CTS-21166 (CoMentis, USA) is the first β-secretase inhibitor, and its phase I clinical trial has been completed in which the plasma level of Aβ was shown to be reduced in healthy young men (Hey et al., 2008).

Semagacestat (Eli Lilly and Company, USA) and tarenflurbil (Myriad Genetics, USA) are the most studied γ-secretase inhibitors. However, two large phase III clinical trials involving semagacestat were interrupted due to its detrimental effects on cognition and the ability to perform activities of daily living (Imbimbo and Giardina, 2011). Tarenflurbil also failed to improve cognitive ability in two large scale phase III studies, and it is no longer being pursued (Imbimbo and Giardina, 2011).

Based on the surprising results that passive immunization with antibodies against human Aβ decreased the level of Aβ, resulting in improvement in memory functions in transgenic AD mice (Schenk et al., 1999, Janus et al., 2000), anti-amyloid immunotherapy has emerged as one of the promising strategies to clear Aβ, and a majority of pharmaceutical companies are indeed working on this aspect. The most notable antibody drugs are bapineuzumab (Élan and Wyeth Pharmaceuticals, USA) and solanezumab (Eli Lilly and Company). They were each tested in two large phase III

trials for mild-to-moderate AD, but neither drug showed improvement in cognition or functional ability compared with a placebo (Salloway et al., 2014, Doody et al., 2014).

4. TKM approach and purpose of this study

There are several advantages of using the knowledge and database from TKM for the development of innovative therapeutics for dementia. First, TKM has a long history of treating dementia patients. Therefore, a bulk of data has been accumulated in the form of medical literatures. Second, TKM adopts a holistic approach by nature and aims at multiple targets as opposite to a single target as in the case of developing drugs based on small molecules or biologics. In TKM, various plant sources are often used in the form of mixture, generally to reduce the toxicity and strengthen the efficacy, so it is ideal for chronic or complex diseases involving many different factors.

In order for TKM to become a viable treatment method, however, several issues have to be addressed. First, extensive laboratory and clinical studies are required to demonstrate their claimed therapeutic effects as well as to unravel the underlying mechanism(s). Safety tests for candidate products have also been carried out in compliance with GLP (good laboratory practice) guidelines. Second, it is necessary to develop reliable and standardized methods to secure raw materials and prepare the reagent (product) in a consistent and reproducible manner, because in most cases, active compounds have not been identified, which makes the quality control of the experimental reagent extremely difficult. This problem is indeed the single most important bottleneck during the modernization efforts of TKM.

Based on the theory and practice of TKM, the pathologies of AD can be classified into two patterns: one is age-related functional and structural degeneration,

and the other is stress generated from various pathological substances, such as the aggregates of amyloid and tau. To deal with them, I developed a botanical formulation consisting of 4 plants, named HX106N. *Dimocarpus longan* and *Liriope platyphylla* were chosen to compensate for the degeneration in the brain on the basis of their nourishing properties in TKM. Recent studies have also shown that they contained neurotrophic activities. For example, *Dimocarpus longan* increased the expression of brain-derived neurotrophic factor (BDNF) in the hippocampus of mice (Park et al., 2010), while spicatoside A, a major compound in *Liriope platyphylla*, was found to induce neurite outgrowth (Hur et al., 2009). *Salvia miltiorrhiza* and *Gastrodia elata* were selected to remove the pathological substances and prevent stress damage through their promoting effects on blood circulation. Antioxidative and anti-inflammatory effects of *Salvia miltiorrhiza* have been reported by Zhao *et al*.(2006) and Kim *et al*.(2005), and the ether fraction of methanol extracts of *Gastrodia elata* has also been reported to have neuroprotective effects in kainic acid-treated rats (Kim et al., 2001).

My goal was to first test this formulation, HX106N, for possible preventive and therapeutic effect in animal models of AD-type amnesia. After obtaining highly encouraging and reproducible data showing significant improvement in cognitive functions, a variety of *in vitro* cell culture systems were used to understand the underlying mechanisms. Because I could not identify active compounds responsible for bioactivities of HX106N, I needed to develop a method which could allow me to make HX106N in a reproducible manner at different times, even with raw plant sources purchased at different times. This was achieved by developing cell-based bioassay systems, using several parameters (or factors) involved in the pathogenesis of AD. Although it was not the scope of this thesis work, HX106N was investigated in a randomized, double-blind, placebo-controlled human study. This study showed that

HX106N could improve working memory performance in a statistically significant manner relative to placebo. Taken together, I demonstrated the potential of HX106N as a safe and effective therapeutic for dementia, especially AD. My thesis shows the power of using TKM theory and its database for the development of new and innovative therapeutics for human diseases in a time-honored and cost-effective way.

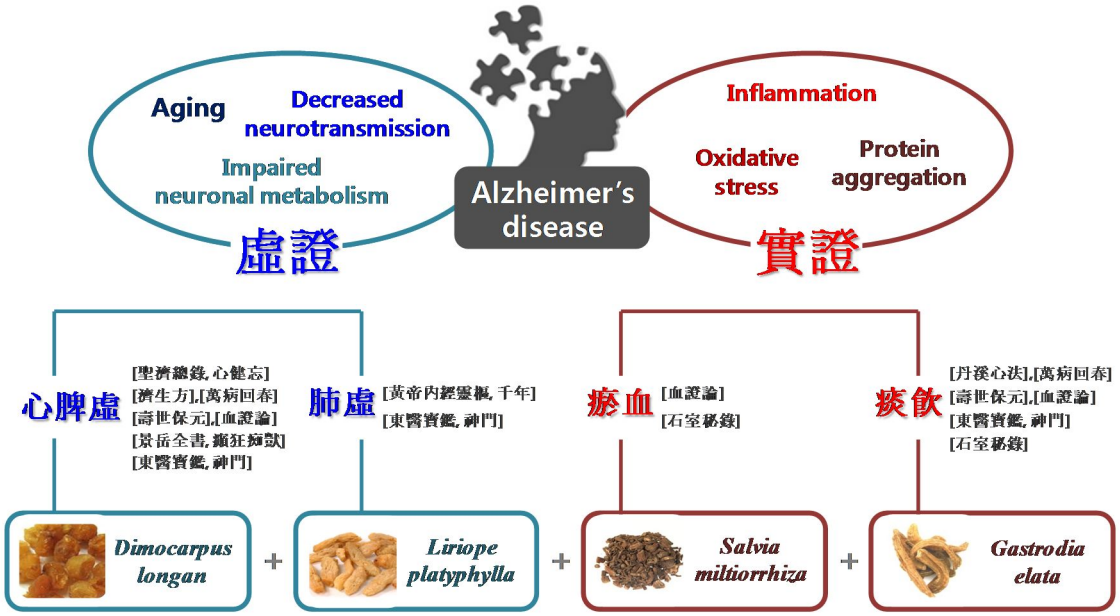

Figure 3. TKM interpretation of AD and rationale for HX106N formulation. Based on the theories of TKM, the pathologies of AD have been classified into two categories. One is heojeung (虛證), which indicates the pathological conditions resulting from the deficiency of the essential elements for body homeostasis. In TKM, heojeung stems from age-related functional and structural degenerations, such as decreased neurotransmission and metabolism. The other one is siljeung (實證), which means the accumulation of pathological substances and stresses generated from such conditions. HX106N was designed to treat both heojeung and siljeung. *Dimocarpus longan* and *Liriope platyphylla* were chosen to counter heojeung, for example to compensate the degeneration in the brain through their nourishing properties. On the other hand, *Salvia miltiorrhiza* and *Gastrodia elata* were selected to solve the problems associated with siljeung, for example to remove the pathological substances and prevent stress damages through their promoting effects on blood circulation.

CHAPTER II

Materials and Methods

1. Preparation and quality control of HX106N

1.1 Cell culture and reagents

BV-2 cells (a gift from Dr. Eui-Ju Choi, Korea University, Seoul, Korea) and HT22 cells (a gift from Dr. Yong-Keun Jung, Seoul National University, Seoul, Korea) were cultured in Dulbecco's modified Eagle's medium (DMEM) containing 10% fetal bovine serum (Gibco, Grand Island, NY, USA) and antibiotics (100 U/mL penicillin and 100 μg/mL streptomycin) at 37°C under 5% CO_2. Gastrodin was purchased from 2A pharmachem (Lisle, IL, USA). Spicatoside A was kindly provided from Dr. Ki-Dong Yoon, the catholic University of Korea, bucheon, Korea. Salvianolic acid B, ellagic acid, lipopolysaccharide (LPS, Escherichia coli, 0111:B4), L-glutamic acid monosodium salt hydrate, acetylthiocholine iodide and 5,5-dithiobis-2-nitrobenzoate were purchased from Sigma (St. Louis, MO, USA).

1.2 Preparation of HX106N

All plants used in the preparation of HX106N were purchased from Kyung Dong Market (Seoul, Korea). The following plants were used: *Dimocarpus longan* Lour. (*Longanae Fructus*, 6 g); *Liriope platyphylla* Wang et Tang. (*Liriopes Radix*, 10 g); *Salvia miltiorrhiza* Bunge (*Salvia miltiorrhiza Radix*, 6 g); and *Gastrodia elata* Blume (*Gastrodiae Rhizoma*, 2 g). The plants (total dry weight, 24 g) were mixed, minced using a grinder (Rong Tong Iron Works, Taichung, Taiwan), and extracted by boiling in distilled water (DW) for 3 h. The extract was filtered with 10-μm cartridge paper and concentrated using a rotary evaporator (Eyela, Tokyo, Japan), followed by a freeze-drying process. This process generally produced approximately 10–11 g of brown powder. To validate the quality of HX106N, high-performance liquid chromatography

(HPLC) analysis was employed, using salvianolic acid B, gastrodin, and spicatoside A for *Salvia miltiorrhiza*, *Gastrodia elata*, and *Liriope platyphylla,* respectively. For *Gastrodia elata*, liquid chromatography-tandem mass spectrometry (LC-MS/MS) analysis was performed, using ellagic acid as a marker. A cell-based bioassay was also used to prepare HX106N in a consistent manner, using nitric oxide (NO), acetylcholinesterase (AChE) activity, and cell viability (upon treatment with glutamate) as indicators. The IC_{50} and EC_{50} values of these parameters were determined when new batches of HX106N were produced. Only the batches whose IC_{50} and EC_{50} values fell within 20% of those from the reference batch were used for the experiments.

1.3 HPLC analysis of salvianolic acid B for *Salvia miltiorrhiza*

5 mg of salvianolic acid B was dissolved in 1 mL 75% methyl alcohol filtered through 0.45-μm PTFE syringe filter (Sartorius, Gottingen, Germany). It was diluted with 75% methyl alcohol and used as a standard stock. 100 mg of the sample extract was extracted with 5 mL 75% methyl alcohol for 30 min by sonication, and then filtered through the PTFE filter for HPLC analysis, followed by HPLC analysis. The experimental conditions are as shown in Table 4.

1.4 HPLC analysis of gastrodin for *Gastrodia elata*

5 mg of gastrodin was dissolved in 1 mL DW. The solution was filtered through the PTFE filter, and diluted with DW for use as a standard stock. 100 mg of the extract was extracted with 5 mL DW for 30 min by sonication. It was filtered through the PTFE filter and analyzed using HPLC. The experimental conditions are as shown in Table 4.

Table 4. Experimental conditions for HPLC and LC-MS/MS analyses

<table>
<tr><td>Indicated components</td><td>Salvianolic acid B</td><td>Gastrodin</td><td>Spicatoside A</td><td>Ellagic acid</td></tr>
<tr><td>Instrument</td><td colspan="2">Agilent 1100</td><td>Agilent 1200</td><td>Agilent 1290 Infinity Binary HPLC system with 6410B triple quadrupole LC/MS system</td></tr>
<tr><td>Detector</td><td colspan="2">Diode Array Detector</td><td>Evaporative Light Scattering Detector
<table><tr><td>Drift tube temp</td><td>90°C</td></tr><tr><td>N2 gas flow</td><td>2.0 SLPM</td></tr><tr><td>Gain</td><td>1</td></tr></table></td><td></td></tr>
<tr><td>Wavelength</td><td>288 nm</td><td>220 nm</td><td></td><td></td></tr>
<tr><td>Column</td><td colspan="4">Shiseido Capcell PAK C18 MG(250 mm × 4.6 mm, 5 μm)</td></tr>
<tr><td>Mobile phase</td><td><table><tr><td>Time</td><td>A (%)</td><td>B (%)</td></tr><tr><td>0</td><td>98</td><td>2</td></tr><tr><td>20</td><td>77</td><td>23</td></tr><tr><td>35</td><td>71.5</td><td>28.5</td></tr><tr><td>40</td><td>71.5</td><td>28.5</td></tr><tr><td>45</td><td>98</td><td>2</td></tr></table>A : 0.026% Phophoric acid
B : Acetonitrile</td><td><table><tr><td>Time</td><td>A (%)</td><td>B (%)</td></tr><tr><td>0</td><td>100</td><td>0</td></tr><tr><td>5</td><td>100</td><td>0</td></tr><tr><td>10</td><td>0</td><td>100</td></tr><tr><td>15</td><td>0</td><td>100</td></tr><tr><td>17</td><td>100</td><td>0</td></tr><tr><td>20</td><td>100</td><td>0</td></tr></table>A : DW
B : 10% Acetonitrile in DW</td><td><table><tr><td>Time</td><td>A (%)</td><td>B (%)</td></tr><tr><td>0</td><td>72</td><td>28</td></tr><tr><td>7</td><td>72</td><td>28</td></tr><tr><td>17</td><td>30</td><td>70</td></tr><tr><td>30</td><td>30</td><td>70</td></tr><tr><td>32</td><td>72</td><td>28</td></tr><tr><td>35</td><td>72</td><td>28</td></tr></table>A : DW
B : Acetonitrile</td><td><table><tr><td>Time</td><td>A (%)</td><td>B (%)</td></tr><tr><td>0</td><td>70</td><td>30</td></tr><tr><td>7</td><td>50</td><td>50</td></tr><tr><td>13</td><td>10</td><td>90</td></tr><tr><td>15</td><td>70</td><td>30</td></tr><tr><td>18</td><td>70</td><td>30</td></tr></table>A : 0.1% Formic acid
B : Methyl alcohol</td></tr>
<tr><td>Flow rate</td><td colspan="2">1.0 mL/min</td><td>0.8 mL/min</td><td></td></tr>
<tr><td>Injection volume</td><td colspan="2">5 μL</td><td>10 μL</td><td></td></tr>
<tr><td>Oven temperature</td><td>20℃</td><td>25℃</td><td>27℃</td><td>40℃</td></tr>
<tr><td>Mass spectrometry conditions</td><td colspan="3"></td><td><table><tr><td>Ionization type</td><td>ESI Negaitve</td></tr><tr><td>Gas temp.(℃)</td><td>320</td></tr><tr><td>Gas flow (L/min)</td><td>9</td></tr><tr><td>Nebulizer (psi)</td><td>15</td></tr><tr><td>Capillary (V)</td><td>4000</td></tr><tr><td>Scan mode</td><td>MRM</td></tr></table></td></tr>
</table>

1.5 HPLC analysis of spicatoside A for *Liriope platyphylla*

5 mg of spicatoside A was dissolved in 5 mL methyl alcohol. The solution was diluted with methyl alcohol for use as a standard stock after filtering through the PTFE filter. 2 g of the extract powder was extracted with 25 mL DW for 30 min by sonication. The extract was transferred into a separatory funnel, and water-saturated butanol was added. The mixture was shaken and allowed to stand until it separate into two layers. The upper layer was collected and concentrated by vacuum concentration. Then it was dissolved in 5 mL methyl alcohol and filtered through the PTFE filter for use as a test sample. An evaporative light scattering detector (ELSD) was used to detect sensitively spicatoside A. The experimental conditions are as shown in Table 4.

1.6 LC-MS/MS analysis of ellagic acid for *Dimocarpus longan*

To prepare a standard stock of ellagic acid, 5 mg of ellagic acid was dissolved in 5 mL methyl alcohol and filtered through the PTFE filter, and then it was diluted with methyl alcohol. 100 mg of the extract powder was sonicated with 5 mL methyl alcohol for 30 min. It was filtered through the PTFE filter and used as a test sample. The conditions used for LC-MS/MS analysis are as described in Table 4.

1.7 Measurement of nitric oxide

BV-2 cells were seeded in 24-well plates (5×10^4 cells/well). After 24 h, the cells were treated with 100 ng/mL LPS and various concentrations of HX106N for 24 h. The culture supernatants were used to measure the level of NO with a nitric oxide assay kit (R&D Systems, Minneapolis, MN, USA).

1.8 Determination of cell viability

HT22 cells were plated at 3×10^3 cells/well in 96-well plates. After 24 h, cells were treated with 4 mM glutamate and various concentrations of HX106N for 18 h. Cell viability was measured using the 3-(4,5-dimethylthiazol-2-yl)-2,5-diphenyl-2H-tetrazolium bromide (MTT) assay kit, according to the manufacturer's protocol (Roche, Mannheim, Germany).

1.9 Measurement of acetylcholinesterase activity

The assay for *in vitro* AChE activity was conducted using the modified method described by Ellman *et al* (Kosasa et al., 1999). Briefly, a reaction buffer containing 134 μL of sodium phosphate buffer (100 mM, pH 7.0), 1 μL of acetylthiocholine iodide (75 mM), and 5 μL of 5,5-dithiobis-2-nitrobenzoate (10 mM) was mixed with 50 μL of diluted HX106N solution and incubated for 10 min at 25°C. Then, 10 μL of mouse brain homogenates (100 mg brain/mL of 12.5 mM sodium phosphate buffer, pH 7.0) was added as an enzyme source. The absorbance was measured at 405 nm after 30 min of incubation at 25°C. AChE activity was expressed as the percentage of absorbance relative to the control (50 μL of DW in reaction buffer).

2. Anti-Amnesic Effects of HX106N in Animal Models of AD

2.1 Animals

Male ICR mice (5-week-old) were obtained from Samtako, Bio Korea (Kyoung-Ki, Korea). The animals were housed 5–6 per cage under a 12:12 h light-dark cycle (light on from 08:00 to 20:00 h) with access to food and water *ad libitum*. All experimental procedures were performed in accordance with the guidelines established by the Institutional Animal Care and Use Committee of Seoul National University.

2.2 $A\beta_{25-35}$-induced amnesia model

Mice were treated orally with HX106N (50, 100, or 200 mg/kg body weight) or donepezil (1 mg/kg body weight, Sigma) on a daily basis from day -7 to day 8. On day 0, they were injected with $A\beta_{25-35}$-peptide via the intracerebroventricular (i.c.v.) route. The Y-maze test and the acquisition trial of the passive avoidance test were carried out on days 7 and 8, respectively.

2.3 Intracerebroventricular injection

$A\beta_{25-35}$ peptide (Sigma) was dissolved in DW and aggregated for 7 days at 37°C. Aggregated $A\beta_{25-35}$ peptide (5 or 10 nmol/5 μL) or vehicle (DW, 5 μL) was administered by i.c.v. injection, as previously described (Maurice et al., 1996). Briefly, the mice were lightly anaesthetized with ether, a 27-gauge stainless steel needle (Hamilton, Reno, NV, USA) was inserted into the lateral ventricle, and peptide or vehicle was delivered over an approximately 30-s interval. The mice returned to normal behavior within 1 min following the injection. In the preliminary experiments, the injection site was confirmed with 1% methylene blue injections.

2.4 Y-maze test

The maze apparatus was made of dark opaque polyvinyl plastic with three arms at 120° angles. Each arm was 40 cm long, 13 cm high, 3 cm wide at the bottom, and 10 cm wide at the top. The mice were initially placed at the end of one arm and allowed to move freely for 7 min. The series of arm entries was recorded manually. Spontaneous alternation was defined as successive entries into the three arms in overlapping triplet sets. The alternation percentage was calculated as the ratio of actual alternations to

maximum alternations (defined as the total number of arm entries minus 2) multiplied by 100.

2.5 Step-through passive avoidance test

The apparatus was composed of two chambers, one clear and one dark, separated by a guillotine door. The floor of both chambers consisted of 2-mm stainless steel rods spaced 1 cm apart. The clear chamber contained a 15W bulb. During the acquisition trial, the mice were initially placed in the clear chamber. After 30 seconds, the guillotine door was opened to allow the mice to enter the dark chamber. Once all four limbs of the mouse were inside the dark chamber, the door was closed, and an electric foot shock (0.5 mA, 3 s) was delivered. Twenty-four hours after the acquisition trial, mice were returned to the clear chamber for the retention trial. Latency was defined as the time required for a mouse to enter the dark chamber and was recorded for up to 300 s.

2.6 Measurement of lipid peroxidation

After the retention trial of the passive avoidance test, the mice were sacrificed, and the hippocampus and cortex were isolated. The hippocampal and cortical tissues were homogenized in ice-cold PBS (10% w/v) containing 0.05% BHT and centrifuged at 10,000 × *g* for 10 min at 4°C. The TBARS levels of the homogenates were determined using the OxiSelect TBARS Assay Kit (Cell Biolabs, San Diego, CA, USA), according to the manufacturer's protocol.

2.7 Western blot analysis

Total proteins were prepared from isolated hippocampus for general Western blot analysis. Membranes containing the blotted proteins were incubated with antibodies

against synaptophysin (1:1,000, Millipore, Billerica, MA, USA) and β-actin (1:5,000, Sigma). For visual detection, a horseradish peroxidase (HRP)-conjugated anti-rabbit IgG or anti-mouse IgG antibody (1:100,000, Sigma) was used with chemiluminescence reagents (Millipore).

2.8 Northern blot analysis

Mice were sacrificed at the indicated time points after $A\beta_{25-35}$ injection. The hippocampus was dissected on ice and stored at -80°C. The tissue was homogenized, and total RNA was isolated using TRIzol reagent, following the manufacturer's instructions (Invitrogen, Carlsbad, CA, USA). The RNA was resolved by electrophoresis in an 1% agarose-formaldehyde gel and transferred to a nylon membrane (Hybond-N; Amersham, Buckinghamshire, UK). The membranes were hybridized with a specific [^{32}P]-labeled probes overnight at 68°C with Expresshyb solution (Clontech, Palo Alto, CA, USA). The membrane was washed and exposed to autoradiography film. Specific cDNA probes for mouse TNF-α, IL-1β and GAPDH were labeled by random priming using the Klenow fragment of DNA polymerase I (Stratagene, La Jolla, CA, USA) and [α-^{32}P]dCTP (Perkin Elmer, Norwalk, CT, USA). The PCR primer sequences were as follows: TNF-α (forward, TGG CCT CCC TCT CAT CAG TTC TATG; reverse, GTC TAA GTA CTT GGG CAG ATT GAC C) and GAPDH (forward, ACG GCA AAT TCA ACG GCA CAG; reverse, GGC GGC ACG TCA GAT CC).

2.9 Quantitative RT-PCR analysis

First-strand cDNA was synthesized using an oligo(dT) primer and AMV reverse transcriptase (Takara, Shiga, Japan) and amplified by PCR using a specific primers for

TNF-α, IL-1β, HO-1 and GAPDH using SYBR Premix Ex TaqTM (Takara). The primer sequences were as follows: TNF-α (forward, CCC TCA CAC TCA GAT CAT CTT CT; reverse, GCT ACG ACG TGG GCT ACA G), IL-1β (forward, GCA ACT GTT CCT GAA CTC AAC T; reverse, ATC TTT TGG GGT CCG TCA ACT), HO-1 (forward, GTG ATG GAG CGT CCA CAG C; reverse, TGG TGG CCT CCT TCA AGG), and GAPDH (forward, AGC CTC GTC CCG TAG ACA A; reverse, AAT CTC CAC TTT GCC ACT GC). The reaction was started at 95°C for 30 s followed by 40 cycles of denaturation at 95°C for 5 s and annealing/extension at 60°C for 20 s. The threshold cycle (Ct) of each gene was determined as PCR cycles during which an increase in reporter fluorescence was observed above a baseline. GAPDH was amplified simultaneously as an internal control. The relative expression levels of the target genes were calculated using the $2^{-\Delta\Delta Ct}$ method, as described previously (Johnson et al., 2013).

2.10 Scopolamine-induced amnesia model

Mice were orally administered with HX106N (100 mg/kg body weight) or donepezil (1 mg/kg body weight). One hour later, amnesia was induced by scopolamine (1 mg/kg body weight, i.p.). The mice were introduced to the Y-maze test and the acquisition trial of the passive avoidance test 30 min after the injection.

2.11 Measurement of acetylcholinesterase activity

Mice were sacrificed 1 h after the oral administration of HX106N (100 mg/kg body weight) or donepezil (1 mg/kg body weight). The hippocampal and cortical tissues were isolated and homogenized in ice-cold sodium phosphate buffer (100 mM, pH 7.0). The homogenates were centrifuged at 10,000 × *g* for 10 min at 4°C, and the supernatant was assayed for the determination of AChE activity using the Amplex Red

Acetylcholine/acetylcholinesterase assay kit (Invitrogen), according to the manufacturer's protocol.

2.12 Statistics

The data are presented as the mean ± SEM. Behavioral tests and biochemical analysis were analyzed using Student's *t*-test or a one-way analysis of variance (ANOVA), with Dunnett's multiple comparison test employed for multiple comparisons. P-values of less than 0.05 were considered significant.

3. Antioxidative effects of HX106N in microglia and neuronal cells

3.1 Cell culture and reagents

BV-2 cells and HT22 cells were cultured in DMEM containing 10% fetal bovine serum and antibiotics (100 U/mL penicillin and 100 μg/mL streptomycin) at 37°C under 5% CO_2. Primary cortical microglia were isolated from ICR mice on postnatal day 1-3 (P1-3) with a mild trypsinization method (Saura et al., 2003). Primary cortical neurons were prepared from ICR mice or C57BL/6 mice (wild type or Nrf2 knockout mice provided by Dr. Masayuki Yamamoto, Tohoku University, Sendai, Japan) at embryonic day 15 (E15), as described previously (Koh et al., 2009). LPS (Escherichia coli, 0111:B4), L-glutamic acid monosodium salt hydrate, actinomycin D (ActD), cycloheximide (CHX), Zinc (II) protoporphyrin-IX (ZnPP), hemoglobin (Hb) and carbon monoxide releasing molecule 3 (CORM-3) were purchased from Sigma.

3.2 Measurement of cytokines and NO

The amount of TNF-α and IL-6 in the supernatant was measured with specific enzyme-linked immunosorbent assay (ELISA) kits (Thermo, Woburn, MA, USA) according to the manufacturer's protocols. The level of NO present in culture supernatants was measured using a nitric oxide assay kit (R&D Systems) according to the manufacturer's instruction.

3.3 Western blot analysis

Following HX106N treatment, cells were harvested and lysed in phosphosafe extraction buffer (Novagen, Madison, WI, USA). The protein were separated by 10% SDS-PAGE and transferred to PVDF membrane. To block nonspecific binding, the membrane was incubated in TBST (150mMNaCl, 10mMTris-HCl, 0.1 % Tween-20) containing 5% skim milk at room temperature for 1 h. Membranes were then incubated in TBST containing 5% skim milk with primary antibodies against iNOS (1:1,000, BD Biosciences, Franklin Lakes, NJ, USA), HO-1 (1:4,000, Stressgen, Victoria, Canada), Nrf2 (1:500, Santa Cruz Biotechnology, Santa Cruz, CA, USA), β-actin (1:5,000, Sigma) or TFIIB (1:500, Santa Cruz) overnight at 4°C. After three times washing with TBST, the membranes were incubated with HRP-conjugated anti-mouse or anti-rabbit IgG (Sigma) antibodies. The blot was developed by the enhanced chemiluminescence (Millipore, Billerica, MA, USA) and visualized by exposure to autoradiography film. The band density was quantitated using Image J software.

3.4 Northern blot analysis

After treatment, total RNA was prepared from the cells using TRIzol reagent (Invitrogen). Twenty micrograms of RNA were separated by electrophoresis in agarose-

formaldehyde gel and transferred to a nylon membrane (Amersham). The membranes were hybridized with the respective [^{32}P]-labeled probes overnight at 68°C with Expresshyb solution (Clontech). The membrane was washed and exposed to autoradiography film. The PCR primer sequences used to generate these probes were as follows: mouse iNOS (forward, ACC CGT CCA CAG TAT GT; reverse, TGT TGG TGG CAT AAA GTA TGT), NQO1 (forward, CAT TCT GAA AGG CTG GTT TGA; reverse, CTA GCT TTG ATC TGG TTG TCA G), GCLm (forward, CAT GGC ATG CTC CGT CCT TG; reverse, AGC AGT TCT TTC GGG TCA TT) and GAPDH (forward, ACG GCA AAT TCA ACG GCA CAG; reverse, GGC GGC ACG TCA GAT CC).

3.5 Luciferase reporter plasmid assay

The 1,749-bp fragment of the 5'-flanking region of iNOS was designed as the full-length promoter sequence, as previously described (Xie et al., 1993). The fragment was inserted into pGL3-basic luciferase reporter vector (Promega, Madison, WI, USA) to form the construct piNOS-Luc. BV-2 cells were transiently transfected with a piNOS-Luc (3 μg) and a β-galactosidase plasmid (1 μg; Invitrogen) using FuGENE6 according to the manufacturer's protocols (Roche, Indianapolis, IN, USA). Twenty-four hours later, the cells were treated with LPS and HX106N for 24h, and the luciferase activity was measured using the Luciferase Reporter kit according to the manufacturer's protocol (Promega) with a microplate luminometer (MicroLumat Plus LB96V, Berthold, Germany). Luciferase activity was normalized to β-gal activity.

3.6 Electrophoretic mobility shift assay (EMSA)

BV-2 cells were treated with LPS and HX106N for 6 h, and the cells were harvested.

The cells were incubated with 200 μL of lysis buffer A [10 mM HEPES (pH 7.9), 10 mM KCl, 1.5 mM MgCl2, 0.1 mM EDTA, 1 mM DTT and protease inhibitor cocktail (Roche)] for 20 min. The same volume of lysis buffer B (lysis buffer A containing 0.5% Nonidet-P40) was added and incubated for an additional 20 min followed by centrifugation. The pellets were washed with 400 μL of lysis buffer A. After centrifugation, the pellets were resuspended in 20 μL of lysis buffer C [10 mM HEPES (pH 7.9), 400 mM NaCl, 1.5 mM MgCl2, 1 mM EDTA, 1 mM DTT and protease inhibitor cocktail (Roche)] and incubated on ice for 1 h. A centrifugation step generated the nuclear extracts. 10 μg of nuclear proteins were incubated with in 20 μL binding buffer containing containing 0.01 unit of poly(dI-dC), 2 μg of salmon sperm DNA, 0.05 pmol [^{32}P]-labeled DNA probe for 30 min on ice. The reaction was analyzed on non-denaturing polyacrylamide gels that were electrophoresed using 0.5X TBE buffer [44.5 mM Tris base, 22.3 mM boric acid and 1 mM EDTA (pH 8.0)]. The gels were exposed to X-ray film at -80°C. Oligonucleotide sequences used to prepare the probes were as follows (the binding motif is underlined and the lowercase letters indicate mutated nucleotides): AP-1 (WT, GCTTGATGACTCAGCCGGAA; MT, CGCTTGATGAgggA GCCGGAA) and NF-kB (WT, AGTTGAGGGGACTTTCCCAGGC; MT, AGTTGAGc tcACTTTCCCAGGC). The specificity of the retarded complexes was confirmed by competition with 100-fold excess unlabeled WT or MT oligonucleotide.

3.7 Determination of cell viability

MTT assay kit (Roche) was used to determine cell viability, according to the manufacturer's protocol.

3.8 Measurement of reactive oxygen species (ROS)

The intracellular ROS levels were measured using the fluorescence probe 5-(and-6)-chloromethyl-2',7'-dichlorodihydrofluorescein diacetate, acetyl ester (CM-H_2DCFDA; Invitrogen). After treatment, cells were washed twice with PBS and were then incubated with 5 μM CM-H_2DCFDA for 30 min at 37°C. The fluorescence was determined by flow cytometry using a FACS Calibur (BD, San Jose, CA, USA).

3.9 Measurement of glutathione (GSH)

The monochlorobimane (MCB) assay was used to measure the contents of GSH, as described previously (Juurlink et al., 1996). In brief, MCB was added to the culture medium to a final concentration of 100 μM. After 30 min, cells were harvested and MCB-glutathione adduct was measured at excitation/emission wavelengths of 380 and 470 nm.

3.10 Immunofluorescence assay

After treatment, primary cortical neurons were fixed with 4% paraformaldehyde for 10 min, and permeabilized with 0.5% triton X-100 for 15 min. After washing three times with PBS, the cells were blocked in 10% FBS for 1h, and then incubated overnight at 4°C with anti-tuj1 antibody (1:500, Millipore). After several rinses in PBS, the cells were incubated with Alexa 588-conjugated anti-rabbit IgG (1:200) for 1 h and then Hoechst (Polyscience, Warrington, PA) for 5 min. Cells were rinsed with PBS, and observed using an inverted immune-fluorescence microscope (Axiovert 200 M, Zeiss, Gottingen, Germany)

3.11 Transfection of siRNA

The small interfering RNAs (siRNA) specific for HO-1 (siHO-1) and a non-specific

control siRNA (siCon; SN-1001) were purchased from Bioneer (Daejeon, Korea). Lipofectamine2000 reagent (Invitrogen) was used for transfection of siRNA into BV-2 cells according to the manufacturer's protocol. The cells were used for assays 24 h after the transfection.

3.12 Statistics

The data are presented as the mean ± SD. Significant differences between the experimental groups were analyzed using Student's *t*-test. P-values less than 0.05 were considered significant.

4. Mechanism study of HX106N-mediated HO-1 expression

4.1 Cell culture and reagents

BV-2 cells were cultured in DMEM containing 10% fetal bovine serum and antibiotics (100 U/mL penicillin and 100 μg/mL streptomycin) at 37°C under 5% CO_2. Primary splenocytes were prepared from wild type or Nrf2 knockout C57BL/6 mice (provided by Dr. Masayuki Yamamoto, Tohoku University, Sendai, Japan), using the mechanical dissociation method (Kweon et al., 1998), and cultured in RPMI-1640 containing 10% fetal bovine serum and antibiotics. SB203580, SP600125 and BAY 11-7802 were purchased from Sigma. PD98059 were purchased from Calbiochem (La Jolla, CA, USA).

4.2 Western blot analysis

After treatment, cells were washed with cold PBS and lysed with Phosphosafe extraction buffer (Novagen). The lysates were then separated by 10% SDS-PAGE and

electrophoretically transferred to PVDF membranes. The membranes were incubated with primary antibodies specific for HO-1 (1:4,000, Stressgen), Nrf2 (1:500, Santa Cruz), c-Jun (1:500, Santa Cruz), p-JNK (1:1,000, Cell Signaling, Beverly, MA, USA), JNK (1:1,000), p-p38 (1:1,000, Cell Signaling), p38 (1:1,000, Santa Cruz), p-IKKα/β (1:1,1000, Cell Signaling), IKKα (1:500, Santa Cruz), IκBα (1:500, Santa Cruz), p65 (1:500, Santa Cruz), β-actin (1:5,000, Sigma) or TFIIB (1:500, Santa Cruz). The membranes were then incubated with HRP-conjugated anti-mouse or anti-rabbit IgG (Sigma) antibodies. The bands were visualized by enhanced chemiluminescence (Millipore, Billerica, MA, USA) using X-ray film, and the band density was quantitated using Image J software.

4.3 Northern blot analysis

Total RNA was isolated using TRIzol reagent (Invitrogen). The RNA was separated with 1% agarose-formaldehyde gel electrophoresis and transferred to a nylon membrane (Amersham). The membrane was hybridized with ^{32}P-labeled mouse HO-1 and GAPDH probes overnight at 68°C. The blot was then washed and exposed to autoradiography film. The band density was measured using Image J software. Specific probes for mouse HO-1 and GAPDH were labeled by random priming using the Klenow fragment of DNA polymerase I (Stratagene) and [α-^{32}P]dCTP (Perkin Elmer). The PCR primer sequences were as follows: HO-1 (forward, TAC ACA TCC AAG CCG AGA AT; reverse, GTT CCT CTG TCA GCA TCA CC) and GAPDH (forward, ACG GCA AAT TCA ACG GCA CAG; reverse, GGC GGC ACG TCA GAT CC).

4.4 Luciferase reporter plasmid assay

Reporter plasmids containing the 15 kb *ho-1* promoter (pHO15-Luc), E1 (pE1-Luc) and

E1M (pE1M-Luc) sequences were provided by Dr. Eun-Hye Joe (Ajou University School of Medicine, Suwon, Korea). Reporter plasmid with five copies of an NF-κB response element (pNF-κB-Luc) was purchased from Promega (Madison, WI, USA). These plasmids encode luciferase as a reporter gene. BV-2 cells were transiently transfected with various reporter plasmids (3 μg) and a β-galactosidase plasmid (1 μg; Invitrogen) using FuGENE6 according to the manufacturer's protocols (Roche, Indianapolis, IN, USA). Twenty-four hours after transfection, the cells were treated with HX106N in the presence or absence of pharmacological inhibitors and incubated for another 9 h. Cell lysates were prepared, and a luciferase activity assay was performed using the Luciferase Reporter kit according to the manufacturer's protocol (Promega) with a microplate luminometer (MicroLumat Plus LB96V). Luciferase activity was normalized to β-gal activity.

4.5 Electrophoretic mobility shift assay

Following HX106N treatment, cells were harvested and nuclear proteins were extracted as described above. The binding reaction was performed in binding buffer (Novagen) containing 0.01 unit of poly(dI-dC), 2 μg of salmon sperm DNA, 0.05 pmol [^{32}P]-labeled DNA probe and 10 μg of nuclear extracts. After incubation for 30 min on ice, the reaction was analyzed on non-denaturing 6% polyacrylamide gels that were electrophoresed using 0.5X TBE buffer [44.5 mM Tris base, 22.3 mM boric acid and 1 mM EDTA (pH 8.0)]. The gels were exposed to autoradiography film at -80°C. Oligonucleotide sequences designed for probe preparation were as follows (the binding motif is underlined and the lowercase letters indicate mutated nucleotides): AP-1 (GCTTGATGACTCAGCCGGAA), ARE (TGGGGAACCTGTGCTGAGTCACTGGAG) and NF-κB (AGTTGAGGGGACTTTCCCAGGC). The specificity of the retarded

complexes was confirmed by competition with 100-fold excess unlabeled oligonucleotide. For supershift/interference assays, the nuclear extracts were preincubated with 4 μg of anti-Nrf2, c-Jun or p65 antibody (Santa Cruz) for 30 min on ice before the addition of the probe.

4.6 Transfection

The small interfering RNAs (siRNA) specific for Nrf2 (siNrf2), c-Jun (sic-Jun), IKKα (siIKKα), HO-1 (siHO-1) and a non-specific control siRNA (siCon; SN-1001) were synthesized by Bioneer. The siRNA was transfected into BV-2 cells using the Lipofectamine2000 reagent according to the manufacturer's protocol (Invitrogen). After 24 h, the cells were used for assays.

4.7 Statistics

The data are presented as the mean ± SD. Significant differences between the experimental groups were analyzed using Student's *t*-test. P-values less than 0.05 were considered significant.

CHAPTER III

Development of Bioassay Systems

1. Background

The quality control (QC) of botanical extracts is an extremely important issue in the context of the modernization efforts of TKM. This is because biologically active compounds in most traditional medicines are not known precisely. Indeed, traditionally made medicinal products contain a wide range of compounds in the form of extracts, and their contents are easily influenced by various factors, such as climate, harvest time and extraction conditions. Indeed, a lack of precise knowledge in the identity of biological active compounds was the single most important factor causing difficulties in controlling raw materials, manufacturing process and producing the reagents with consistent quality.

For a long time, QC of botanicals has been heavily dependent on crude methods, such as shape, color and smell. However, recent progresses made in the area of high-throughput analytical methods, including various qualitative and quantitative chemical analytical instruments, allowed investigators to overcome these problems. Chromatographic fingerprinting, a method comparing the complex chromatographic pattern of the chemical components present in plant sources, is now used for the QC of medicinal products when manufacturing TCM products (Zhong et al., 2009). However, the lack of information on the identity of active compounds still imposes a great deal of uncertainties in the context of the final product sold to consumers.

To overcome the disadvantage of this type of random chemical analysis, we have developed a cell-based bioassay system to evaluate biological activities of raw materials as well as their final products (Kim et al., 2009, Choi et al., 2012). This cell-based bioassay system has also been useful for the study of the underlying molecular mechanisms and the efforts in identifying the active compound(s) (Kim et al., 2013, Lee

et al., 2012).

HX106N is a water-soluble extract prepared from a mixture of 4 plants, and it has the same problems as described above. Furthermore, I needed to develop a system(s) that could allow me to prepare HX106N in a reproducible manner when they were made at different times with plants purchased at different times. To overcome this hurdle, I introduced cell-based bioassay systems using biologically meaningful markers, such as nitric oxide (NO), which is known to play important roles in the pathogenesis of various neurodegenerative diseases, including AD (Brown and Bal-Price, 2003). Under pathological conditions, NO is produced mainly by glial cells, such as microglia and astrocytes, and can induce neurotoxicity through the formation of reactive nitrogen species. The neuroprotective effect of HX106N against glutamate-induced neurotoxicity was also evaluated. A high concentration of glutamate has been reported to cause cell death via glutamate-induced oxidative neurotoxicity, a well-known cause of neurodegenerative diseases (Coyle and Puttfarcken, 1993). Acetylcholinesterase (AChE) inhibitors have been shown to improve cognitive functions by the enhancement of cholinergic neurotransmission (Hirai, 2000). Therefore, the effect of HX106N on AChE was also used to measure the bioactivity of HX106N. So as biological markers, NO, cell death upon glutamate treatment and AChE activity were used.

In this chapter, I present the methods for evaluating the quality of HX106N. Whenever new batches were made during the thesis work, HX106N was subjected to qualitative and quantitative analysis described in this chapter, allowing me to prepare reagents (HX106N) and obtain data in a reproducible manner.

2. Results

2.1 Development of semiquantitative cell-based bioassays

Effect of HX106N on NO production in LPS-stimulated BV-2 cells

The effect of HX106N on NO production was examined using BV-2 cells, a murine microglia cell line. Cells were treated with LPS in the presence or absence of various concentrations of HX106N for 24 h, and the culture supernatants were analyzed with the Griess assay to measure the amount of nitrite, a stable end product of NO. When BV-2 mouse microglia cell line was stimulated with LPS, the level of nitrite was highly increased. However, the production of nitrite was inhibited by HX106N in a dose-dependent manner, and an 89.8% decrease was observed at 1 mg/mL concentration (Figure 4). The IC_{50} value was 305.2 μg/mL. There was no significant effect of HX106N on cell viability at all concentrations used in this study, as measured by MTT assay (data not shown). These data indicated that HX106N inhibited NO production, and this effect could be quantitatively measured.

Effect of HX106N on glutamate-induced neurotoxicity in HT22 cells

To investigate whether HX106N has any effect on glutamate-induced oxidative neurotoxicity, HT22 cells, a murine hippocampal neuronal cell line, were used. Cells were treated for 18 h with 4 mM glutamate and various concentrations of HX106N, and cell death was measured using MTT assay. The level of cell death in glutamate-treated group was regarded as 100%. As shown in Figure 5, treatment with HX106N decreased cell death in a dose-dependent manner, and the IC_{50} value was 992.5 μg/mL. These data suggested that HX106N protected cells from glutamate-induced oxidative neurotoxicity.

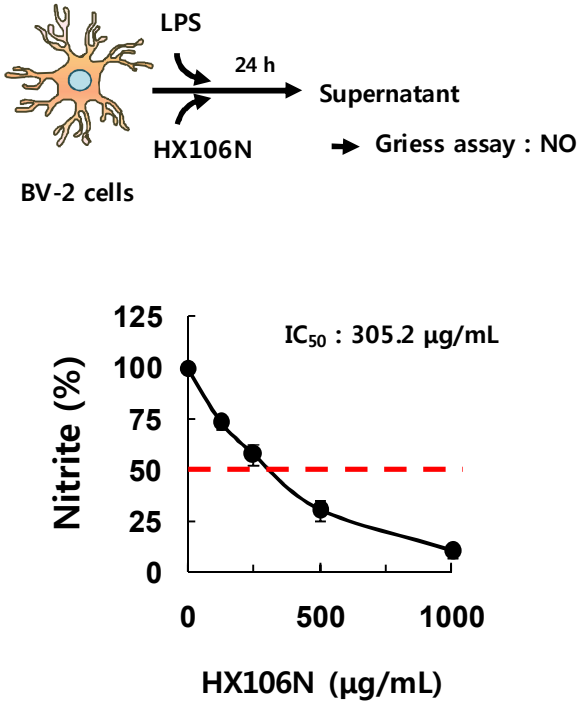

Figure 4. Effect of HX106N on the production of NO in BV-2 cells. BV-2 cells were treated with 100 ng/mL LPS and various concentration of HX106N for 24 h. The supernatants were harvested and the level of NO was measured using a Griess assay. The values are expressed as a percentage relative to LPS-treated cells (set to 100% ± SD). Data are presented as the mean ± SD of triplicate samples from a representative experiment. The dotted line indicates the IC50 value.

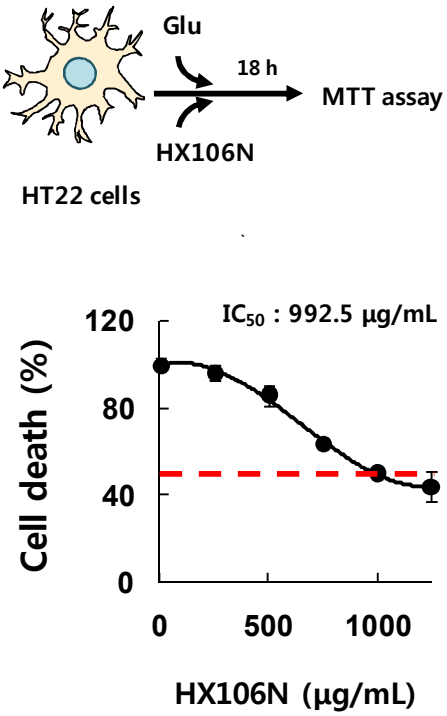

Figure 5. Effect of HX106N on glutamate-induced neurotoxicity in HT22 cells.

HT22 cells were treated with 4 mM glutamate in the presence or absence of various concentrations of HX106N. After 18 h, cell viability was determined by the MTT assay. The results are presented relative to the glutamate-treated cells. Data are presented as the mean ± SD of triplicate samples from a representative experiment. The dotted line indicates the EC_{50} value.

Effect of HX106N on AChE activity

The effect of HX106N on AChE acitivity was tested using mouse brain homogenates as a source of AChE enzyme. The homogenates were treated with various concentrations of HX106N, and then the enzyme activity was measured by the modified Ellman's method as described in the Materials and Methods. HX106N inhibited AChE activity in a dose-dependent manner and the IC_{50} value was 4.7 mg/mL (Figure 6). These results indicate that HX106N has AChE inhibitory activity, which could be used as a quantitative biological marker.

2.2 Application of bioassays for the quality control of HX106N

I employed above cell-based bioassays to evaluate the biological quality of HX106N made at different times. The IC_{50} values of these three parameters (effects on NO, cell death upon glutamate treatment and AChE activity), were determined whenever new batches of HX106N were made. Only the batches whose IC_{50} value was fell within a 20% of those from the reference stock, were used for the actual experiments.

One example of using the bioassay systems is as follows. HX106N #1 was a reference batch which showed a positive outcome in original animal experiments, and HX106N #2, #3, #4 and #5 were batches produced at different times. The individual plants used for the preparation of these batches were purchased at different times, and their agricultural origins were also different, as shown in Table 5.

In the LPS-stimulated BV-2 cells, all batches of HX106N reduced the level of nitrite in a dose-dependent manner, and the IC_{50} values of HX106N #1, #2 and #3 were 361.5, 339.9 and 331.5 μg/mL, respectively (Figure 7A). To examine the neuroprotective effect of each batch, HT22 cells were treated with various

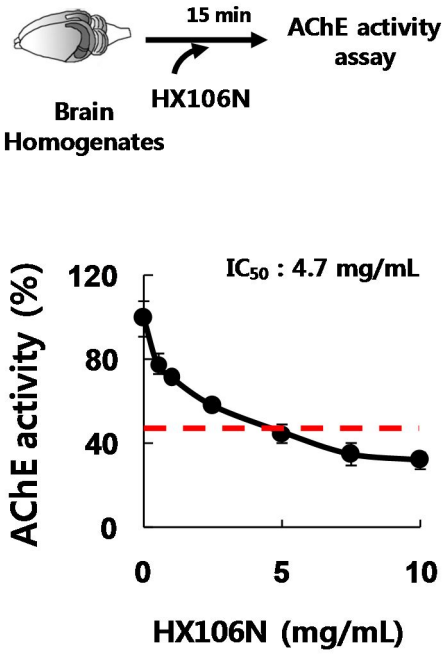

Figure 6. Effect of HX106N on AChE acitivity. Adult mouse brain homogenates were used as a source of the enzyme. Various concentrations of HX106N were added to the brain homogenates. AChE activity was measured using the modified Ellman's method as described in the materials and methods section. The values are expressed as a percentage relative to the untreated group (set to 100% ± SD). Data are presented as the mean ± SD of triplicate samples from a representative experiment. The dotted line indicates the IC_{50} value.

Table 5. Origins of each plant used for the preparation of HX106N batches

	Dimocarpus longan	***Salvia miltiorrhiza***	***Gastrodia elata***	***Liriope platyphylla***
Batch #1 (Reference)	Thailand	China	Hwasun, Chonnam, Korea	Miryang, Gyeongnam, Korea
Batch #2	Thailand	China	Jinan, Chonbuk, Korea	Buyeo, Chungnam, Korea
Batch #3	Thailand	China	Jinan, Chonbuk, Korea	Chungyang, Chungnam, Korea
Batch #4	Thailand	China	Jinan, Chonbuk, Korea	Buyeo, Chungnam, Korea
Batch #5	Thailand	China	Jinan, Chonbuk, Korea	Chungyang, Chungnam, Korea

concentrations of different HX106N batches in the presence of 4 mM glutamate. As shown in Figure 7B, HX106N #1, #2 and #3 inhibited glutamate-induced neurotoxicity in a dose-dependent manner, and their IC_{50} values were 815.6, 887.7 and 875.1 μg/mL, respectively. AChE inhibitory activity was also evaluated. The level of AChE activity was decreased in a dose-dependent manner with the IC_{50} values of 4.5, 5.3 and 4.5 mg/mL for batches #1, #2 and #3, respectively (Figure 7C). The IC_{50} values of respective parameters were within a 20% range of difference compared to the reference batch #1.

However, in the case of batches #4 and #5, their IC_{50} values for the three markers were over 20% compared to those of the reference batch (Figure 7D, 7E and 7F), although the geographic origins of raw plants used for the preparation of batches #4 and #5 were the same to those of batches #2 and #3, respectively. These results suggested that the time of the purchase (probably harvest or other processes) might have affected the quality of products.

2.3 Chemical analysis of HX106N

We also had to employ a chemical method in compliance with KFDA guidelines (otherwise, the botanical formulation cannot be used in Korea.) This was done using high-performance liquid chromatography (HPLC) and liquid chromatography-tandem mass spectrometry (LC-MS/MS).

Compounds used as indicators of each plant were shown in Table 6. The HPLC and LC-MS/MS analytical conditions used to determine the content of these compounds are described in the Materials and Methods. Salvianolic acid B and gastrodin were quantitatively detected using HPLC with UV detection. They were recognized by comparing the retention times and UV spectra with standard compounds. Peak specific

Figure 7. Quality control of various HX106N batches using the bioassay systems. (A and D) For NO, BV-2 cells were treated with 100 ng/ml LPS and various concentrations of HX106N batches for 24 h. The level of nitrite in medium was determined with Griess assay. (B and E) To investigate the neuroprotective effects of each batch, HT22 cells were treated with 4 mM glutamate and various concentrations of HX106N batches for 18 h. Cell death was measured by MTT assay. (C and F) To measure the effects on AChE activity, various concentrations of HX106N batches were added to mouse brain homogenates. AChE activity was measured using modified Ellman method. Data are presented as the mean ± SD of triplicate samples from a representative experiment. The dotted line indicates the IC_{50} value.

A

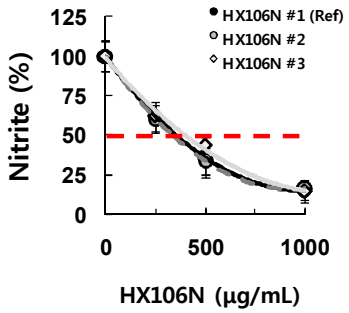

IC_{50}

#1 : 361.5 µg/mL

#2 : 339.9 µg/mL

#3 : 331.5 µg/mL

B

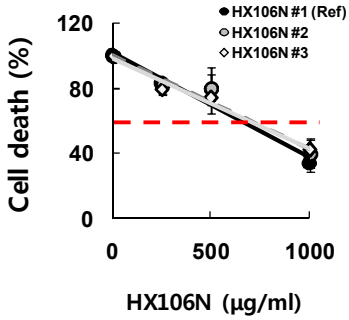

IC_{50}

#1 : 815.6 µg/mL

#2 : 887.7 µg/mL

#3 : 875.1 µg/mL

C

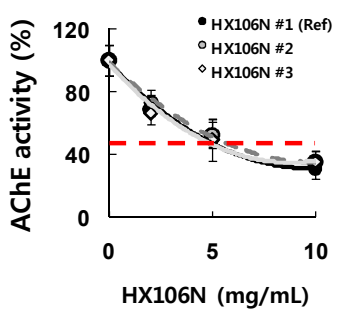

IC_{50}

#1 : 4.5 mg/mL

#2 : 5.3 mg/mL

#3 : 4.5 mg/mL

D

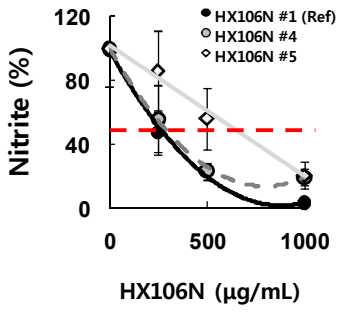

IC_{50}

#1 : 258.4 µg/mL

#4 : 280.3 µg/mL

#5 : 635.8 µg/mL

E

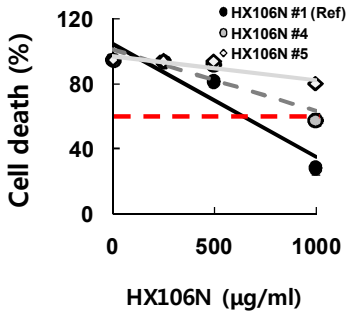

IC_{50}

#1 : 792.8 µg/mL

#4 : 1378,4 µg/mL

#5 : 3347.9 µg/mL

F

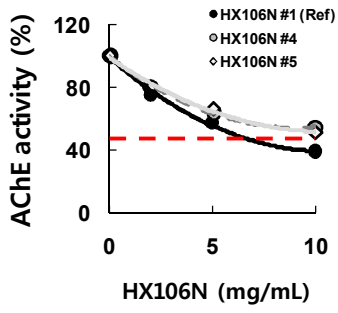

IC_{50}

#1 : 6.0 mg/mL

#4 : 9.1 mg/mL

#5 : 11.2 mg/mL

Table 6. Chemical characteristics of the indicated compounds used in this study

Structural formula	Chemical name	CAS number	Molecular formula	Molecular weight	Plant name
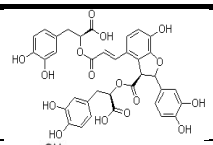	Salvianolic acid B	115939-25-8	$C_{36}H_{30}O_{16}$	718.62	*Salvia miltiorrhiza*
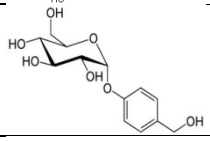	Gastrodin	62499-27-8	$C_{13}H_{18}O_7$	286.28	*Gastrodia elata*
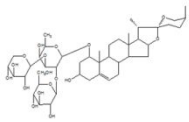	Spicatoside A	128397-47-7	$C_{44}H_{70}O_{17}$	870	*Liriope platyphylla*
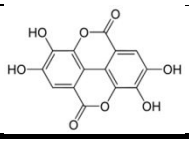	Ellagic acid	476-66-4	$C_{14}H_6O_8$	302.19	*Dimocarpus longan*

for salvianolic acid B or gastrodin was found only in *Salvia miltiorrhiza* or *Gastrodia elata*, respectively, among the four kinds of plants (data not shown). HPLC chromatograms of standard products and HX106N showed that HX106N contained these compounds, indicating salvianolic acid B and gastrodin could be used as a specific chemical marker for *Salvia miltiorrhiza* and *Gastrodia elata* (Figure 8). It was found that HX106N contained salvianolic acid B and gastrodin at the rage of 7.40 ± 0.95 and 0.67 ± 0.09 mg/g, respectively.

Spicatoside A and ellagic acid were qualitatively, rather than quantitatively, detected using evaporative light scattering detector (ELSD) and mass spectrometry, respectively, because of their extremely low levels in the raw materials. Spicatoside A or ellagic acid was found to be present specifically in *Liriope platyphylla* or *Dimocarpus longan*, respectively (data not shown), and both were also detected in HX106N, suggesting that they are appropriate markers that can be used as specific indicators (Figure 8 and 9).

3. Discussion

It is certain that multiple active compounds are responsible for the biological effects of HX106N (and probably of a majority of traditional medicinal products) in later chapters. Because their identities were not known at the time of this thesis research, the single most important hurdle in the scientific characterization of HX106N was the difficulties associated with preparing research reagents in a reproducible manner.

Conventionally, industry and academic communities working with botanical production (drugs and nutraceuticals with health claim) have been using chemical analysis methods to control the quality of raw materials and final products. However,

	A. Standard	B. HX106N
Salvianolic acid B	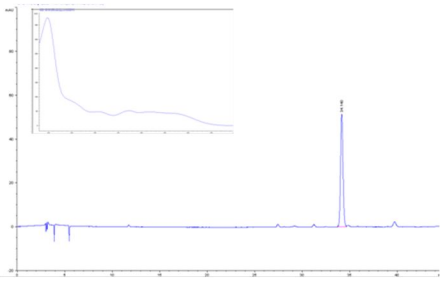	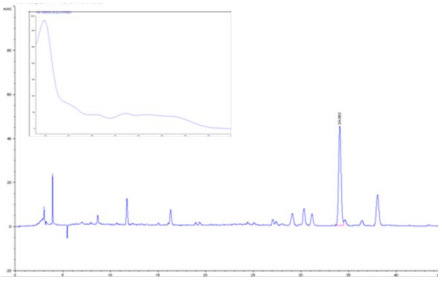
Gastrodin	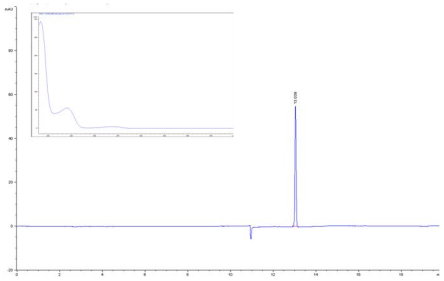	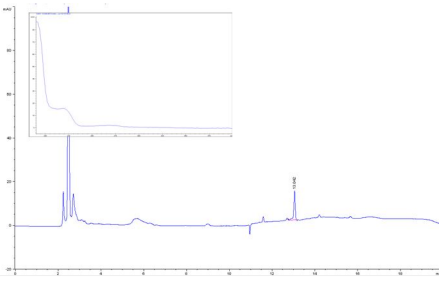
Spicatoside A	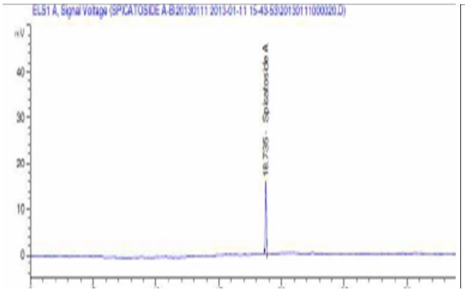	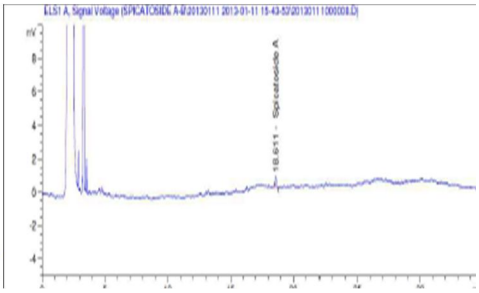

Figure 8. Representative HPLC chromatograms of standard compound (A) and HX106N (B)

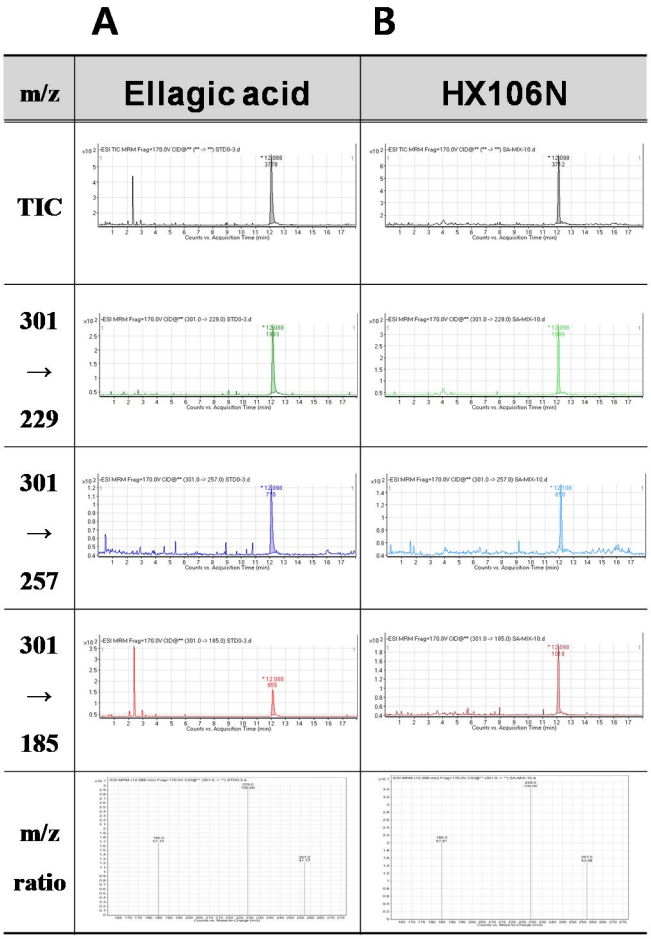

Figure 9. LC-MS/MS chromatogram of ellagic acid standard (A) and HX106N (B).

almost all markers used in these analyses are either “surrogate” markers or compounds with a minimum level of bioactivities, if there is any. In this study, I tried to overcome this fundamental problem by employing cell-based bioassay systems. The effects of HX106N on NO production, cell death following glutamate exposure, and AChE activity were used because they are meaningful biological markers involved in memory functions and the pathogenesis of AD, as discussed in later chapters. The IC_{50} value was calculated, and only reagents showing less than 20% variation were chosen for the experiments. This method appears to be reliable, because HX106N made at different times gave very reproducible results in animal experiments as well as in cell culture systems.

This type of cell-based bioassays can be useful for other purposes too. For example, these three markers are actually involved in AD pathogenesis and many other neurodegenerative diseases. Therefore, these assays can be used to identify active compounds and also to unravel the underlying mechanisms at the molecular and cellular levels. Various fractions can be prepared and single compounds can be isolated, followed by cell-based bioassays which will measures the level of bioactivities present in respective fractions or compounds.

This is not to say that cell-based bioassays can solve all problems. For example, cell-based bioassays are more cumbersome, more time-consuming and probably produce more variation than chemical analytical methods. Furthermore, if biologically active compounds are the metabolites of microorganisms in the body, cell-based assay system would not be able to measure the activities of responsible molecules.

In conclusion, cell-based bioassay systems described in this chapter were useful to prepare HX106N in a reproducible manner. The combination of bioassays with chemical analytical methods will give more meaningful data regarding actual

bioactivities in botanical products, especially when they are made for specific health claims in the real world as in my case. This method was shown to be able to help the modernization process of TKM by complementing the current weaknesses of chemical analyses that are widely used for the quality control of botanical products.

CHAPTER IV

Anti-Amnesic Effects of HX106N

in Animal Models of AD

1. Background

AD is a progressive neurodegenerative disorder characterized by a global cognitive decline in memory, orientation, judgment, and reasoning (Tanzi and Bertram, 2005). Various cellular and molecular pathologies have been suggested as causes of cognitive deficits in AD. One of them is Aβ peptide-mediated neurotoxicity.

Aβ is a peptide fragment of 39-43 amino acids derived from proteolytic cleavage of amyloid precursor protein, and its deposition in the brain is assumed to initiate a pathological cascade that results in synaptic dysfunction, synaptic loss, neuronal death and memory impairment (Walsh and Selkoe, 2004). A number of studies have shown that the deleterious toxicity of Aβ is due to free radical damage to neurons (Butterfield et al., 2002, Rogers et al., 1996, Tuppo and Arias, 2005). Aβ stimulates microglia to release a large array of toxic factors such as NO, superoxide and tumor necrosis-factor α (TNF-α), and also directly produces reactive oxygen species through interaction with metal ions such as Cu^{+} and Fe^{2+} (Block et al., 2007, Medeiros et al., 2007, Wilkinson and Landreth, 2006, Jomova et al., 2010). Because of abundant lipid content and small amount of antioxidants in the brain, these free radicals can readily oxidize cellular molecules such as lipids and proteins, possibly leading to neuronal dysfunction and death (Gandhi and Abramov, 2012). According to these findings, many attempts have been made to prevent Aβ-induced neurotoxicity by inhibiting oxidative stress.

Cholinergic dysfunction is suggested as one of the key pathogenesis contributing to the cognitive decline observed in AD patients. Acetylcholine (ACh) is an important neurotransmitter mediating fundamental cognitive processes, such as learning and memory (Sarter and Parikh, 2005). However, in the brain of AD, reduced choline

uptake, ACh synthesis and loss of cholinergic neurons have been found, and which appeared to correlate with loss of cognitive function (Francis et al., 1999, Terry and Buccafusco, 2003). This finding has given rise to present therapeutic strategies aimed to compensate for cholinergic deficits, especially by inhibition of AChE. Current drugs, such as donepezil, rivastigmine, and galantamine, belong to this category. These drugs have been reported to improve cognitive function in patients with AD (Rogers et al., 1998, Rosler et al., 1999, Tariot et al., 2000), but they often cause adverse side-effects and are ineffective at preventing the progression of AD (Benzi and Moretti, 1998). Therefore, there is a need for the development of safer and more effective therapeutic approaches.

In this study, we established the amnesia animal models associated with AD using $A\beta_{25-35}$ peptide and scopolamine, and investigated whether HX106N has an anti-amnesic effect in these models. Both the Y-maze and passive avoidance tests were used to evaluate memory function of mice. Effect of HX106N on inflammation and oxidative stress induced by $A\beta_{25-35}$ in brain, was examined using measurement of lipid peroxidation and RNA level of inflammatory and antioxidant genes. Moreover, AChE activity in hippocampus and cortex of mice treated with HX106N was analyzed. Here, we show that HX106N has great potential for prevention and/or treatment of AD.

2. Results

2.1 Establishment of $A\beta_{25-35}$ peptide-induced amnesia mouse model

To establish a mouse model of AD-type amnesia, aggregated $A\beta_{25-35}$ peptide was intracerebroventricularly (i.c.v) administrated into mouse brain. This acute injection of Aβ has frequently been used as an animal model of AD to evaluate the anti-amnesic

effects of various reagents (Yamada and Nabeshima, 2000). $A\beta_{25-35}$ is a core fragment containing essential residues for the aggregation and toxicity of full-length Aβ peptide. According to a previous study, neurotoxicity was occurred at 6 days after an acute treatment of $A\beta_{25-35}$ (Lockhart et al., 1994). Therefore, after 7 days $A\beta_{25-35}$ injection, its effects on memory function were examined in mice. A Y-maze or passive avoidance tests were used for the evaluation of spatial working memory or long-term memory performance, respectively (Maurice et al., 1996). To determine a suitable concentration of $A\beta_{25-35}$ with significant toxicity, mice were exposed to two different concentrations of $A\beta_{25-35}$.

Effects of $A\beta_{25-35}$ on the performances in Y-maze and passive avoidance tests

Mice were administered with vehicle (distilled water; DW) or 5 or 10 nmol of aggregated $A\beta_{25-35}$ by i.c.v. injection, and subjected to the Y-maze test and passive avoidance test, at 7 and 8 days after the injection, respectively, together with untreated naïve mice. In the Y-maze test, there was no significant difference of alternation behavior between naïve and vehicle-injected mice, indicating that vehicle injection did not affect working memory function (Figure 10A). However, $A\beta_{25-35}$ injection decreased the alternation behavior of mice in a dose-dependent manner. These data suggested that $A\beta_{25-35}$ injection into the brain could induce memory impairment in mice.

In the passive avoidance test, mice injected with vehicle showed no significant change in the latency time of passive avoidance compared to naïve mice, while it was significantly decreased by 10 nmol of $A\beta_{25-35}$ injection (Figure 10B). On the basis of this result, 10 nmol was used in subsequent experiments.

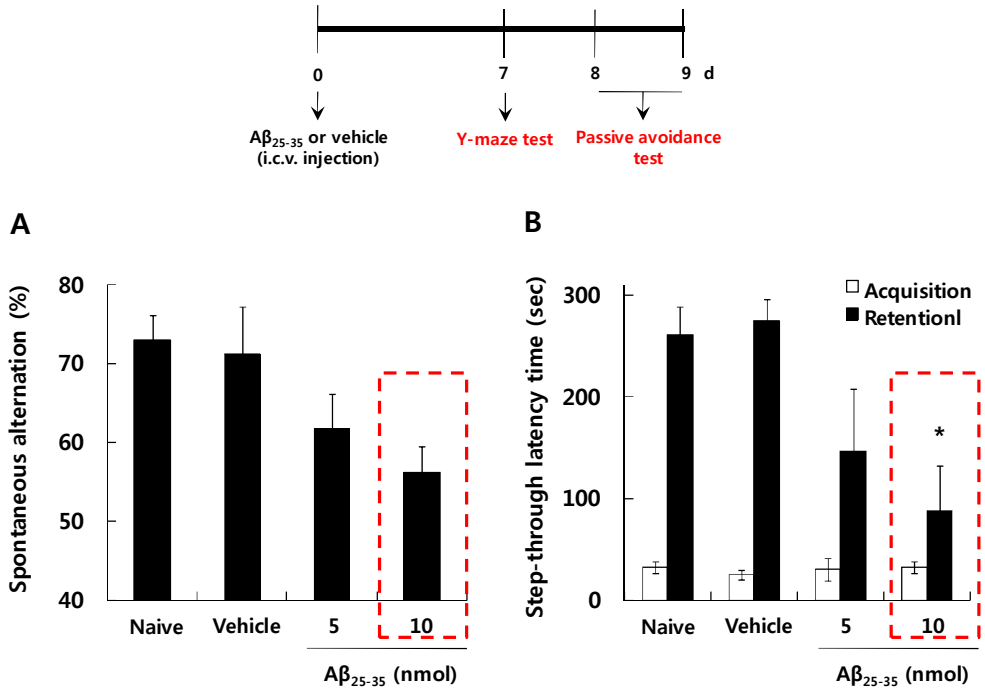

Figure 10. Effects of Aβ$_{25-35}$ on performance in the Y-maze and passive avoidance tests. Aβ$_{25-35}$ (5 or 10 nmol) or the same volume of sterile DW (vehicle) was delivered to the brain of mice by i.c.v. injection. (A) The Y-maze test was performed on day 7. (B) The acquisition and retention trials of the passive avoidance test were conducted on day 8 and 9, respectively. The data are presented as the mean ± SEM (n = 6). *$P < 0.05$ vs. the vehicle-injected control group

Effects of $A\beta_{25-35}$ on the expression of synaptophysin in the hippocampus

Biochemical analysis on various markers affected by $A\beta_{25-35}$ peptide, was done. Synaptic dysfunction induced by Aβ plays a critical role in memory impairment in AD (Hardy and Selkoe, 2002). To investigate whether there is any change in synaptic function in this particular model, the level of synaptophysin, a key protein for presynaptic function, was measured (Sze et al., 1997). After the last behavior test, mice were sacrificed, and the hippocampus tissue was isolated. Total proteins were prepared followed by Western blot analysis, using a specific antibody for synaptophysin. As shown in Figure 11A and 11B, $A\beta_{25-35}$ injection had no significant effect on the protein level of synaptophysin in the hippocampus.

Effects of $A\beta_{25-35}$ on lipid peroxidation and inflammatory response in the hippocampus

Because it is reported that oxidative stress plays an important role in Aβ-induced neurotoxicity (Butterfield et al., 2002), the level of oxidative damage was examined by measuring the level of TBARS (thiobarbituric acid-reactive substances), a lipid peroxidation marker, in the hippocampal tissue. The level of TBARS in the hippocampus of $A\beta_{25-35}$-injected mice was increased by 1.9-fold compared to that of the control mice (Figure 12A), indicating that $A\beta_{25-35}$ injection could induce oxidative stress.

Inflammatory cytokines, such as TNF-α and IL-1β, have been reported to mediate the deleterious effects of Aβ, including the inhibition of long-term potentiation (LTP) and production of free radicals (Medeiros et al., 2007, Minogue et al., 2003, Wang et al., 2005). The expression levels of TNF-α and IL-1β in the hippocampus were measured at different time points, after $A\beta_{25-35}$ injection. The RNA levels of TNF-α and

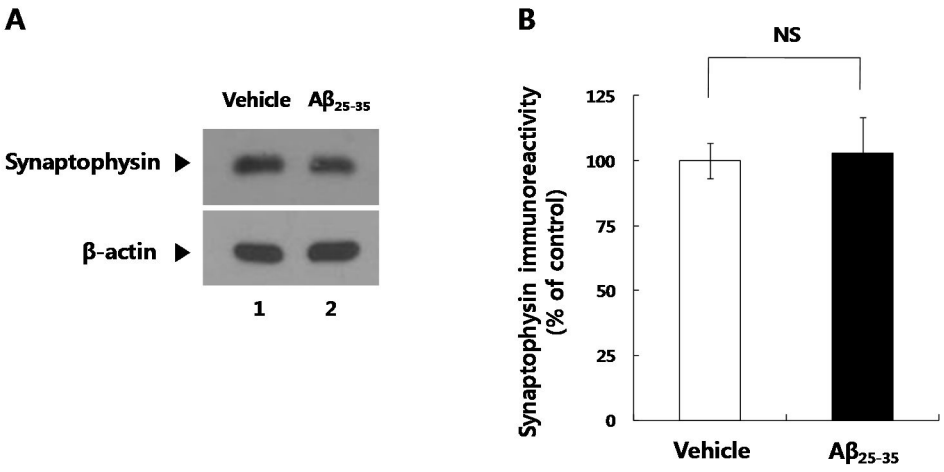

Figure 11. Effects of $A\beta_{25-35}$ on the protein level of synaptophysin in the hippocampus. (A) Mice were sacrificed after the passive avoidance test. The hippocampus was isolated to determine the protein level of synaptophysin by Western blot analysis. β-actin was used as a loading control. (B) The density of immunoreactive bands was measured using NIH ImageJ software program. The data are presented as the mean ± SEM (n = 4).

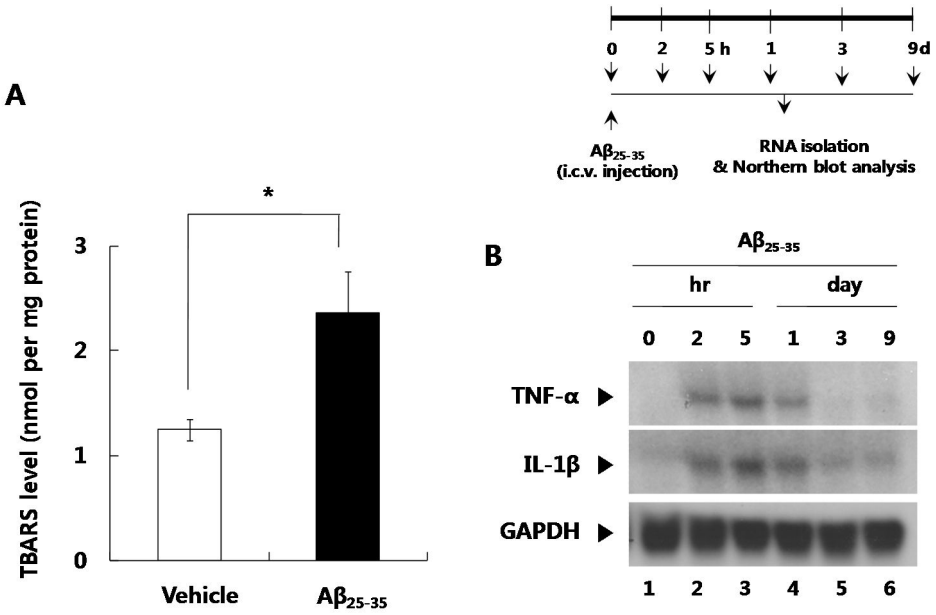

Figure 12. Effects of $A\beta_{25-35}$ on the lipid peroxidation and inflammatory response in the hippocampus of mice. (A) The level of lipid peroxidation in the hippocampus of mice treated with $A\beta_{25-35}$ or vehicle was determined, using TBARS as a marker. The data are presented as the mean ± SEM (n = 4–5). *$P < 0.05$ vs. the vehicle-injected control group. (B) Mice were sacrificed, and the hippocampal tissue was isolated at indicated time points after injection of $A\beta_{25-35}$ peptide. The RNA levels of TNF-α and IL-1β were measured by Northern blot analysis. GAPDH was used as a loading control.

IL-1β were elevated 2 h after $A\beta_{25-35}$ injection, remained high on day 1, and returned to the baseline level by day 3 (Figure 12B). These data showed that neuroinflammation occurred after injection of $A\beta_{25-35}$.

2.2 Effects of HX106N on memory deficits and oxidative stress in $A\beta_{25-35}$-injected mice

Effects of HX106N on Y-maze spontaneous alternation in Aβ25-35-injected mice

The effect of HX106N on working memory was examined using a Y-maze spontaneous alternation test in $A\beta_{25-35}$-injected mice. Mice were orally administered three different doses of HX106N (50, 100, or 200 mg/kg body weight) or donepezil (1 mg/kg body weight) on a daily basis from 7 days before to 7 days after $A\beta_{25-35}$ peptide delivery. Control mice were administered distilled water and injected with a vehicle solution. The Y-maze test was performed on day 7. Following the i.c.v. injection of $A\beta_{25-35}$, the alternation behavior of mice was significantly decreased, indicating that $A\beta_{25-35}$ impaired their working memory (Figure 13A). Treatment with HX106N inhibited the alternation behavior impairment in a dose-dependent manner (Figure 13A). The effect of HX106N at 200 mg/kg was comparable to that of donepezil. Based on this result, HX106N at 200 mg/kg was used for subsequent experiments. The total number of entries into the three arms was similar among the groups, suggesting that neither HX106N nor donepezil affected locomotor activity (Figure 13B).

Effects of HX106N on performance of passive avoidance test in Aβ25-35-injected mice

To evaluate the effect of HX106N on the long-term memory impairment

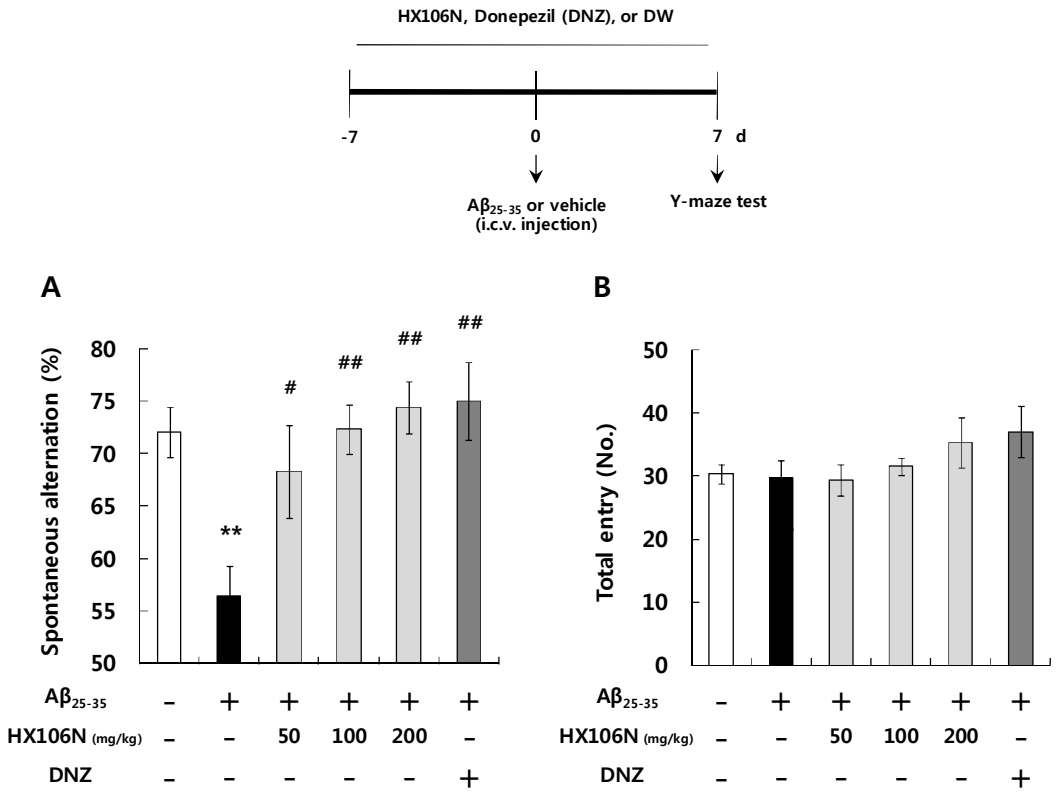

Figure 13. Effects of HX106N on impairment of working memory induced by $A\beta_{25-35}$ in the Y-maze test. Mice were orally treated with HX106N (50, 100 or 200 mg/kg body weight) or donepezil (1 mg/kg body weight) once a day from day -7 to day 7. Amnesia was induced by an i.c.v. injection of $A\beta_{25-35}$ peptides on day 0, and mice were examined for spontaneous alternation behavior in the Y-maze test on day 7. (A) Spontaneous alternation behavior was examined as an index of working memory using the Y-maze test on day 7. (B) The total number of arm entries was measured as an indicator of locomotor activity. The data are presented as the mean ± SEM (n = 10-11). $^{**}P < 0.01$ vs. the vehicle-injected, DW-treated control group; $\#P < 0.05$, $\#\#P < 0.01$ vs. the $A\beta_{25-35}$-injected, DW-treated group. DNZ, donepezil.

induced by $A\beta_{25-35}$, the mice were subjected to an acquisition trial of the step-through passive avoidance test on day 8. One day later, the step-through latency was measured as an index of long-term memory in a retention trial. The step-through latency time was significantly lower in the $A\beta_{25-35}$-injected mice than in the control mice and was dramatically increased following the daily administration of 200 mg/kg HX106N or 1 mg/kg donepezil (Figure 14). The latency times during the acquisition trial were similar across all groups (Figure 14). The effect of HX106N was comparable to that of donepezil. These results demonstrate that HX106N may help ameliorate the memory impairment induced by $A\beta_{25-35}$ in mice.

Effects of HX106N on lipid peroxidation in the hippocampus and cortex of Aβ25-35-injected mice

To investigate whether HX106N had any effect on the oxidative stress induced by an $A\beta_{25-35}$ injection, lipid peroxidation levels were measured in the hippocampus and cortex using a TBARS assay. A 2.7-fold increase of TBARS level was observed in the hippocampus of $A\beta_{25-35}$-injected mice compared to that of the control mice (Figure 15A). This increase was prevented by the oral administration of HX106N or donepezil (Figure 15A). The TBARS production induced by $A\beta_{25-35}$ injection was also inhibited in the cortex of the mice treated with HX106N or donepezil (Figure 15B). These results suggest that the ameliorating effect of HX106N, as observed in the present experiments, might be due to its ability to suppress oxidative stress induced by $A\beta_{25-35}$.

Effects of HX106N on the expression of TNF-α, IL-1β, and HO-1 in the hippocampus of $A\beta_{25-35}$-injected mice

Based on above result of expression pattern of TNF-α and IL-1β RNA after the

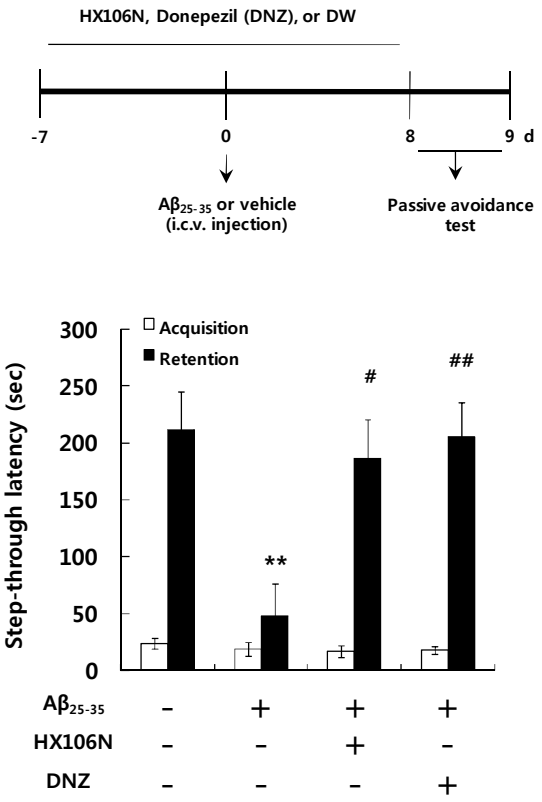

Figure 14. Effects of HX106N on $A\beta_{25-35}$-induced long-term memory impairment in the passive avoidance test. Mice were treated orally with HX106N (200 mg/kg body weight) or donepezil (1 mg/kg body weight) once a day from day -7 to day 8. $A\beta_{25-35}$ peptide was injected into mouse brain on day 0. Mice were trained for the acquisition of passive avoidance response on day 8, and step-through latency was measured in a retention trial 24h after acquisition. The data are presented as the mean ± SEM (n = 10-11). $^{**}P < 0.01$ vs. the vehicle-injected, DW-treated control group; $\#P < 0.05$, $\#\#P < 0.01$ vs. the $A\beta_{25-35}$-injected, DW-treated group. DNZ, donepezil.

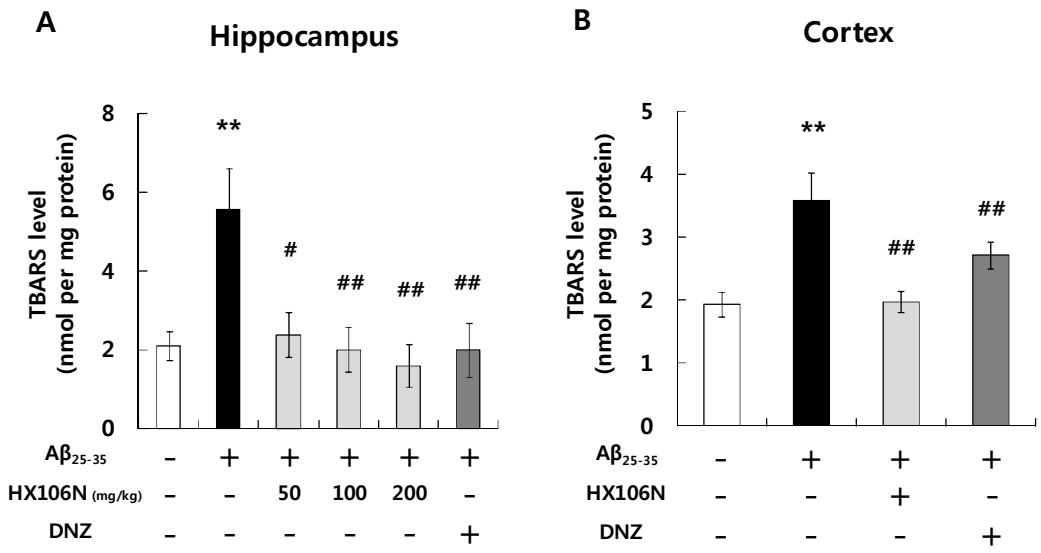

Figure 15. Effects of HX106N on $A\beta_{25-35}$-induced lipid peroxidation in the hippocampus and cortex. Mice were sacrificed on day 9, and levels of lipid peroxidation in the hippocampus (A) and cortex (B) were assessed using the TBARS assay. The data are presented as the mean ± SEM (n = 4–5). $^{**}P < 0.01$ vs. the vehicle-injected, DW-treated control group; $^{\#}P < 0.05$, $^{\#\#}P < 0.01$ vs. the $A\beta_{25-35}$-injected, DW-treated group. DNZ, donepezil.

injection of $A\beta_{25-35}$ peptide, the effect of HX106N on the production of these cytokines was analyzed on day 1. Mice were treated orally with 200 mg/kg HX106N once a day for 7 days and injected with $A\beta_{25-35}$ peptide. One day later, mice were sacrificed, and quantitative RT-PCR was used to measure the hippocampal levels of TNF-α and IL-1β. As shown in Figure 16A and 16B, the RNA levels of TNF-α and IL-1β increased 3.0- and 10.1-fold, respectively, compared to the control mice after $A\beta_{25-35}$ injection. This increase was not attenuated by treatment with HX106N, indicating that HX106N might not have an anti-inflammatory effect in this model (Figure 16A and 16B).

Because of the critical roles of HO-1 in the cellular defense responses against oxidative stress (Ryter et al., 2006), the effect of HX106N on the expression of HO-1 was tested. The time course of the RNA level of HO-1 in the hippocampus of $A\beta_{25-35}$-treated mice is shown in Figure 15C. When $A\beta_{25-35}$ peptide was injected, HO-1 expression increased more than two-fold on day 1 but decreased on day 3, and it remained relatively low on day 9. However, in HX106N-treated mice, the rate of decrease in the level of HO-1 expression was much lower, and on day 9, the RNA level of HO-1 was significantly higher than in the $A\beta_{25-35}$-injected, DW-treated mice (Figure 16C). These data suggest that HX106N may upregulate the expression of HO-1, and the antioxidative effect of HX106N on $A\beta_{25-35}$-induced lipid peroxidation may have resulted from the upregulation of HO-1.

2.3 Effect of HX106N on amnesia in scopolamine-injected mice

Effects of HX106N on Y-maze spontaneous alternation in scopolamine-injected mice

Cognitive decline in patients with AD is known to be correlated with decreased cholinergic neurotransmission (Francis et al., 1999, Terry and Buccafusco, 2003).

Figure 16. Effects of HX106N on the RNA level of TNF-α, IL-1β, and HO-1 in the hippocampus of $A\beta_{25-35}$-injected mice. Mice were orally treated with 200 mg/kg HX106N, on a daily basis from days -7 to 8, and were sacrificed at the indicated time points after $A\beta_{25-35}$ injection on day 0. Total RNA was isolated from the hippocampus of mice, and RNA levels of TNF-α (A), IL-1β (B), and HO-1 (C) were measured by quantitative RT-PCR. The data are presented as the mean ± SEM (n = 5). $^{*}P < 0.05$, $^{**}P < 0.01$ vs. the vehicle-injected, DW-treated control group; $\#P < 0.05$ vs. the $A\beta_{25-35}$-injected, DW-treated group.

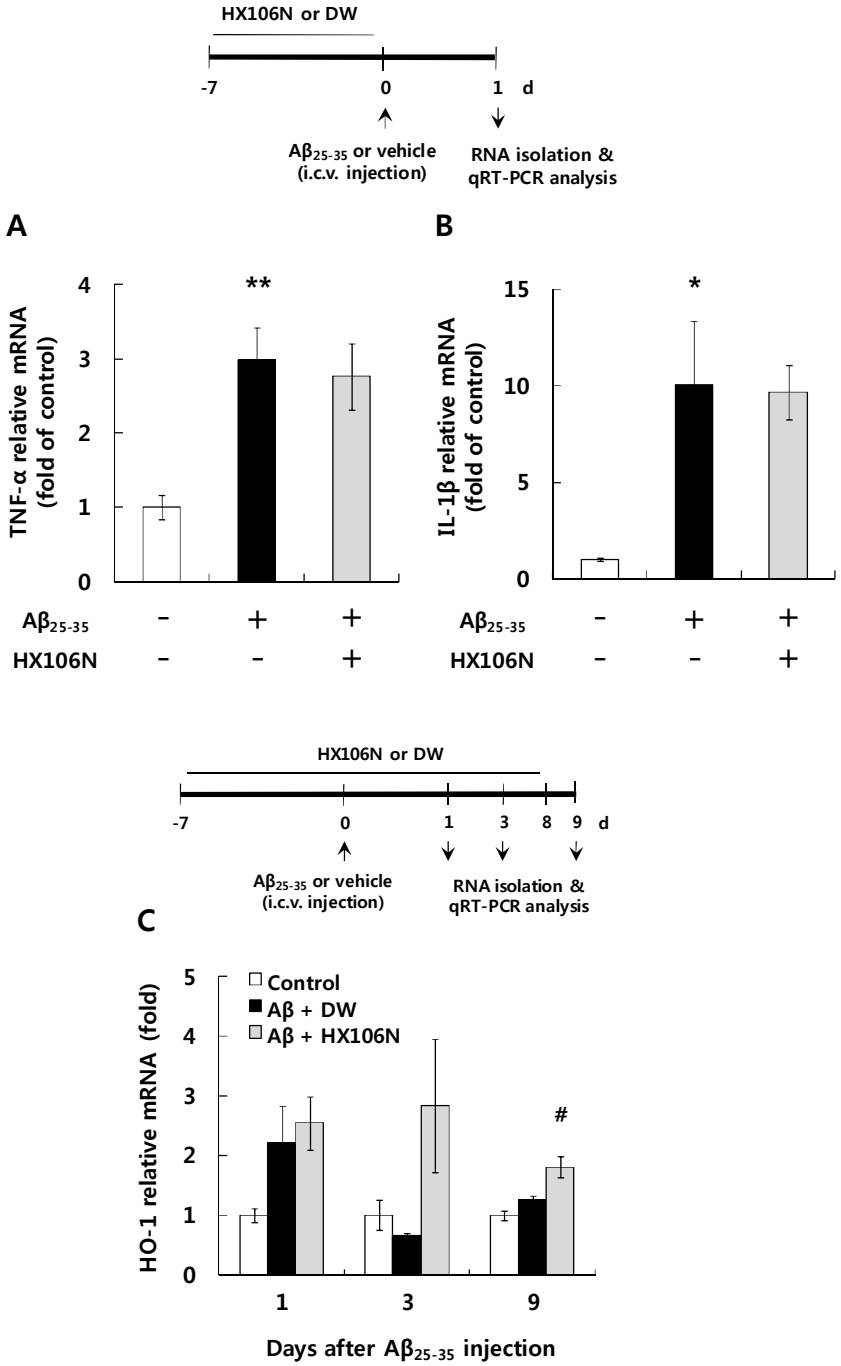
HX106N or DW
-7
0
1 d
Aβ25-35 or vehicle
(i.c.v. injection)
RNA isolation &
qRT-PCR analysis
A
B
TNF-α relative mRNA
(fold of control)
IL-1β relative mRNA
(fold of control)
**
*
Aβ25-35
HX106N
HX106N or DW
-7
0
1
3
8
9 d
Aβ25-35 or vehicle
(i.c.v. injection)
RNA isolation &
qRT-PCR analysis
C
HO-1 relative mRNA (fold)
Control
Aβ + DW
Aβ + HX106N
#
Days after Aβ25-35 injection

Scopolamine-induced amnesia is used as a model for AD because it causes cognitive deficits by blocking cholinergic signaling (Klinkenberg and Blokland, 2010). To examine the effect of HX106N on the memory impairment caused by cholinergic dysfunction, behavioral tests, including the Y-maze and passive avoidance tests, were performed in scopolamine-injected mice. The animals were orally administered with HX106N (100 mg/kg body weight) or donepezil (1 mg/kg body weight) 1 h before an intraperitoneal (i.p.) injection of scopolamine. The Y-maze test was conducted 30 min after the injection. The percentage of spontaneous alternation was significantly lower in scopolamine-injected mice compared to control mice, but this effect was prevented by the oral administration of HX106N (Figure 17A). The administration of donepezil also increased the alternation behavior in scopolamine-injected mice, but not in a statistically significant manner (Figure 17A). No difference was observed in the total number of entries between the groups (Figure 17B). These data showed that HX106 could improve scopolamine-induced impairment of working memory in this model.

Effects of HX106N on performance of passive avoidance test in scopolamine-injected mice

The effect of HX106N on passive avoidance was investigated in scopolamine-injected mice. The animals were trained for the passive avoidance test 30 min after the injection of scopolamine. One day later, step-through latency was measured as an index of long-term memory in the retention trial. Scopolamine-injected mice showed significantly decreased latency times in the retention trial compared to control mice (Figure 18). However, a significant increase in step-through latency was observed when the mice were treated with HX106N (100 mg/kg body weight) 1 h before the injection of scopolamine, and this effect was comparable to that of donepezil (Figure 18).

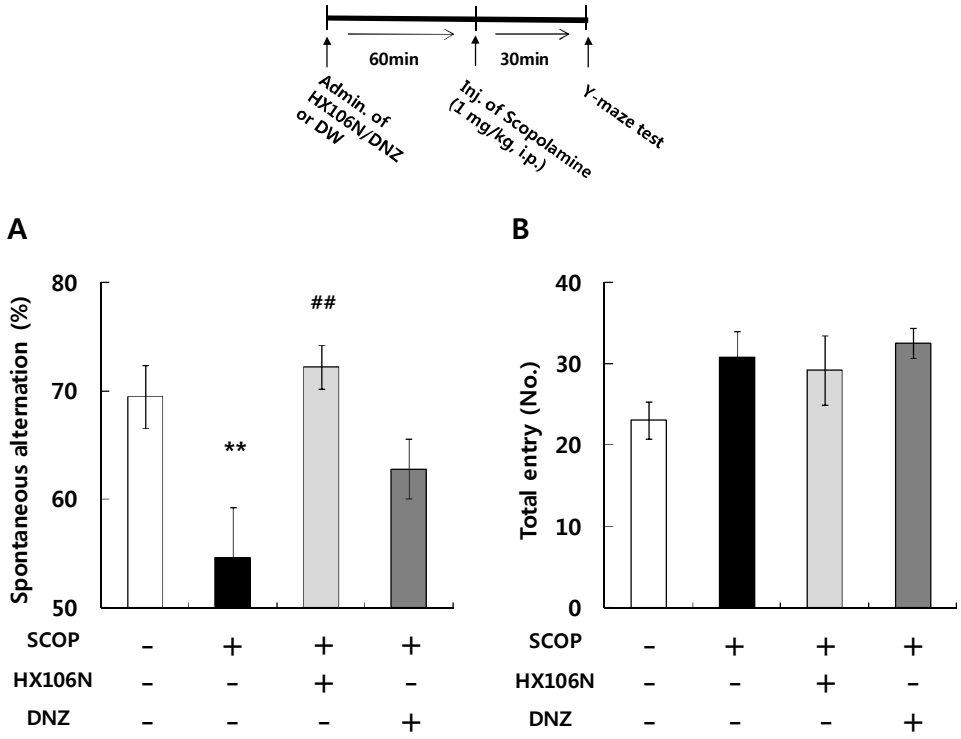

Figure 17. The effects of HX106N on scopolamine-induced working memory impairment in the Y-maze test. Mice were orally treated with HX106N (100 mg/kg body weight) or donepezil (1 mg/kg body weight) 90 min before the test. Memory impairment was induced by the i.p. injection of scopolamine. After 30 min, mice were subjected to the Y-maze test. The percentages of spontaneous alternation (A) and number of total entry (B) are shown as indicated. The data are presented as the mean ± SEM (n = 7-8). $^{**}P < 0.01$ vs. the PBS-injected, DW-treated control group; $^{\#\#}P < 0.01$ vs. the scopolamine-injected, DW-treated group. DNZ, donepezil.

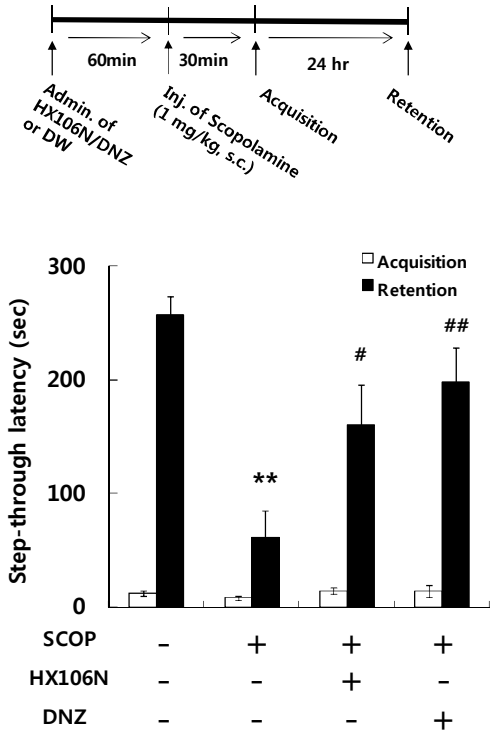

Figure 18. The effects of HX106N on long-term memory impairment induced by scopolamine in the passive avoidance test. Scopolamine was delivered to mice by an i.p. injection, one hour after oral administration of HX106N (100 mg/kg body weight) or donepezil (1 mg/kg body weight). Thirty minutes later, mice were subjected to the acquisition trial of step-through passive avoidance test, and retention trial was performed 24 h after the acquisition. The data are presented as the mean ± SEM (n = 8-10). $^{**}P < 0.01$ vs. the PBS-injected, DW-treated control group; $^{\#}P < 0.05$, $^{\#\#}P < 0.01$ vs. the scopolamine-injected, DW-treated group. DNZ, donepezil.

These results demonstrated that HX106N can attenuate the long-term memory deficit induced by scopolamine in the mouse.

Effects of HX106N on AChE acitivity

Enhancing cholinergic neurotransmission by inhibiting AChE activity is a major strategy for improving cognitive function in patients with AD (Hirai, 2000). To examine whether AChE activity was affected by treatment with HX106N, AChE activity in the hippocampus and cortex of mice was measured 1 h after the oral administration of HX106N (100 mg/kg body weight). HX106N inhibited AChE activity by 42.5% ± 3.1% in the hippocampus and by 47.5% ± 6.3% in the cortex compared to control mice, respectively (Figure 19A). The AChE inhibitor donepezil also decreased AChE activity (Figure 19A). These results suggest that HX106N might improve scopolamine-induced cholinergic amnesia by inhibiting AChE activity in mice.

The level of AChE activity in hippocampal tissue was also measured 6 h after oral administration of HX106N or donepezil. As shown in Figure 19B, HX106N treatment reduced AChE activity in a dose-dependent manner. A significant decrease was observed in 25 mg/kg of HX106N-treated group, and the magnitude of this reduction was comparable to that of donepezil-treated group (Figure 19B). These data indicated that AChE inhibitory activity of HX106N was dose-dependent and was maintained up to 6 h after administration.

3. Discussion

In this study, the anti-amnesic effects of HX106N were tested in two different mouse models of AD-type amnesia through the acute injection of $A\beta_{25-35}$ peptide or

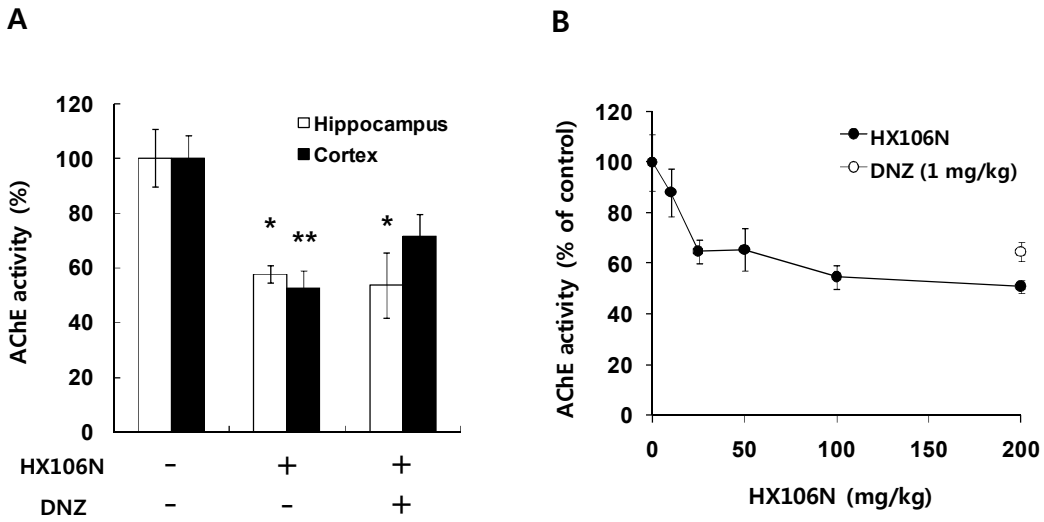

Figure 19. The effects of HX106N on AChE activity. (A) Mice were orally treated with HX106N (100 mg/kg body weight) or donepezil (1 mg/kg body weight). After 1 h, the hippocampus and cortex were isolated, total proteins were prepared, and AChE activity was measured. The data are presented as the mean ± SEM (n = 3). **P* < 0.05, ***P* < 0.01 vs. the DW-treated, control group. (B) Mice were administrated with various concentrations of HX106N or 1 mg/kg donepezil. 6 h later, the mice were sacrificed and the hippocampal tissue was examined to evaluate AChE activity. The data are presented as the mean ± SEM (n = 3). DNZ, donepezil.

scopolamine. In $A\beta_{25-35}$-injected mice, oral administration of HX106N significantly improved memory deficits in the Y-maze alternation and passive avoidance tests, which coincided with a marked reduction in the level of TBARS, an indicator for lipid peroxidation, in the hippocampus and cortex.

Elevated level of HO-1 expression was found to correlate with oxidative damage in many neurodegenerative diseases, including AD (Schipper et al., 1995), and the increase of HO-1 are believed to be a part of cellular defense mechanisms to protect neurons against various oxidative stimuli (Chen et al., 2000, Le et al., 1999). In our experiment, $A\beta_{25-35}$ injection itself briefly and transiently increased the level of HO-1 expression, while treatment with HX106N appears to maintain the increased level of HO-1 for a relatively long time, which might provide a protective effect against $A\beta_{25-35}$-induced oxidative damage.

The cholinergic amnesia induced by scopolamine was also rescued by HX106N. The level of AChE activity was significantly reduced in the hippocampus and cortex of mice treated with HX106N. A significant decrease of AChE acitivty was observed at one hour after HX106N administration. This finding suggested that the presence of some compound(s) in HX106N would be able to rapidly penetrate into the brain and exert an AChE inhibitory effect. This possibility is also supported by the fact that many compounds containing AChE inhibitory activity, such as physostigmine, have been identified from plant sources (Mukherjee et al., 2007). Further studies to identify compound(s) responsible for the AChE inhibitory effects of HX106N are warranted.

Amnesia caused by Aβ toxicity has been reported to be associated with the damage in cholinergic neuron that can be improved by enhancement of cholinergic neurotransmission through the inhibition of AChE activity (Maurice et al., 1996, Tran et al., 2002). Based on our data it can be thought that the improvement of memory

functions in $A\beta_{25-35}$-injected mice might be the result of AChE inhibitory activity of HX106N.

The safety of the plants used for the preparation of HX106N has been established through a long history of human use (Park and Lee, 2000, Kang et al., 2000). Indeed, no toxic effects of HX106N have been observed in acute or repeated-dose toxicity studies involving rats and dogs (unpublished data). Taken together, our results demonstrate that HX106N has the potential to act as a preventive and/or therapeutic agent for AD.

CHAPTER V

Antioxidative Effects of HX106N in Microglia and Neuronal Cells

1. Background

The generation of free radicals is a common outcome of normal aerobic cellular metabolism, and their level is regulated by endogenous antioxidant enzyme system. However, exposure to various oxidants or imbalanced antioxidant defense can cause overproduction of free radicals, damaging biomolecules including lipids, proteins and nucleotides and eventually lead to serious medical problems (Uttara et al., 2009). The brain is particularly vulnerable to oxidative stress due to its high consumption of oxygen, abundance of highly peroxidisable lipids, and low expression of antioxidant enzymes (Gandhi and Abramov, 2012). There are growing evidences indicating that oxidative stress plays a key role in the pathogenesis of neurodegenerative diseases, including AD.

A variety of cellular and molecular factors have been reported as direct or indirect mediators of oxidative stress (Figure 20). Microglia, resident innate immune cells in the central nervous system, is one of them. Under pathological conditions, microglia is known to be activated and induce oxidative damage through excessive production of various neurotoxic factors, such as inflammatory cytokines, NO, superoxide, and prostaglandins (Liu and Hong, 2003). In particular, NO appears to play a critical role in microglia-mediated neurotoxicity. Neuron is highly sensitive to NO because NO can generate free radicals and also induce release of glutamate from both astrocytes and neurons, resulting in glutamate-mediated neurotoxicity (Brown and Bal-Price, 2003).

Glutamate has been known to be a direct neurotoxin. It is the most abundant neurotransmitter in the brain, mediating excitatory signals. However, large amounts of glutamate can induce neurotoxicity through two different mechanisms. (Brown and Bal-Price, 2003). One of them is oxidative glutamate neurotoxicity, a process called oxytosis.

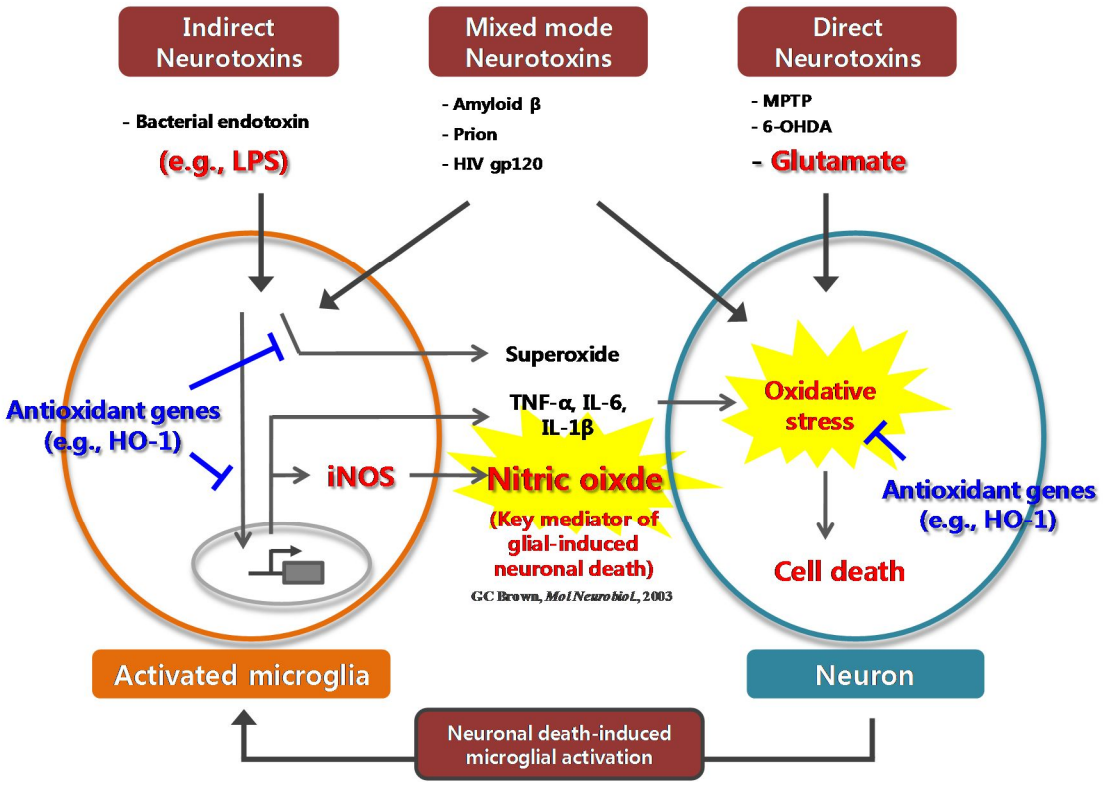

Figure 20. Overview of oxidative neurotoxins associated with neurodegenerative diseases. Adopted and modified from a review of (Liu and Hong, 2003).

In this case, excessive extracellular glutamate inhibits the uptake of cystine by blocking the activity of cystine/glutamate antiporter. Because cysitine is a rate-limiting amino acid for glutathione (GSH) synthesis, which is a major antioxidant in neuron, the reduced level of this amino acid can cause depletion of GSH, consequently leading to oxidative stress and cell death (Tan et al., 2001, Murphy et al., 1989).

During evolution, mammalian cells have developed various antioxidant defense mechanisms to counter the cellular damage caused by free radicals (Ho et al., 1998). HO-1 has recently been implicated as a key antioxidant enzyme in cellular defense responses in the central nervous system. Its expression is rapidly induced by various oxidative stimuli and it confers the anti-inflammatory and antioxidative activities by itself or through its enzymatic byproducts, such as biliverdin, carbon monoxide (CO), and ferrous iron (Stocker et al., 1987, Dore et al., 1999, Otterbein et al., 2000, Balla et al., 1992, Choi et al., 2013). In the nervous system, the neuroprotective role of HO-1 has been well documented. Transgenic mice that overexpress HO-1 in the brain are resistant to ischemic brain damage (Panahian et al., 1999), and HO-1 overexpression protects neurons from various oxidative stimuli, such as glutamate and hydrogen peroxide (Chen et al., 2000, Le et al., 1999).

In the present study, I investigated the antioxidative effects of HX106N in microglia and neurons. In BV-2 cells, a murine microglia cell line, and primary microglia, HX106N suppressed LPS-induced production of NO and iNOS by regulating the level of iNOS RNA at the post-transcriptional level. The expression of HO-1 was found to be increased by HX106N, which contributed to HX106N-inhibited NO production. In primary cortical neurons and HT22 cells, a murine hippocampal neuronal cell line, HX106N inhibited glutamate-induced neuronal cell death and ROS production. I found that the neuroprotective effect of HX106N was not associated with HX106N-

mediated expression of Nuclear factor E2-related factor 2 (Nrf2)-dependent antioxidant genes, including HO-1, suggesting that HX106N might not use HO-1 to exert its neuroprotective activity.

2. Results

2.1 Effects of HX106N on LPS-induced inflammatory mediator productions in BV-2 cells

A variety of inflammatory and neurotoxic factors secreted by activated microglia are believed to play a critical role in neurodegeneration (Liu and Hong, 2003). I investigated the effects of HX106N on the production of microglia-derived inflammatory mediators, including TNF-α, IL-6 and NO, using BV-2 cells. BV-2 cells were treated with 100 ng/mL LPS and various concentrations of HX106N for 24 h, and the culture supernatants were analyzed for the level of TNF-α, IL-6 and nitrite. The basal levels of TNF-α, IL-6 and nitrite were very low or undetectable, but LPS markedly increased their levels to 2.9 nM, 13.9 nM and 14.7 μM, respectively. When cells were treated with HX106N, no significant change was observed in the level of TNF-α and IL-6 (Figure 21A and 21B), while the nitrite level was reduced in a dose-dependent manner (Figure 21C). The IC_{50} value of HX106N for NO was 0.4 mg/mL. These results suggested that HX106N could inhibit the production of nitrite, but not that of TNF-α and IL-6.

2.2 Effects of HX106N on the expression of iNOS in LPS-stimulated BV-2 cells

iNOS is a key enzyme to produce continuously high level of NO in activated microglia (Brown and Bal-Price, 2003). To test the effect of HX106N on the expression of iNOS,

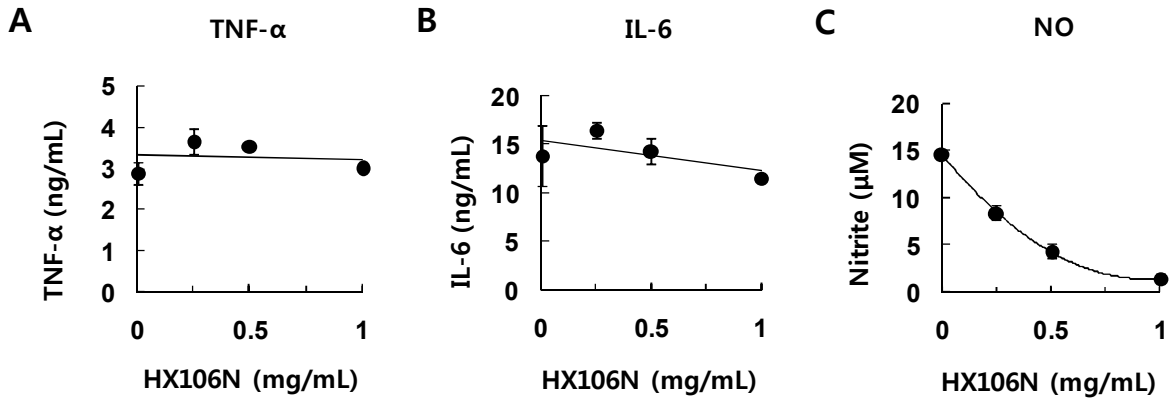

Figure 21. Effects of HX106N on the production of inflammatory mediators in LPS-stimulated BV-2 cells. BV-2 cells were treated for 24 h with 100 ng/mL LPS and various concentrations of HX106N and the culture supernatant was harvested. The level of TNF-α and IL-6 was measured using the ELISA kits (A and B), and that of NO was determined by a Griess assay (C). The values are presented as the means ± SD of triplicate samples from a representative experiment.

BV-2 cells were treated with 100 ng/mL LPS and various concentrations of HX106N for 24 h, and the total proteins were extracted, followed by Western blot analysis using a specific antibody for iNOS. The iNOS protein was not detectable in normal BV-2 cells, but when the cells were stimulated with LPS for 24 h, the protein level of iNOS increased by approximately 7-fold compared to the controls (Figure 22A). The elevated level of iNOS was dose-dependently reduced to basal levels by 1 mg/mL of HX106N (Figure 22A).

To determine at what level HX106N regulates iNOS expression, Northern blot analysis was performed. The LPS-mediated increase in iNOS RNA level was inhibited by HX106N in a dose-dependent manner (Figure 22B). These results indicated that HX106N inhibited the LPS-induced production of NO by controlling iNOS expression at the RNA level.

2.3 Effects of HX106N on iNOS transcription in LPS-stimulated BV-2 cells

Expression of iNOS is mainly regulated at the transcription level (Aktan, 2004). To investigate whether HX106N regulates iNOS transcription, its effects on the iNOS promoter were examined using a luciferase reporter plasmid, piNOS-Luc, containing the murine 1.7 kb full-length iNOS promoter sequence. BV-2 cells were transfected with piNOS-Luc and treated with LPS (100 ng/mL) and HX106N (1 mg/mL). After 24 h, whole cell lysates were prepared and subjected to a luciferase assay. Stimulation with LPS caused a 7.9-fold increase in luciferase activity, and this increase was not affected by HX106N (Figure 23A). These data indicated that HX106N might not regulate iNOS gene expression at the transcription level.

Effects of HX106N on AP-1 and NF-κB, key transcription factors responsible for iNOS transcription, were examined by EMSA. The amount of DNA-protein

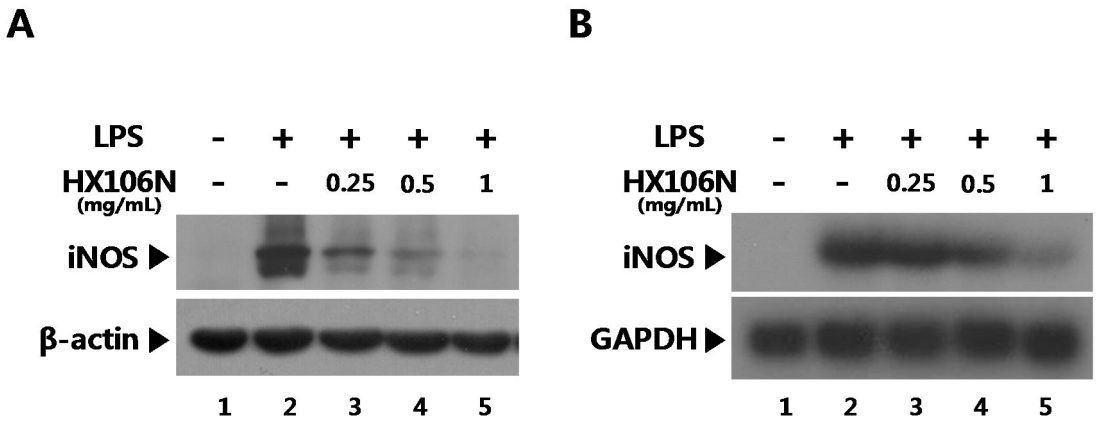

Figure 22. Effects of HX106N on the expression of iNOS in LPS-stimulated BV-2 cells. (A) BV-2 cells were treated with 100 ng/mL LPS and various concentration of HX106N. Twenty-four hours later, whole cell lysates were prepared, followed by Western blot analysis for iNOS. β-actin was used as a loading control. (B) BV-2 cells were treated for 12 h with 100 ng/mL LPS and various concentrations of HX106N. Total RNA was extracted and analyzed for iNOS and GAPDH mRNA expression by Northern bolt hybridization. GAPDH was used as a loading control.

complexes for AP-1 and NF-κB was highly increased by LPS stimulation (Figure 23B and 23C). These DNA–protein complexes were specific because they were effectively competed by unlabeled cold oligonucleotides, but not by mutant sequences. HX106N did not decrease the amount of DNA-protein complex for both AP-1 and NF-κB (Figure 23B and 23C). These results again suggested that HX106N might not control the transcription of iNOS.

2.4 Effects of HX106N on RNA level of iNOS at the post-transcriptional stage

Because it has been reported that the RNA expression of iNOS can be regulated at the post-transcriptional level (Korhonen et al., 2001, Vodovotz et al., 1993, Geng and Lotz, 1995), it was examined whether HX106N affected the stability of iNOS RNA. BV-2 cells were stimulated with 100 ng/mL LPS, and 12 h later, it was removed from the media, and then 1 μg/mL actinomycin D (ActD) was added to stop further transcription. In the presence of 1 mg/mL HX106N, the kinetics of iNOS RNA expression was not significantly different from that of the control (Figure 24B). These results indicated that HX106N might not directly affect the stability of iNOS RNA.

To investigate whether *de novo* protein synthesis is required for HX106N-mediated suppression of iNOS RNA expression, BV-2 cells were treated with LPS and HX106N in the presence or absence of 1 μM cyclohexamide (CHX) for 12 h. Total RNAs were prepared and subjected to Northern blot analysis to determine the level of iNOS RNA. As shown in Figure 24C, the suppression of iNOS RNA expression by HX106N was dramatically attenuated in the presence of CHX, suggesting that HX106N might induce the synthesis of new protein(s) that can regulate the level of iNOS RNA.

Figure 23. Effects of HX106N on the transcription of iNOS. (A) BV-2 cells were transfected with a reporter plasmid containing the 1.7 Kb full-length mouse iNOS promoter using FuGene6 reagent. Cells were stimulated with 100 ng/mL LPS in the presence or absence of 1 mg/mL HX106N for 24 h, and whole cell lysates were prepared followed by a luciferase assay. The values are presented as the means ± SD of triplicate samples from a representative experiment. NS = non-significant compared to the LPS-treated group. (B and C) BV-2 cells were treated with 100 ng/mL LPS and 1 mg/mL HX106N for 6 h, and nuclear extracts were prepared. EMSA was performed using [^{32}P]-labeled nucleotide sequences for AP-1 (B) or NF-κB (C). Competition analysis was carried out to demonstrate the specificity of the DNA-protein complex, using unlabeled cold or mutant-type (MT) oligonucleotides.

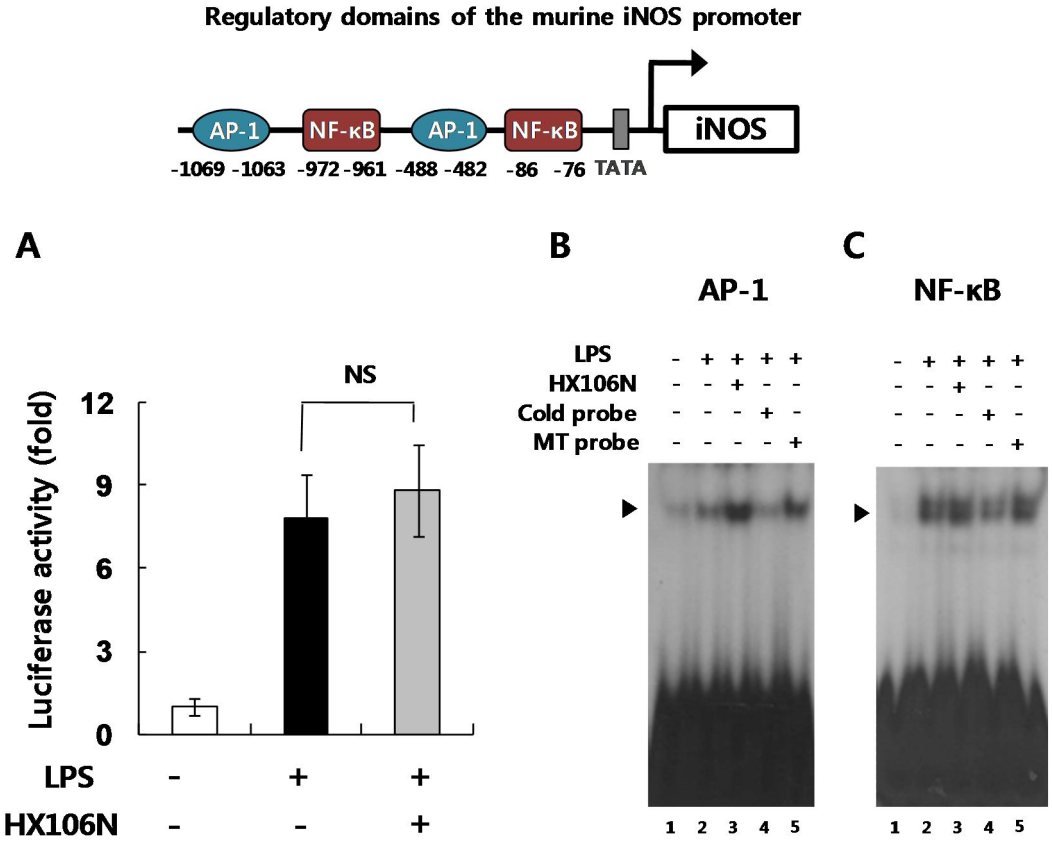
Regulatory domains of the murine iNOS promoter
AP-1
NF-κB
AP-1
NF-κB
iNOS
-1069 -1063 -972 -961 -488 -482 -86 -76 TATA
A
B
C
AP-1
NF-κB
Luciferase activity (fold)
12
9
6
3
0
NS
LPS - + +
HX106N - - +
LPS - + + + +
HX106N - - + - -
Cold probe - - - + -
MT probe - - - - +
1 2 3 4 5
1 2 3 4 5

Figure 24. Effects of HX106N on the leve of iNOS RNA at the post-transcriptional stage. (A) Potential mechanisms of HX106N-mediated regulation of iNOS RNA level. (B) BV-2 cells were pretreated with 100 ng/mL LPS for 12 h, and washed with PBS to remove LPS. Cells were treated with 1 μg/mL actinomycin D (ActD) in the presence or absence of 1 mg/mL HX106N at the indicated time points, and the total RNA was isolated. The RNA level of iNOS was determined by Northern blot analysis. GAPDH was used as a loading control. (C) BV-2 cells were treated with 100 ng/mL and 1 mg/mL HX106N in the presence or absence of 1 μM cycloheximide (CHX). After 12 h, the total RNAs were prepared followed by Northern blot analysis.

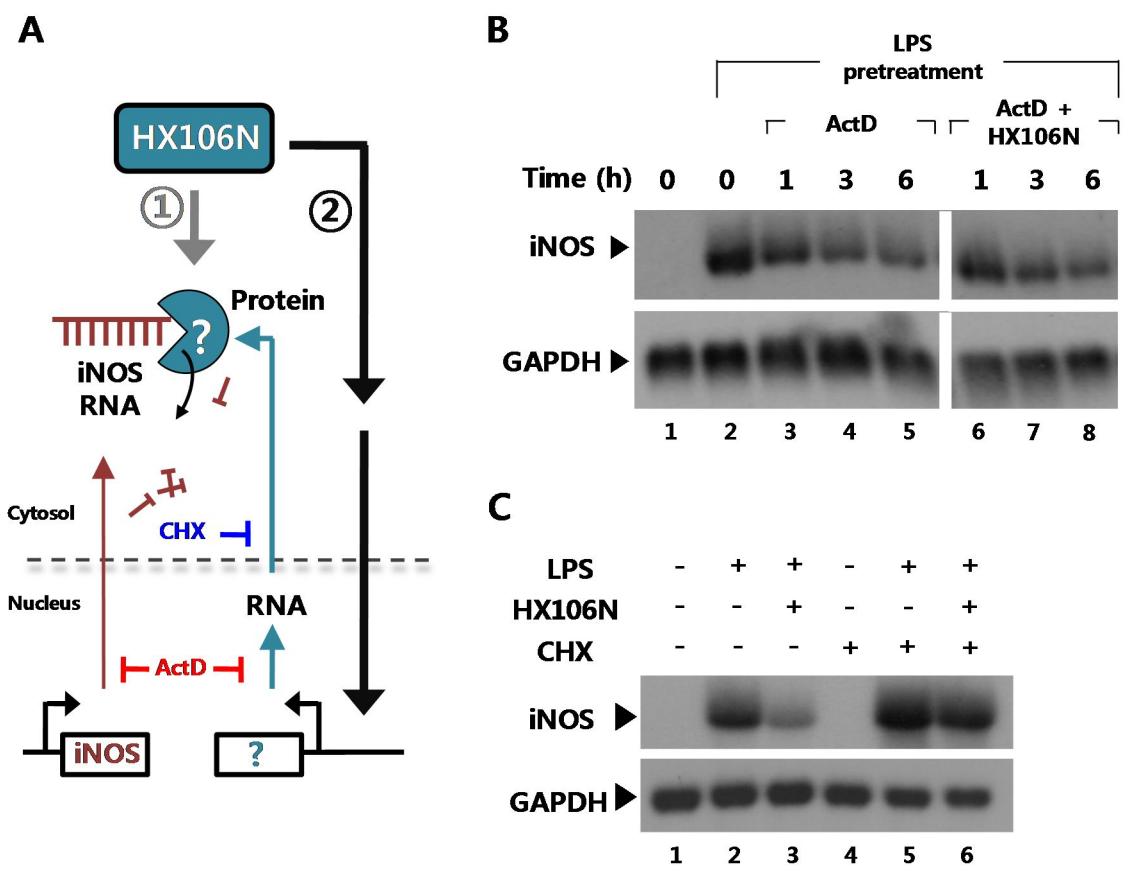
A
HX106N
①
②
Protein
?
iNOS
RNA
Cytosol
CHX
Nucleus
RNA
ActD
iNOS
?
B
LPS
pretreatment
ActD
ActD +
HX106N
Time (h) 0 0 1 3 6 1 3 6
iNOS
GAPDH
1 2 3 4 5 6 7 8
C
LPS - + + - + +
HX106N - - + - - +
CHX - - - + + +
iNOS
GAPDH
1 2 3 4 5 6

2.5 Effects of HX106N on HO-1 expression

Because it is well-established that HO-1 plays a key role in the control of NO production in many cell types (Tsoyi et al., 2008, Vareille et al., 2008), I investigated whether HX106N has any effect on HO-1 expression. BV-2 cells were treated with 1 mg/mL HX106N for various time periods, and whole cell lysates were prepared for the detection of HO-1 by Western blot analysis. The amount of HO-1 protein increased 6 h after treatment with HX106N, remained at a high level for 24 h, and then returned to the basal level after 48 h (Figure 25A). The effect on HO-1 was dose-dependent, as shown in Figure 25B. When the cells were treated with HX106N at a 1 mg/mL concentration for 24 h, the protein level of HO-1 was increased 11-fold (Figure 25B). To test whether this result was restricted to a particular cell type, primary microglia were isolated from the cortex of P1-P2 mice and treated with 1 mg/mL HX106N for 24 h. When measured by Western blot analysis, treatment with HX106N increased HO-1 expression 3-fold compared to the control level (Figure 25C). These data indicated that HX106N could effectively induce HO-1 expression in cells of microglial origin.

2.6 Roles of HO-1 in HX106N-suppressed NO production

Effects of HO-1 inhibitor on HX106N-inhibited NO and iNOS production

To investigate if HO-1 affected HX106N-mediated NO suppression, BV-2 cells were incubated with 100 ng/mL LPS for 24 h in the presence or absence of 1 mg/mL HX106N, and the culture supernatants were analyzed with the Griess assay to measure the amount of nitrite, a stable end product of NO. The nitrite level increased up to 28.2 μM in the supernatant from LPS-stimulated cells but was significantly decreased to 7.0 μM after treatment with HX106N (Figure 26A). When 100 nM zinc (II) protoporphyrin-IX (ZnPP), a pharmacological inhibitor of HO-1, was added to the cells,

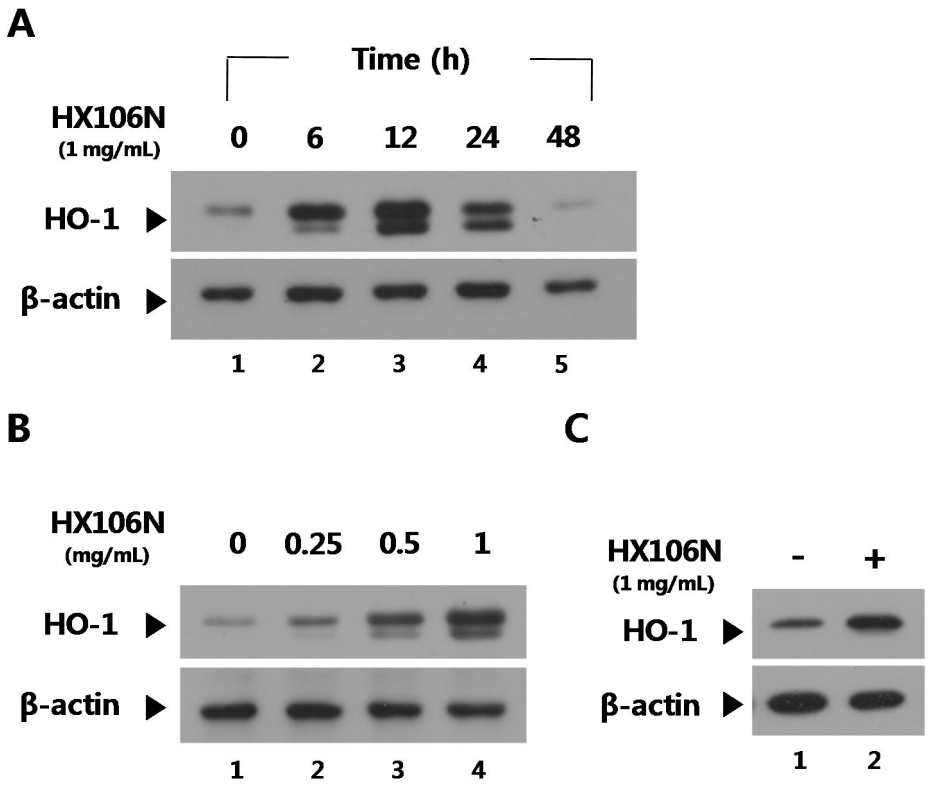

Figure 25. Effects of HX106N on the expression HO-1 in BV-2 cells and primary microglia. (A) BV-2 cells were treated with 1 mg/mL HX106N for the indicated time periods. Whole cell lysates were prepared and subjected to Western blot analysis using antibodies specific for HO-1 and β-actin. β-actin was used as a loading control. (B) Cells were treated with various concentrations of HX106N for 24 h, and HO-1 and β-actin were detected in whole cell lysates by Western blot analysis. (C) Primary microglial cultures were obtained from the cortex of P1-P2 mouse pups as described in the Materials and Methods and treated with 1 mg/mL HX106N for 24 h. The level of HO-1 and β-actin in cell lysates was determined by Western blot analysis.

the nitrite level increased to 15.3 μM (Figure 26A).

To test whether ZnPP has any effect on HX106N-suppressed iNOS expression, whole cell lysates were extracted from the same experiments and subjected to Western blot analysis for the detection of iNOS. As shown in Figure 26B, treatment with HX106N significantly decreased LPS-induced iNOS expression by 83%, and this inhibition was not affected by ZnPP. These data suggested that HO-1 might not contribute to HX106N-mediated iNOS suppression.

Primary cultured microglia were also used to test the effects of HX106N on NO production. The cells were stimulated with 100 ng/mL LPS in the presence or absence of 1 mg/mL HX106N and 100 nM ZnPP for 48 h and the culture supernatant was harvested to detect the nitrite level. Consistent with the results from the BV-2 cells, treatment with HX106N effectively suppressed the increase in the level of nitrite in LPS-stimulated primary microglia, and this suppression was antagonized by ZnPP treatment (Figure 26C). Taken together, HO-1 appears to be involved in the HX106N-mediated inhibition of NO production but not in the control of iNOS expression.

Effects of HO-1 siRNA on HX106N-inhibited NO and iNOS production

I confirmed the above observation by knockdown of HO-1 using a specific siRNA. BV-2 cells were transfected with siRNA specific for HO-1 (siHO-1) or a non-specific siRNA (siControl) and treated with 1 mg/mL HX106N for 24 h. The Western blot analysis showed that siHO-1 significantly decreased HX106N-induced HO-1 expression, by 58%, whereas siControl had no effect (Figure 27A).

SiRNA-transfected cells were stimulated with 100 ng/mL LPS in the presence or absence of 1 mg/mL HX106N for 24 h, and the level of nitrite and iNOS expression was measured in culture supernatants and cellular proteins, respectively. HX106N

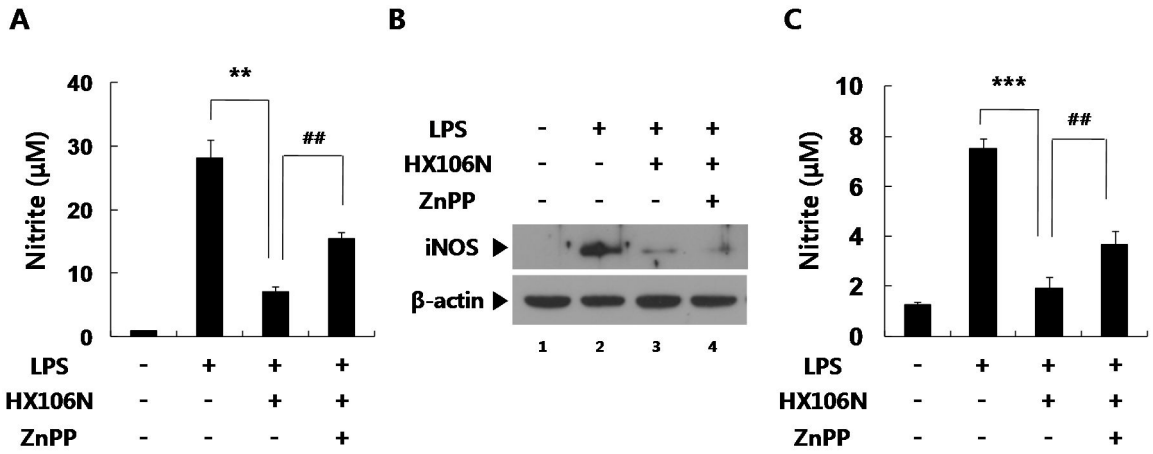

Figure 26. Effects of HO-1 inhibitor on HX106N-suppressed the production of NO and iNOS protein. (A and B) BV-2 cells were stimulated with 100 ng/mL LPS in the presence or absence of 1 mg/mL HX106N and 100 nM ZnPP, an HO-1 inhibitor. After 24 h, the culture supernatant was subjected to the Griess assay to examine the level of nitrite (A), whole cell lysates were harvested for Western blot analysis to detect iNOS and β-actin (B). β-actin was used as a loading control. The values for nitrite are presented as the means ± SD of triplicate samples of a representative experiment. $^{**}P < 0.01$ compared to the LPS-treated group; $^{\#\#}P<0.01$ compared to the LPS and HX106N-treated group. (C) Primary microglial cells were stimulated with 100 ng/mL LPS in the presence or absence of 1 mg/mL HX106N and 100 nM ZnPP. After 48 h, the culture supernatant was prepared and analyzed by Griess assay. The values are presented as the means ± SD of triplicate samples of a representative experiment. $^{***}P < 0.001$ compared to the LPS-treated group; $^{\#\#}P<0.01$ compared to the LPS and HX106N-treated group.

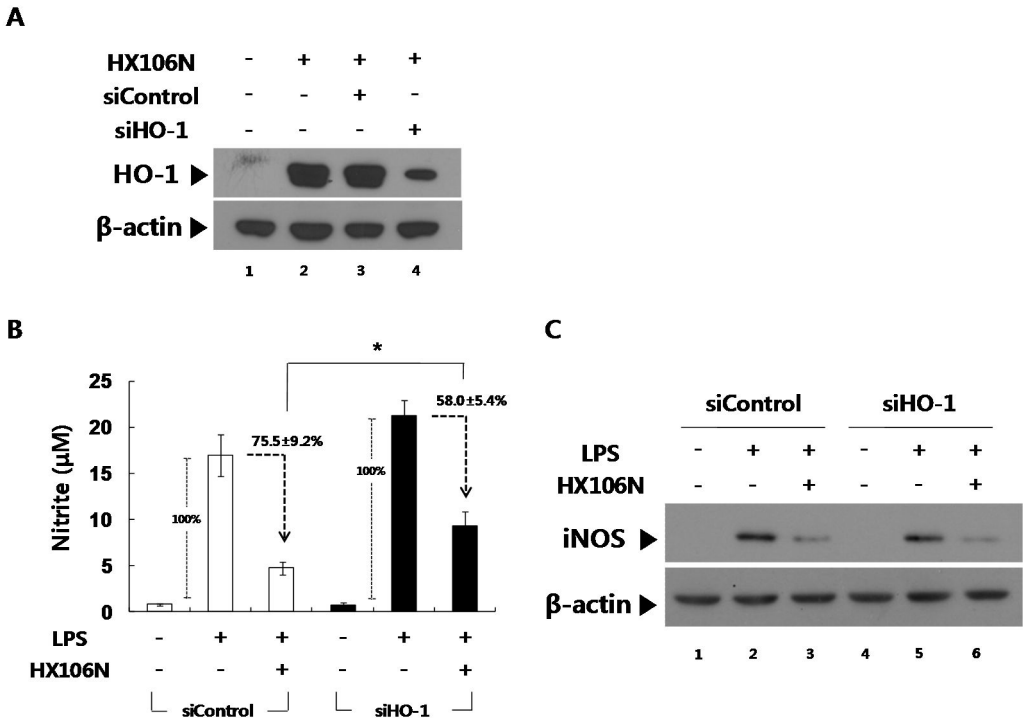

Figure 27. Effects of the knockdown of HO-1 on HX106N-suppressed the production of NO and iNOS protein. (A) BV-2 cells transfected with siHO-1 or siControl were treated with 1 mg/mL HX106N for 24 h. The total protein was prepared for Western blot analysis using antibodies against HO-1 and β-actin. β-actin was used as a loading control. (B and C) Cells transfected with siHO-1 or siControl were stimulated with 100 ng/mL LPS in the presence or absence of 1 mg/mL HX106N. After 24 h, the culture supernatant and total proteins were harvested for the Griess assay (B) and Western blot analysis (C). The values are presented as the means ± SD of triplicate samples of a representative experiment. $^{*}P < 0.05$ compared to the siControl-transfected group.

decreased nitrite production by 75.5 ± 9.2% and 58.0 ± 5.4% in siControl- and siHO-1-transfected cells, respectively, compared to the group treated with LPS (Figure 27B). The relative inhibition rate of nitrite production in siHO-1-transfected cells was significantly lower compared to that of siControl-transfected cells (Figure 27B). These results confirmed the involvement of HO-1 in HX106N-mediated NO suppression. HX106N-mediated suppression of iNOS expression was not affected by siHO-1 transfection, consistent with the results from ZnPP treatment (Figure 27C).

Roles of CO in HX106N-inhibited NO and iNOS production

Carbon monoxide (CO), an enzymatic byproduct of HO-1 activity, has been known to suppress NO production without affecting the iNOS protein level (Sawle et al., 2005, White and Marletta, 1992). Therefore, it was tested whether CO was involved in the HX106N-mediated downregulation of NO. BV-2 cells were incubated with 100 ng/mL LPS in the presence or absence of 1 mg/mL HX106N, 1 μM hemoglobin (Hb), a CO scavenger, and 100 μM carbon monoxide releasing molecule 3 (CORM-3), a CO donor, for 24 h. The supernatant and cell lysates were harvested and used to measure the level of nitrite and iNOS protein, respectively. As expected, Hb attenuated the inhibitory effect of HX106N on LPS-induced NO production, while CORM-3 significantly suppressed the production of NO (Figure 28A). As shown in Figure 28B, the decreased level of iNOS protein by HX106N was not affected by Hb, while CORM-3 also had little effect on LPS-induced iNOS expression. These data indicated that CO is a critical factor for HX106N-mediated NO suppression, but with no effect on iNOS expression.

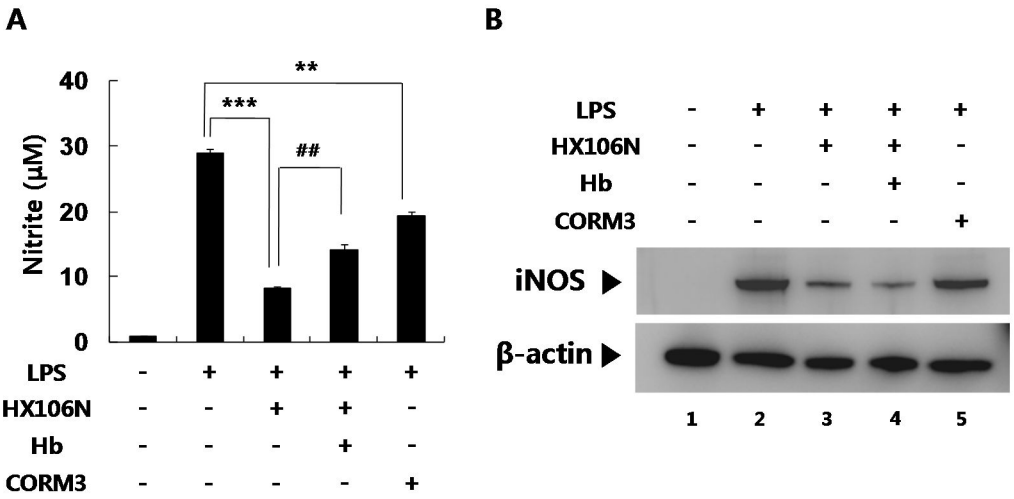

Figure 28. Roles of CO in HX106N-suppressed the production of NO and iNOS protein. BV-2 cells were incubated with 100 ng/mL LPS in the presence or absence of 1 mg/mL HX106N, 1 μM Hb and 100 μM CORM-3. Twenty-four hours later, the levels of nitrite and iNOS were determined by the Griess assay from the supernatant (A) and Western blot analysis using the total proteins (B), respectively. The values for nitrite are presented as the means ± SD of triplicate samples of a representative experiment. $^{**}P < 0.01$, $^{***}P < 0.001$ compared to the LPS-treated group; $^{\#\#}P<0.01$ compared to the LPS and HX106N-treated group.

2.7 Effects of HX106N on glutamate-induced oxidative neurotoxicity

Effects of HX106N on glutamate-mediated cell death and oxidative stress in HT22 cells

It has previously been reported that a high concentration of glutamate induces oxidative neurotoxicity, in which it disturbs cystine uptake through the cystine/glutamate antiporter, leading to glutathione (GSH) depletion (Tan et al., 2001). Therefore, we tested the effect of HX106N on glutamate-induced oxidative neurotoxicity using HT22 cells, a murine hippocampal neuronal cell line. HT22 cells were treated for 18 h with 4 mM glutamate and various concentrations of HX106N, and cell viability was measured using the MTT assay. Glutamate reduced cell viability by 62.3 %, but the viability was dose dependently increased by HX106N, reaching up to 88.1 % at 1 mg/mL HX106N (Figure 29B). The level of ROS was elevated over time, increasing by 6.7-fold 12 h after glutamate treatment (Figure 29C). However, the presence of 1 mg/mL HX106N significantly slowed the rate of ROS accumulation (Figure 29C). The level of intracellular GSH was found to be markedly reduced to 22.2 % compared to that of untreated cells (Figure 29D). HX106N was shown to have no significant effect on GSH depletion (Figure 29D). These data suggested that HX106N protected HT22 cells from the glutamate-induced cell death by inhibiting oxidative stress.

Effects of HX106N on glutamate-mediated cell death and oxidative stress in primary cortical neurons

To confirm that above results were not restricted to a specific cell line, the neuroprotective effects of HX106N on primary cultured cortical neurons were also examined. Primary cortical neurons (DIV 3) were pretreated with three different

Figure 29. Effects of HX106N on glutamate-induced oxidative neurotoxicity in HT22 cells. (A) Mechanism of glutamate-induced oxidative stress and neurotoxicity. (B) HT22 cells were treated for 18 h with 4 mM of glutamate and various concentrations of HX106N. The cell viability was determined by the MTT assay. The results are presented relative to untreated control cells. The values are presented as the mean ± SD of triplicate samples from a representative experiment. (C) Cells were treated with 4 mM glutamate alone or with 1 mg/mL of HX106N for indicated times followed by incubation for 30 min with 5 μM of H_2DCFDA. Intracellular ROS levels were measured by flow cytometry analysis. The results are presented relative to untreated control cells. The values are presented as the mean ± SD of triplicate samples from a representative experiment. $^{*}P < 0.05$, $^{**}P < 0.01$ compared to the glutamate-treated group. (D) Cells were treated with 4 mM glutamate in the presence or absence of 1 mg/mL HX106N for 12 h. Whole cell lysates were prepared and GSH contents were measured using the MCB-based fluorescence assay. The values are presented as the means ± SD of triplicate samples from a representative experiment. NS = non-significant compared to the glutamate-treated group.

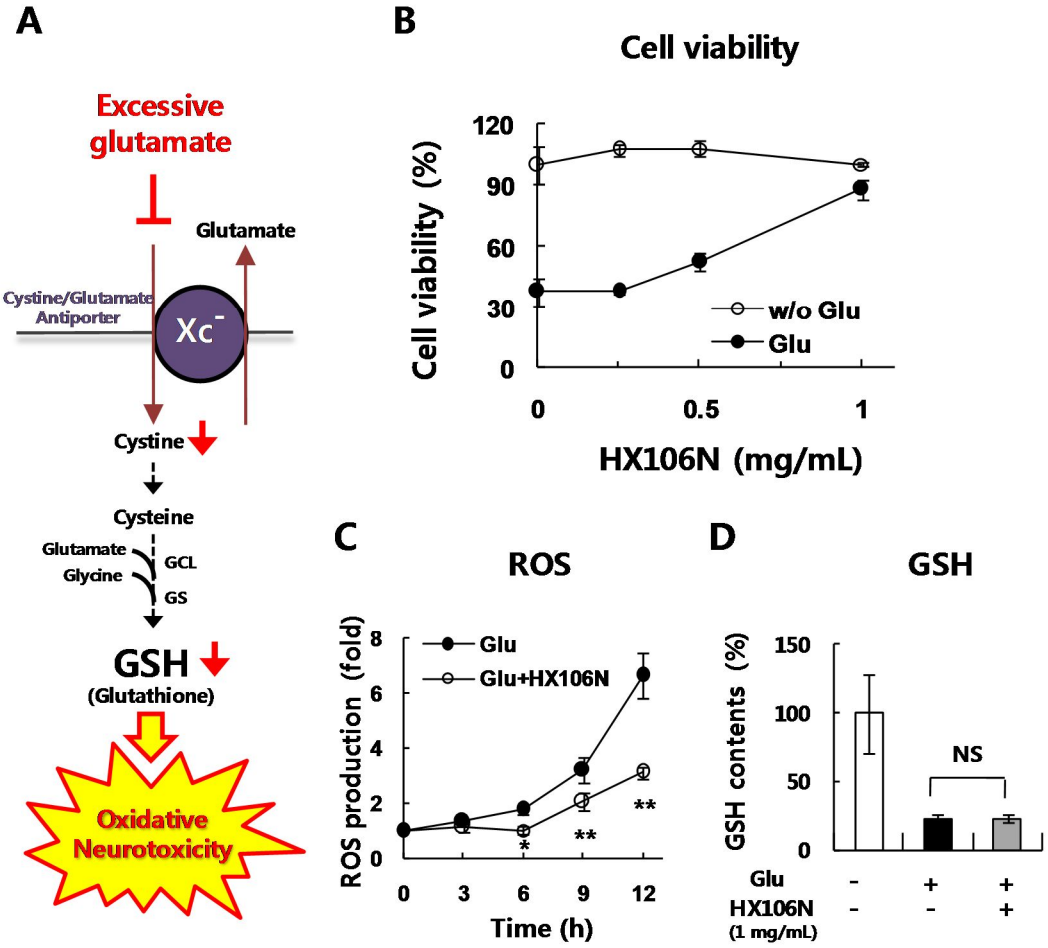
A
Excessive glutamate
Glutamate
Cystine/Glutamate Antiporter
Xc-
Cystine
Cysteine
Glutamate
Glycine
GCL
GS
GSH
(Glutathione)
Oxidative Neurotoxicity
B
Cell viability
Cell viability (%)
120
90
60
30
0
0
0.5
1
HX106N (mg/mL)
w/o Glu
Glu
C
ROS
ROS production (fold)
8
6
4
2
0
Glu
Glu+HX106N
*
**
**
0
3
6
9
12
Time (h)
D
GSH
GSH contents (%)
150
100
50
0
NS
Glu
HX106N
(1 mg/mL)
-
+
+
-
-
+

concentrations (25, 50 and 100 μg/mL) of HX106N for 18 h, and then glutamate (8 mM) was added for another 48 h. Data from the MTT assay indicated that cell viability was decreased by 69.2 % after glutamate treatment, while pretreatment with HX106N increased the viability in a dose-dependent manner (Figure 30A). When HX106N-treated cells were stained with Tuj1 (neuron-specific β-III tubulin), a neuron-specific marker, the number of stained cells was higher than glutamate-treated cells (Figure 30B). These data demonstrated that HX106N could inhibit glutamate-induced cell death in primary cortical neurons.

The effects of HX106N on the level of ROS and GSH were also investigated. Similar to the data obtained from HT22 cells, HX106N inhibited glutamate-induced ROS production but did not affect the level of GSH depletion (Figure 30C and 30D).

2.8 Roles of HO-1 in the protective effect of HX106N against glutamate neurotoxicity

Effects of HX106N on HO-1 expression in HT22 cells and primary cortical neurons

Because the increased expression of HO-1 has been demonstrated to produce neuroprotective effects against glutamate neurotoxicity (Chen et al., 2000, Rossler et al., 2004, Son et al., 2013), the effects of HX106N on HO-1 expression was tested in HT22 cells and primary cortical neurons. HT22 cells were treated with 1 mg/mL HX106N, and whole cell lysates were prepared at various time points to determine the protein level of HO-1 by Western blot analysis. The expression of HO-1 was increased 6 h after HX106N treatment and remained at a high level up to 24 h, and then decreased to the basal level after 48 h (Figure 31A). HX106N also induced the expression of HO-1 in a dose-dependent manner (Figure 31B). When primary cortical neurons were

Figure 30. Effects of HX106N on glutamate-induced oxidative neurotoxicity in primary cortical neurons. (A and B) Primary cortical neurons (DIV 3) were pretreated with various concentrations of HX106N for 18 h and then treated with 8 mM glutamate. After 48 h, cell viability was determined by the MTT assay (A) and immunofluorescence staining for neuron specific marker, Tuj1 (B). The results are presented relative to untreated control cells, as the mean ± SD of triplicate samples from a representative experiment. Scale bar, 50 μm. (C and D) Neurons were pretreated with 100 μg/ml of HX106N for 18 h, followed by treatment with 8 mM glutamate for another 24 h. The intracellular levels of ROS (C) and GSH (D) were measured by the H_2DCFDA and MCB-based fluorescence assays, respectively. The values are presented as the means ± SD of triplicate samples from a representative experiment. $^{**}P < 0.01$, NS = non-significant compared to the glutamate-treated group.

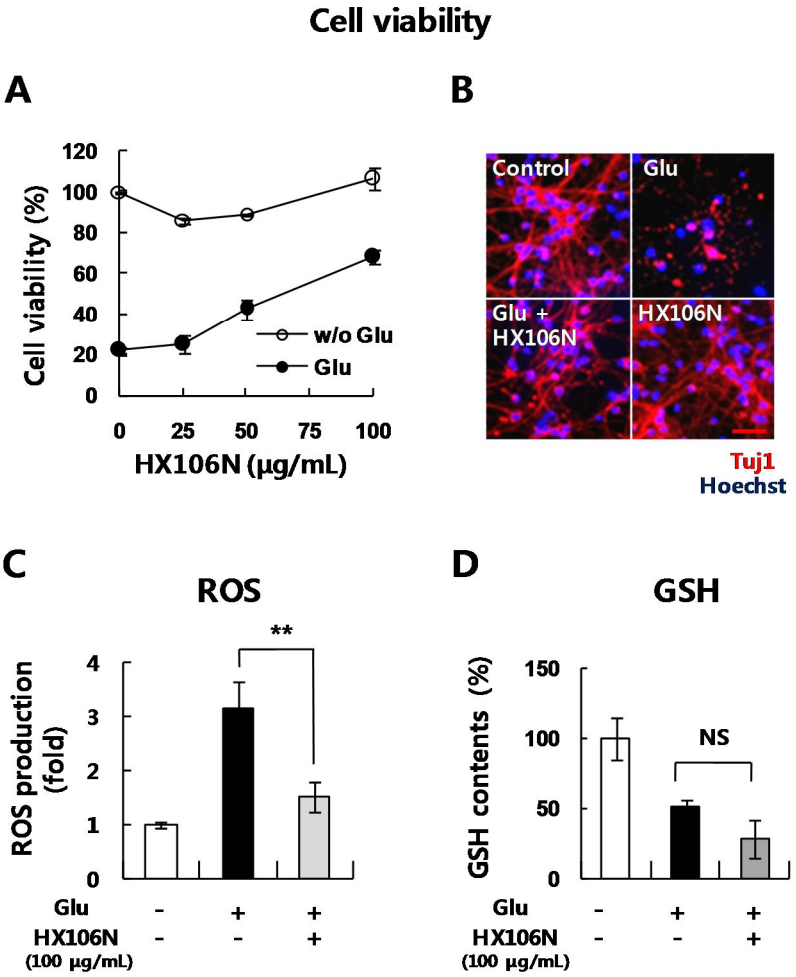
Cell viability
A
B
Cell viability (%)
120
100
80
60
40
20
0
w/o Glu
Glu
0
25
50
75
100
HX106N (μg/mL)
Control
Glu
Glu +
HX106N
HX106N
Tuj1
Hoechst
C
ROS
**
ROS production
(fold)
4
3
2
1
0
Glu
HX106N
(100 μg/mL)
D
GSH
GSH contents (%)
150
100
50
0
NS

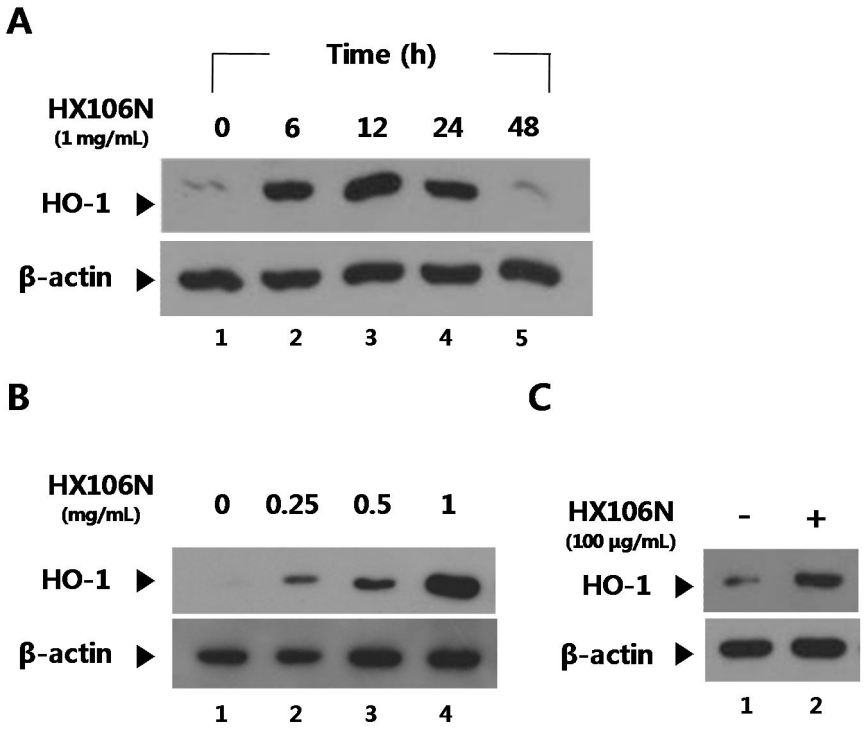

Figure 31. Effects of HX106N on the expression of HO-1 in HT22 cells and primary cortical neurons. (A) HT22 cells were treated with 1 mg/mL HX106N, and total proteins were prepared at the indicated time points. Western blot analysis was performed to determine the levels of HO-1 and β-actin. β-actin was used as a loading control. (B) Cells were treated for 12 h with three different concentrations of HX106N (0.25, 0.5 and 1 mg/mL). Whole cell lysates were prepared and the level of HO-1 was analyzed. (C) Primary cortical neurons were treated with 100 μg/mL HX106N for 18 h. The protein levels of HO-1 and β-actin in cell lysates were measured by Western blot analysis.

treated with 100 μg/mL HX106N for 18 h, a 2.6-fold increase in the level of HO-1 protein was observed (Figure 31C). These results indicated that HX106N could induce HO-1 expression in cells of neuronal origin.

Effects of HO-1 on HX106N-suppressed glutamate neurotoxicity

To examine whether HO-1 plays a role(s) in the neuroprotective effects of HX106N, the expression level of HO-1 was knocked down using a specific siRNA. HT22 cells were transfected with siHO-1 or a non-specific siRNA (siControl), and treated with 1 mg/mL HX106N for 12 h. HX106N-induced HO-1 expression was decreased to 14% of the original level in siHO-1-treated cells, while it was not affected in the control cells (Figure 32A). Cells transfected with siRNA were treated with 4 mM glutamate in the presence or absence of 1 mg/mL HX106N. Cell viability and ROS levels were measured 18 h and 12 h after the treatment, respectively. When the difference between glutamate-treated and untreated groups was regarded as 100%, HX106N increased cell viability by 58.8 ± 4.6% and 50.9 ± 6.9%, and reduced ROS level by 101.0 ± 3.0 % and 83.4±16.2% in siControl- and siHO-1-transfected cells, respectively (Figure 32B and 32B). The percentage changes in viability and ROS level were not significantly different between siControl- and siHO-1-transfected cells. These data suggested that HO-1 might not be involved in HX106N-inhibited glutamate neurotoxicity.

2.9 Roles of Nrf2 in the protective effect of HX106N against glutamate neurotoxicity

Effects of HX106N on Nrf2 activation and Nrf2-dependent gene expression

Figure 32. Effects of the knockdown of HO-1 on HX106N-inhibited glutamate neurotoxicity. (A) HT22 cells transfected with siHO-1 or siControl were treated with 1 mg/mL HX106N for 24 h. Whole cell lysates were prepared for Western blot analysis using specific antibodies for HO-1 and β-actin. β-actin was used as a loading control. (B and C) Cells transfected with siHO-1 or siControl were treated with 4 mM glutamate in the presence or absence of 1 mg/mL HX106N. After 18 h, cell viability was evaluated by the MTT assay (B). 12 h later, the intracellular level of ROS was measured by the H_2DCFDA assay. The results are presented relative to untreated control cells. The values are presented as the mean ± SD of duplicate samples from a representative experiment. NS = non-significant compared to the glutamate-treated group.

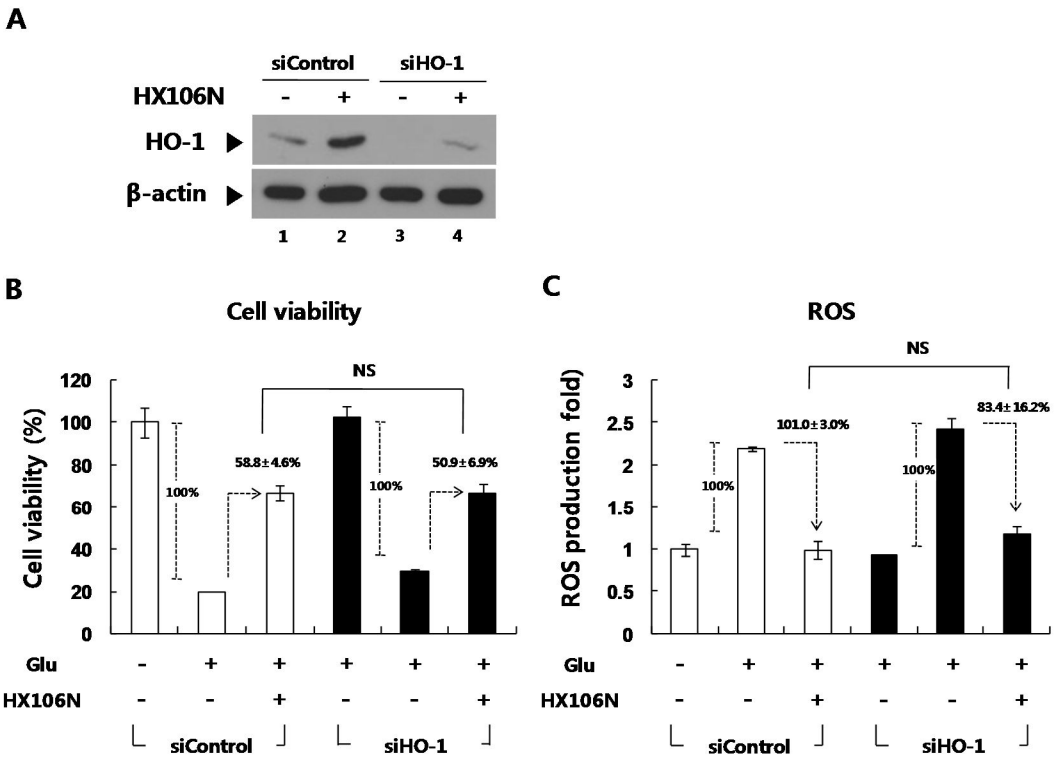
A
siControl
siHO-1
HX106N
- + - +
HO-1
β-actin
1 2 3 4
B
Cell viability
Cell viability (%)
120
100
80
60
40
20
0
NS
100%
58.8±4.6%
100%
50.9±6.9%
Glu - + + + + +
HX106N - - + - - +
siControl
siHO-1
C
ROS
ROS production fold)
3
2.5
2
1.5
1
0.5
0
NS
100%
101.0±3.0%
100%
83.4±16.2%
Glu - + + + + +
HX106N - - + - - +
siControl
siHO-1

Nuclear factor E2–related factor 2 (Nrf2) is a master regulator of antioxidant transcriptional responses. Several antioxidant genes, primarily regulated by Nrf2, have been reported to protect neurons against various toxic stimuli (Calkins et al., 2009). Therefore, it was examined whether HX106N had any effects on Nrf2 activation and the expression of Nrf2-dependent antioxidant genes, including NQO1 (NAD(P)H, quinone oxidoreductase 1), and GCLm (glutamate-cysteine ligase modifier subunit). HT22 cells were treated for 6 h with various concentrations of HX106N or 25 μM tBHQ (tert-butylhydroquinone), an Nrf2 activator. Nuclear extracts were prepared and analyzed to measure the nuclear level of Nrf2 using Western blot hybridization. Both HX106N and tBHQ were found to increase the nuclear accumulation of Nrf2 (Figure 33A). When the cells were treated with HX106N for 9 h, the RNA level of NQO1 and GCLm was increased in a dose-dependent manner (Figure 33B). These data indicated that HX106N could activate Nrf2 and subsequently control the expression of Nrf2-dependent genes.

Effects of HX106N on glutamate-induced cell death in primary cortical neurons from Nrf2-KO mice

To test the involvement of Nrf2 in the neuroprotective effect of HX106N, primary cortical neurons were isolated from Nrf2-KO or WT mice. Cells (DIV 3) were pretreated with 100 μg/mL HX106N for 18 h, and then treated with glutamate (8 mM). As neuronal death in KO cells occurred relatively quickly than that in WT cells, cell viability was measured at 24 h and 48 h time points after glutamate treatment, respectively. As shown in Figure 33C, a significant increase in neuronal cell viability was observed in both WT and KO cells when cells were treated with HX106N. These data indicated that HX106N might protect neuronal cells in Nrf2-independent manner.

Figure 33. Roles of Nrf2 on HX106N-inhibited glutamate neurotoxicity. (A) HT22 cells were treated with various concentrations of HX106N or 25 μM tBHQ. After 6 h, the nuclear extracts were prepared, and the protein level of Nrf2 was measured by Western blot analysis. TFIIB was used as a loading control. (B) Cells were treated for 9 h with various concentrations of HX106N. Total RNAs were prepared and the RNA levels of HO-1, NQO1 and GCLm were analyzed by Northern blot hybridization. GAPDH was used as a loading control. (C) Primary cortical neurons were isolated from the E14.5-15.5 embryos of WT or Nrf2-KO mice, and were pretreated with 100 μg/mL HX106N for 18 h, followed by treatment with 8 mM glutamate. Cell viability of WT and KO cells was determined using the MTT assay, 48 h and 24 h after glutamate treatment, respectively. The values are presented as the mean ± SD of triplicate samples from a representative experiment.

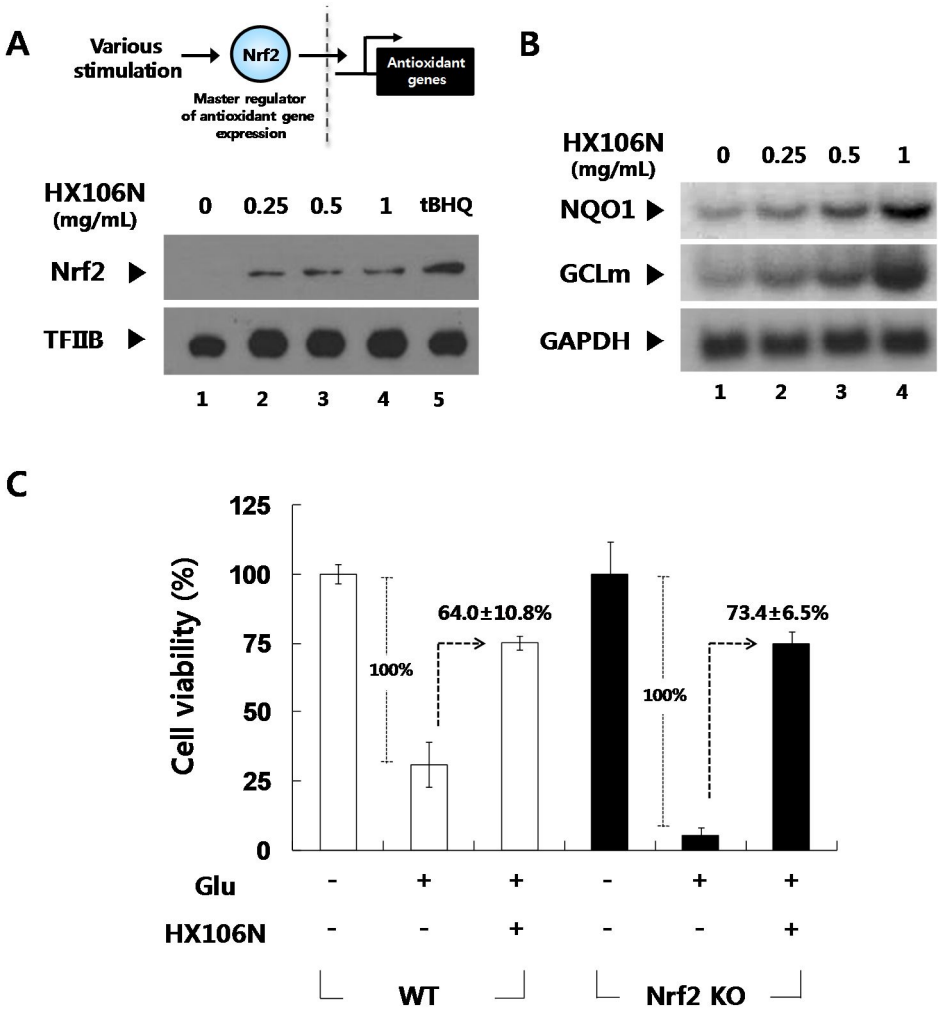
A
Various stimulation
Nrf2
Antioxidant genes
Master regulator of antioxidant gene expression
HX106N (mg/mL)
0 0.25 0.5 1 tBHQ
Nrf2
TFIIB
1 2 3 4 5
B
HX106N (mg/mL)
0 0.25 0.5 1
NQO1
GCLm
GAPDH
1 2 3 4
C
Cell viability (%)
125
100
75
50
25
0
64.0±10.8%
73.4±6.5%
100%
100%
Glu
HX106N
WT
Nrf2 KO

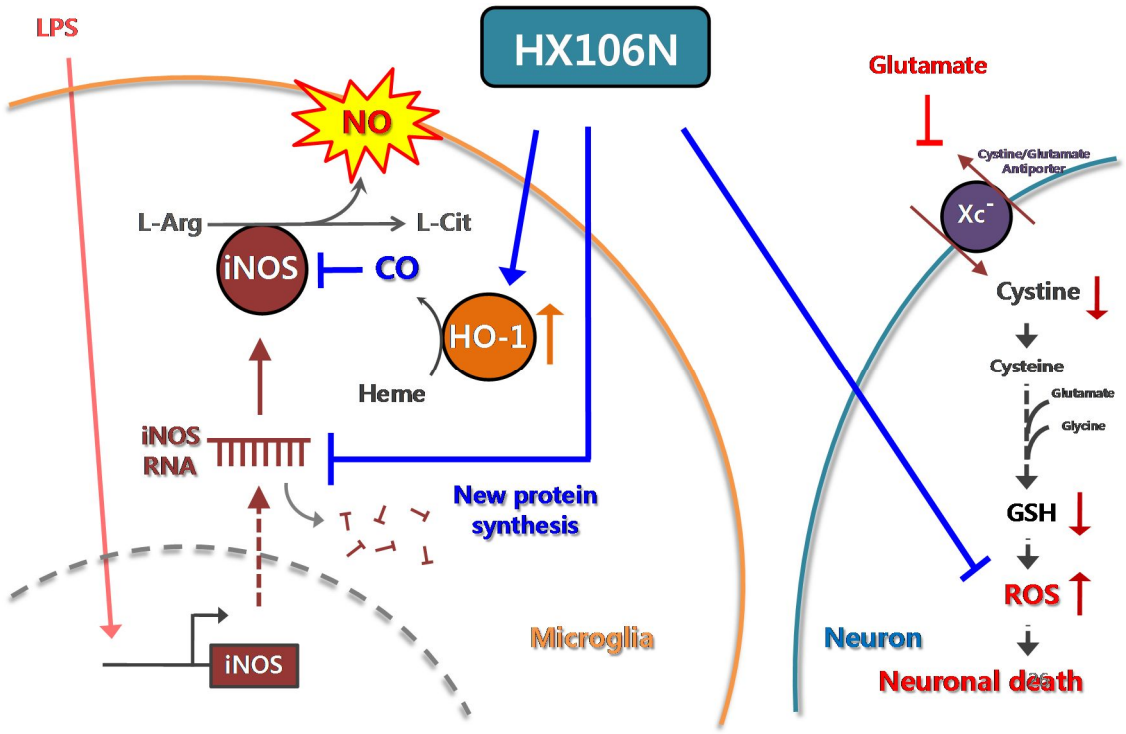

Figure 34. Schematic diagram of working mechanism of HX106N in this chapter. HX106N effectively inhibited LPS-induced production of NO by regulating the expression of iNOS at the level of RNA in microglia cells. In this step, new protein synthesis was needed. The expression HO-1 was increased by HX106N and its enzymatic byproduct CO was found to contribute to HX106N-mediated suppression of NO production. In neuronal cells, HX106N markedly prevent glutamate-induced neuronal cell death by regulating ROS production.

3. Discussion

In the present study, I investigated the antioxidative effects of HX106N and its underlying mechanisms in microglia and neurons. HX106N suppressed LPS-induced NO production by regulating iNOS RNA expression at the post-transcriptional level. Data from the experiment involving cycloheximide (a translational inhibitor), indicated that *de novo* protein synthesis was required for HX106N-mediated decrease of iNOS RNA level. Human, mouse and rat iNOS RNAs contain a sequence motif (AUUUA) in their 3'-UTR (Galea et al., 1994, Geller et al., 1993, Lyons et al., 1992), which is known to play a regulatory role in RNA stability of various cytokines and oncogenes (Caput et al., 1986). Several regulatory proteins which bind to the AUUUA element have been identified. One of them is Hur, a member of the ELAV (embryonic lethal abnormal vision) protein family. Hur is known to increase the RNA stability of several inducible genes (Brennan and Steitz, 2001), and its overexpression is found to upregulate iNOS expression (Rodriguez-Pascual et al., 2000). In contrast to Hur, AUF1 (AU binding factor 1) is reported to destabilize RNA of these genes. The p37 subunit of AUF1 has shown to have a high affinity to the AUUUA element present in the human iNOS 3'-UTR, and promote the degradation of iNOS RNA (Pautz et al., 2009). Therefore, it is possible that HX106N enhances the destabilization of iNOS RNA by regulating the expression of these RNA-binding proteins. It is interesting to note that HX106N selectively inhibited iNOS expression without affecting other inflammatory cytokines, such as TNF-α and IL-6, although their RNAa also contain the AUUUA element present in the 3'-UTR (Dean et al., 2001, Paschoud et al., 2006). Further studies are needed to identify the protein(s) involved in HX106N-mediated downregulation of iNOS RNA.

The production of NO was effectively suppressed by HX106N, and HO-1 played an important role in this process through CO generation. However, HO-1 and CO were not involved in HX106N-mediated suppression of iNOS expression. CO is known to inhibit iNOS activity without affecting the expression of iNOS, by interacting with the heme iron moiety of the enzyme (Sawle et al., 2005, White and Marletta, 1992). Therefore, it is possible that CO released from HO-1-catalyzed reactions may inhibit iNOS activity, resulting in the regulation of NO production by HX106N.

HX106N significantly reduced glutamate-induced neurotoxicity through inhibition of ROS production without affecting GSH depletion. Although several Nrf2-dependent antioxidant genes were found to be induced by HX106N, they had little effects on the neuroprotective properties of HX106N. In the 2,2-diphenylpicrylhydrazyl (DPPH) assay, HX106N showed a direct ROS scavenging effect (data not shown). As it has been reported that ROS scavengers, such as N-acetyl-cysteine (NAC), can protect HT22 cells against oxidative stimuli, such as glutamate (Fukui et al., 2009), it may be possible that the neuroprotective effects of HX106N due to its direct ROS scavenging action. Other potential mechanism would be that HX106N acts on the signaling pathway that is downstream of GSH depletion. These include the activation of 12-lipoxygenase, soluble guanylyl cyclase and Ca^{2+} influx (Tan et al., 2001), which has been reported to mediate oxidative glutamate toxicity (Li et al., 1997, Li et al., 1997, Davis and Maher, 1994).

In this study, HX106N showed to contain strong antioxidative and neuroprotective activities in the cells of microglial and neuronal origin. HX106N was found to affect various factors involved in the regulation of oxidative stress, although further in-depth investigations are still required to unravel the exact mechanism(s). Given the critical role(s) of oxidative stress in neurodegeneration, data contained in this

thesis research indicated HX106N has a great potential as a therapeutic agent for neurodegenerative diseases, such as AD.

CHAPTER VI

Mechanism Study of HX106N-Mediated HO-1 Expression

1. Background

The expression of HO-1 is regulated by complex cooperative interactions between various signaling kinases and transcription factors (Figure 35). Mitogen-activated protein kinases (MAPKs) have been reported to play a major role in HO-1 expression, and other kinases, including phosphatidylinositol 3-kinase (PI3K) and protein kinases A and C, might also be involved (Ryter et al., 2006). Multiple *cis*-acting elements in the HO-1 promoter play critical roles in transcriptional regulation. In particular, the stress-responsive element (StRE), a 10-bp sequence motif in the E1 and E2 enhancers, has been identified as a dominant *cis*-element for the induction of HO-1 gene expression (Alam et al., 1999, Alam and Cook, 2003). Activating protein-1 (AP-1), composed of homo- and heterodimers from the Jun and Fos families, and Nrf2 are StRE-binding activating transcription factors for the HO-1 gene (Alam et al., 1999, Alam and Den, 1992). Two potential binding sequences for NF-κB were also identified within the immediate 5' flanking region of the human HO-1 gene, but it is currently unclear if these sequences are functional (Alam and Cook, 2007). The consensus NF-κB binding sequence has not been observed in other mammalian HO-1 genes (Alam and Cook, 2007). However, accumulating evidence indicates that NF-κB contributes to HO-1 expression. Several agents, including curcumin, resveratrol, and docosahexaenoic acid, have been reported to induce HO-1 expression through NF-κB (Lu et al., 2010, Hill-Kapturczak et al., 2001, Juan et al., 2005).

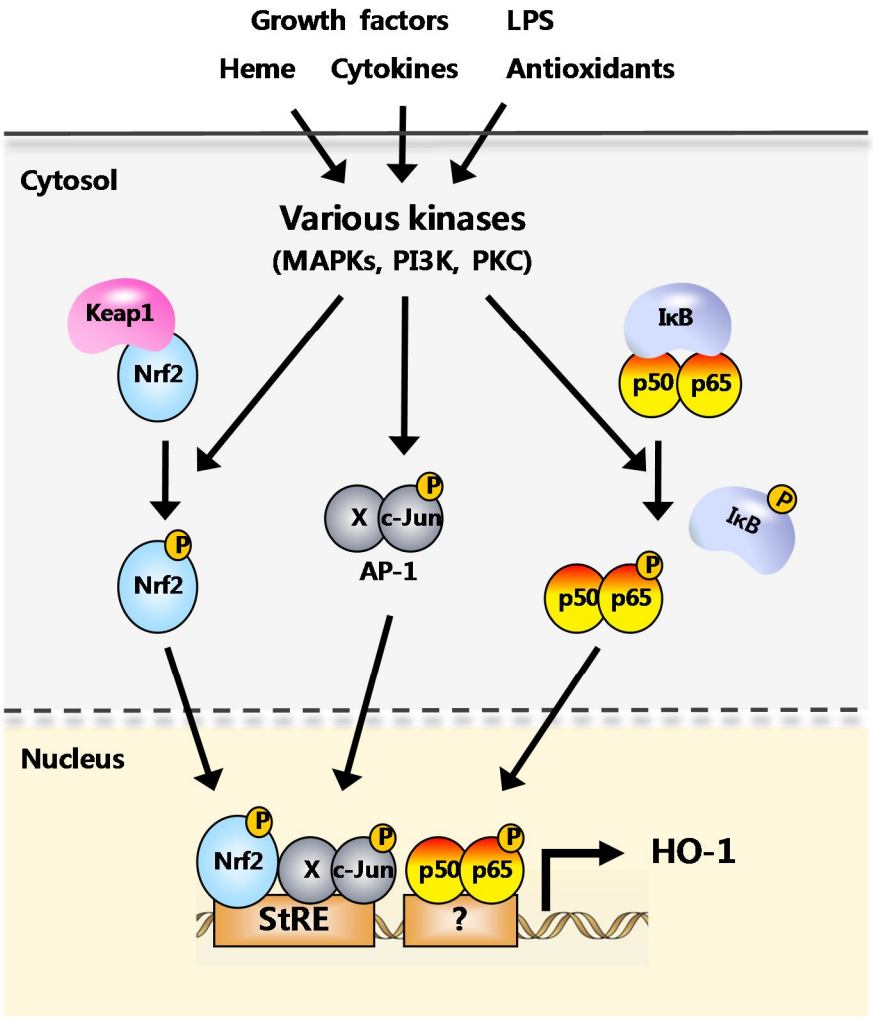

Figure 35. Schematic representation of signaling pathways involved in the regulation of HO-1 expression. A number of signaling kinases and transcription factors are involved in the regulation of HO-1 expression. Nrf2 and AP-1 are the major transcription factors regulating the expression of HO-1 through StRE present in the HO-1 promoter. NF-κB pathway plays an important role in HO-1 expression in response to diverse stimuli, although a functional NF-κB binding site has not yet been identified in the HO-1 gene. Various cellular kinases, such as MAPKs, PI3K and PKC, are known to regulate the stabilization, nuclear translocation and activation of these transcription factors. Adopted and modified from reviews of (Ryter et al., 2006, Alam and Cook, 2007)

HX106N was shown to produce antioxidative effects by upregulating HO-1 expression in the previous chapters, but its underlying molecular mechanism remains elusive. In the chapter, I investigated the molecular mechanisms underlying HX106N-mediated HO-1 expression. HX106N induced the expression of HO-1 RNA by activating various transcription factors and signaling molecules such as Nrf2, NF-κB, JNK and p38 MAPK, all of which are known to be involved in HO-1 expression. Data in this chapter suggested that multiple signaling pathways are involved in HX106N-mediated upregulation of HO-1.

2. Results

2.1 Effects of HX106N on *HO-1* transcription

Effects of HX106N on the RNA level of HO-1

Expression of the HO-1 gene is known to be regulated mainly at the transcription level (Ryter et al., 2006). To investigate the effect of HX106N on HO-1 transcription, BV-2 cells were treated with various concentrations of HX106N for 12 h, and total RNAs were prepared followed by Northern blot hybridization. The basal RNA level of HO-1 was very low but increased substantially after treatment with HX106N in a dose-dependent manner, resulting in an approximately 15-fold increase at a 1 mg/mL concentration (Figure 36). When the RNA level of HO-1 was measured at earlier time points, 3, 6 and 9 h after treatment with 1 mg/mL HX106N, it was increased by 2.9-, 6.5- and 10.0-fold, compared to untreated cells, respectively (data not shown). These results indicated that HX106N regulated the expression of HO-1 at the RNA level.

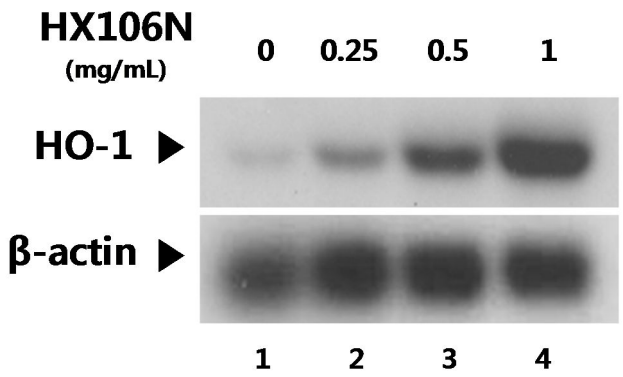

Figure 36. Effects of HX106N on the RNA level of HO-1. BV-2 cells were treated with various concentrations of HX106N. After 12 h, the total RNA was isolated, followed by Northern blot analysis to determine the RNA level of HO-1. GAPDH was used as a loading control.

Effects of HX106N on the promoter activity of HO-1 gene

The effect of HX106N on the HO-1 promoter was examined using a luciferase reporter plasmid, pHO15-Luc, containing the 15 kb full-length HO-1 promoter sequence. BV-2 cells were transfected with pHO15-Luc and treated with various concentrations of HX106N for 9 h. Treatment with HX106N significantly increased the level of luciferase activity in a dose-dependent manner, and a 27-fold increase was observed at the 1 mg/mL concentration (Figure 37B).

The HO-1 promoter contains multiple copies of the stress-responsive element (StRE) in the region called E1 and E2, which have been shown to be the primary loci responsible for HO-1 transcriptional activation in response to various agents (Ryter et al., 2006, Alam et al., 1994, Alam et al., 1995). To test whether these enhancers are also involved in HX106N-mediated HO-1 transcription, BV-2 cells were transfected with the luciferase reporter plasmids containing the wild-type (pE1-Luc) or mutant (pE1M-Luc) E1 enhancer sequence. Treatment with 1 mg/mL HX106N resulted in a 6.9-fold increase in the level of luciferase activity over that of cells transfected with pE1-Luc, while no significant change was found in cells transfected with pE1M-luc (Figure 37C). These data indicated that HX106N regulated the transcription of HO-1 through the StRE-containing enhancer present in the HO-1 promoter.

2.2 Effects of HX106N on Nrf2 and AP-1 activation

Effects of HX106N on nuclear accumulation of Nrf2 and c-Jun

Because the StRE is structurally and functionally similar to the antioxidant response element (ARE) and AP-1 binding site, Nrf2 and AP-1 are reported to be the major transcription factors regulating HO-1 expression in response to various stimuli (Alam et al., 1999, Alam and Den, 1992, Balogun et al., 2003, Camhi et al., 1995).

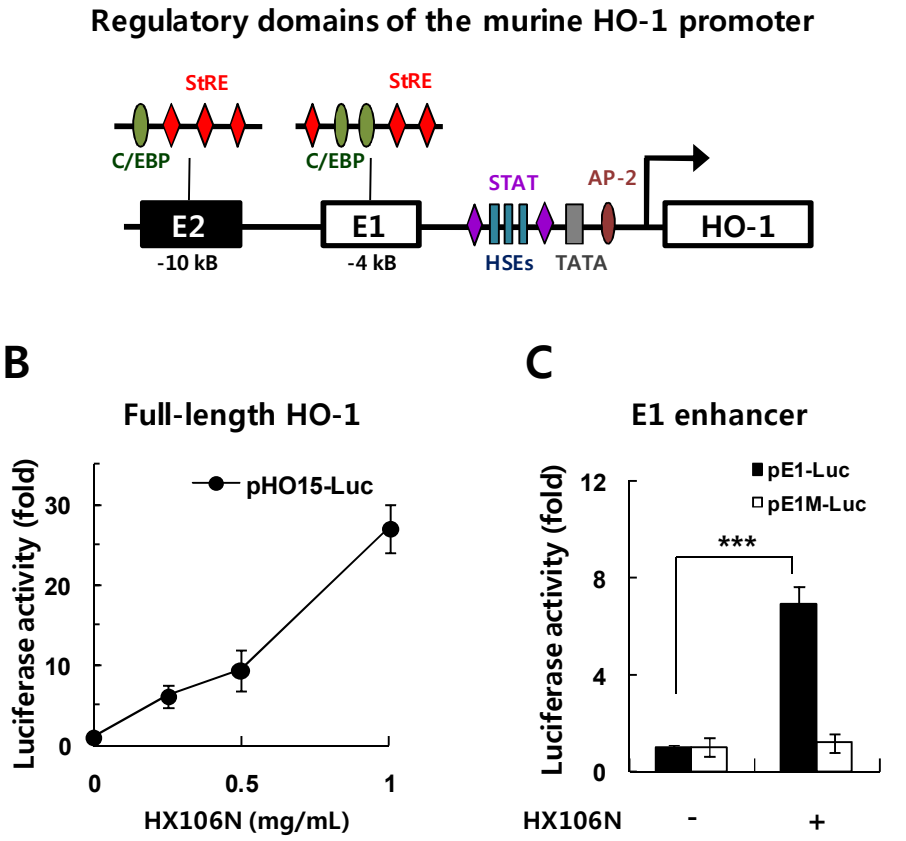

Figure 37. Effects of HX106N on the HO-1 promoter. (A) BV-2 cells were transfected with a luciferase reporter plasmid containing the full-length mouse HO-1 promoter, pHO15-Luc. Twenty-four hours later, the cells were treated with various concentrations of HX106N for 9 h and subjected to a luciferase assay as described in the Materials and Methods. (B) BV-2 cells were transfected with luciferase plasmids containing the original (pE1-Luc) or mutant (pE1M-Luc) sequence of E1. The cells were treated with 1 mg/mL HX106N for 9 h, and the level of luciferase activity was measured. The values are presented as the means ± SD of triplicate samples from one of three independent experiments. ***P < 0.001 compared to the untreated group.

Therefore, the effect of HX106N on the activation of Nrf2 and AP-1 was examined by assessing the nuclear accumulation of Nrf2 and c-Jun, a major component of the AP-1 family. BV-2 cells were treated with 1 mg/mL HX106N, and the nuclear proteins were extracted at various time points, followed by Western blot analysis to determine the levels of these two transcription factors. The levels of Nrf2 and c-Jun remained very low or undetectable at all of the time points examined in untreated cells, but a marked increase was observed after 1 h of HX106N treatment and was maintained throughout the experimental time course (Figure 38).

Effects of HX106N on ARE and AP-1 binding activities

To confirm the effect of HX106N on the activation of Nrf2 and AP-1, a gel retardation assay was performed using ARE and AP-1 oligonucleotide probes. BV-2 cells were treated with 1 mg/mL HX106N for 3 h, and nuclear extracts were prepared, followed by EMSA. Treatment with HX106N significantly increased the amount of DNA-protein complex for both probes (Figure 39A and 39B). These complexes were specific because competition with cold oligonucleotide probes decreased the signal. Supershift/interference assays were carried out to test the binding of Nrf2 or c-Jun to ARE or AP-1 oligonucleotides, respectively. In the presence of Nrf2 or c-Jun antibodies, the formation of DNA-protein complex was inhibited (Figure 39A and 39B).

Effects of Nrf2 or c-Jun on HX106N-mediated HO-1 induction

To examine the roles of Nrf2 and AP-1 in the HX106N-induced HO-1 expression, BV-2 cells were transfected with siRNA specific for Nrf2 (siNrf2), c-Jun (sic-Jun) or a non-specific siRNA (siControl). Twenty-four hours later, the cells were treated with 1 mg/mL HX106N for 6 h, and whole cell lysates were prepared followed

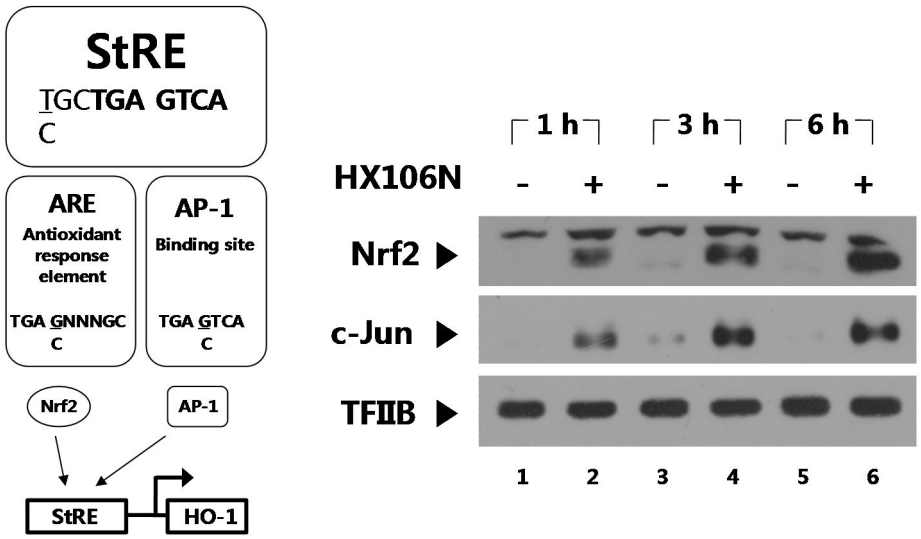

Figure 38. Effects of HX106N on the protein level of Nrf2 and c-Jun in the nucleus. BV-2 cells were treated with 1 mg/mL HX106N for the indicated time periods, and nuclear protein was extracted to determine the level of Nrf2, c-Jun and TFIIB by Western blot analysis. TFIIB was used as a loading control for the nuclear extracts.

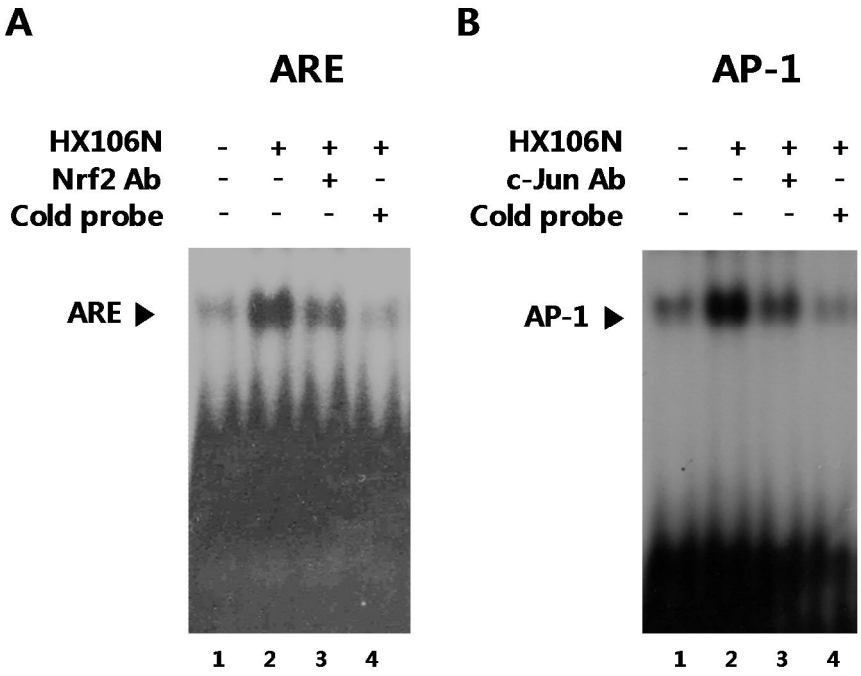

Figure 39. Effects of HX106N on ARE and AP-1 binding activities. BV-2 cells were treated with 1 mg/mL HX106N for 3 h, and nuclear extracts were prepared. EMSA was performed using [^{32}P]-labeled nucleotide sequences for ARE (A) or AP-1 (B). Competition analysis was performed to demonstrate the specificity of the DNA-protein complex using unlabeled cold oligonucleotides. For supershift/interference assays, the nuclear extracts were pre-mixed with 4 μg of Nrf2 or c-Jun antibody for 30 min, and the EMSA assays were performed.

by Western blot analysis. When compared to the case of siControl, siNrf2 and si-cJun transfection downregulated the protein level of Nrf2 and c-Jun by 54% and 62%, respectively (Figure 40A). The level of HO-1 was greatly increased by HX106N treatment in the cells transfected with siControl, while it was reduced by 40% in those with siNrf2 (Figure 40A). Sic-Jun transfection affected the basal level of HO-1, but not HX106N-induced HO-1 expression (Figure 40A). Taken together, these data indicated that Nrf2 played a role in the HX106N-mediated induction of HO-1, although both Nrf2 and AP-1 transcription factors were activated by HX106N.

To confirm the involvement of Nrf2 in HX106N-mediated regulation of HO-1 expression, splenocytes were isolated from Nrf2-knockout (KO) or normal (WT) mice, and treated with 1 mg/mL HX106N. 24 h later, total proteins were prepared and analyzed to determine the protein level of HO-1 by Western blot analysis. The basal level of HO-1 was undetectable in both untreated WT and KO cells (Figure 40B). Treatment with HX106N markedly increased the level of HO-1 in WT cells, while this was not a case in KO cells (Figure 40B). These results confirmed a crucial role of Nrf2 in HX106N-activated induction of HO-1.

2.3 Effects of HX106N on MAPKs activation

Effects of pharmacological inhibitors of MAPKs on HX106N-induced HO-1 expression

Mitogen-activated protein kinases (MAPKs) have been implicated as one of the major regulators of HO-1 expression (Drechsler et al., 2006, Immenschuh and Ramadori, 2000, Ryter et al., 2002). To test whether MAPK signaling has any effect on HX106N-mediated HO-1 expression, pharmacological MAPK inhibitors (i.e., JNK: SP600125; p38 MAPK: SB203580; ERK: PD98059) were applied to the cells. When

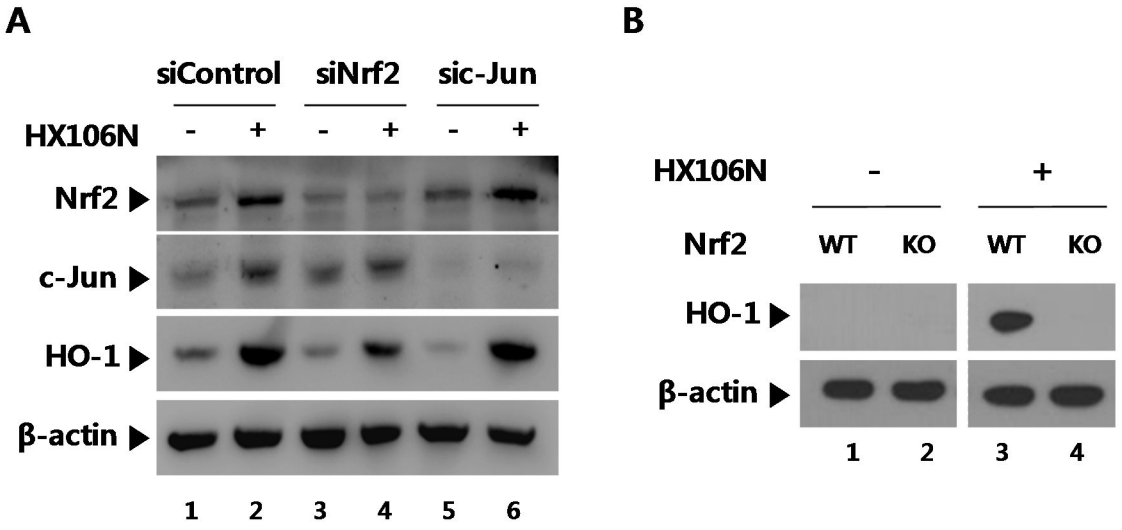

Figure 40. Roles of Nrf2 and c-Jun in HX106N-mediated HO-1 expression. (A) BV-2 cells were transfected with siRNA specific for Nrf2 or c-Jun, and then treated with 1 mg/mL HX106N for 6 h. Whole cell lysates were prepared followed by Western blot analysis to determine the protein level of Nrf2, c-Jun and HO-1. (B) Splenocytes were isolated from wild-type (WT) or Nrf2-knockout (KO) mice, and treated with 1 mg/mL HX106N for 24h. Total proteins were extracted and subjected to Western blot analysis using a specific antibody for HO-1. β-actin was used as a loading control.

BV-2 cells were treated with different concentrations of SP600125 or SB203580 in the presence of HX106N, the induction of HO-1 protein by HX106N was significantly reduced by 63% and 93%, respectively, in a dose-dependent manner at a 20 μM concentration (Figure 41A). The HX106N-mediated increase of HO-1 RNA was also attenuated by both inhibitors (data not shown). Treatment with PD98059 had little effect on the level of HO-1 expression, suggesting that JNK and p38 MAPK but not ERK were involved in HX106N-induced HO-1 expression (Figure 41B).

Effects of HX106N on JNK and p38 MAPK

To test the effects of HX106N on the activation of the JNK and p38 pathways, BV-2 cells were treated with 1 mg/mL HX106N, and total proteins were prepared at various time points followed by Western blot analysis. A marked increase in the phosphorylated JNK and p38 levels was observed after 15 min of HX106N treatment, which subsequently decreased over time (Figure 42). No significant change in the level of total JNK and p38 was observed (Figure 42). These data indicated that HX106N activated JNK and p38 signaling pathways.

Effects of chemical inhibitors of JNK and p38 MAPK on HX106N-mediated activation of Nrf2

Because MAPKs have been implicated in upstream signaling pathways leading to Nrf2 activation, the JNK and p38 signaling pathways were investigated for involvement in HX106N-mediated Nrf2 activation. BV-2 cells were treated with 20 μM SP600125 or SB203580 in the presence of 1 mg/mL HX106N for 6 h, and the nuclear extracts were isolated and analyzed by Western blot analysis for Nrf2. As shown in Figure 43A, HX106N-mediated nuclear accumulation of Nrf2 was not affected by

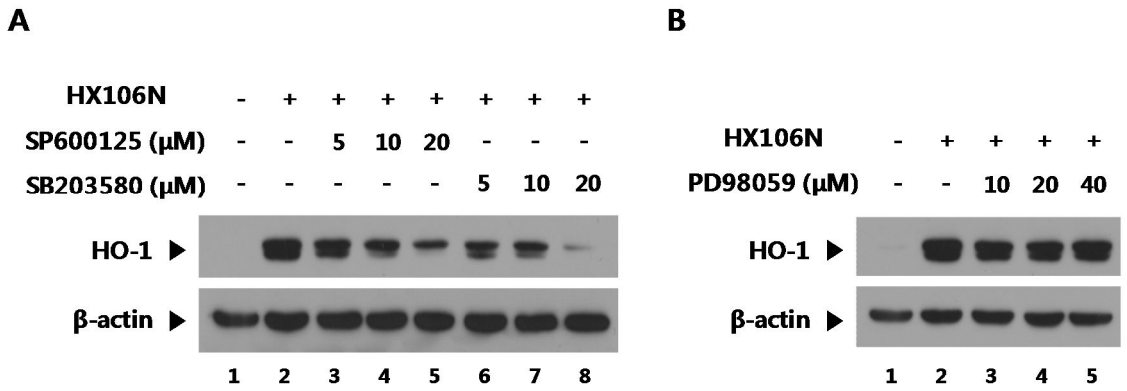

Figure 41. Effects of chemical inhibitors of MAPKs on HX106N-induced HO-1 expression. (A) BV-2 cells were treated with 1 mg/mL HX106N and various concentrations of SP600125 or SB203580, specific inhibitors for JNK or p38 MAPK, respectively. Twenty-four hours later, the total protein was extracted and subjected to Western blot analysis for the detection of HO-1 and β-actin. β-actin was used as a loading control. (B) The same experiment was performed using an ERK inhibitor, PD98059.

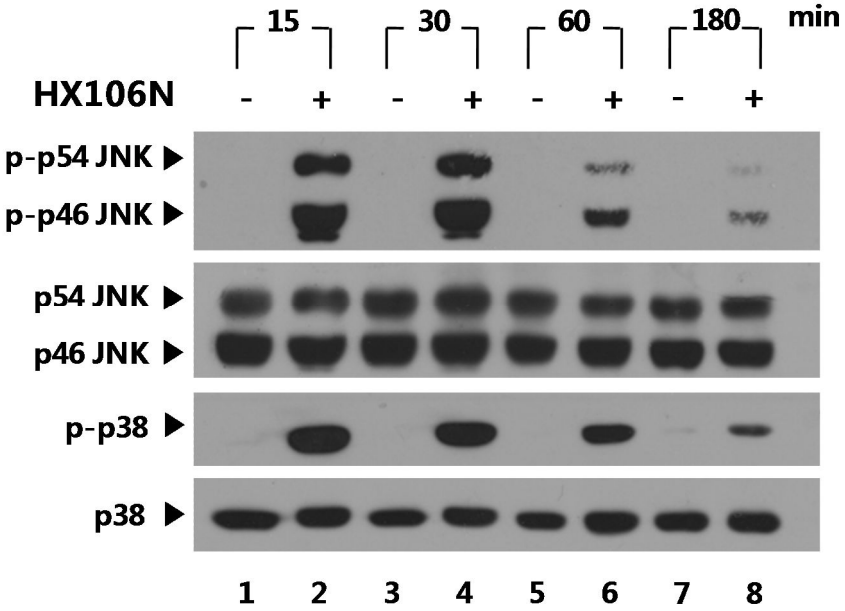

Figure 42. Effects of HX106N on the phosphorylation of JNK and p38 MAPK. BV-2 cells were treated with 1 mg/mL HX106N, and whole cell lysates were prepared at the indicated time points. The level of total and phosphorylated forms of JNK and p38 was determined by Western blot analysis.

treatment with SP600125 or SB203580.

To confirm the above results, the effect of specific inhibitors of JNK and p38 MAPK (SP600125 and SB203580, respectively) on Nrf2-mediated transcriptional activation was examined using a reporter plasmid containing StRE, pE1-Luc. BV-2 cells transfected with pE1-Luc were treated with respective inhibitors and HX106N for 9 h, and the luciferase activity was measured. Neither SP600125 nor SB203580 affected HX106N-mediated increase of luciferase activity (Figure 43B). These data suggested that JNK and p38 MAPK did not act as an upstream kinase in HX106N-mediated activation of Nrf2.

2.4 Effects of HX106N on NF-κB activation

Testing the involvement of NF-κB in HX106N-mediated induction of HO-1

It has been reported that NF-κB is important for HO-1 expression in response to diverse stimuli (Ryter et al., 2006, Alam and Cook, 2007). To test whether the inhibition of NF-κB activation has any effect on HX106N-induced HO-1 expression, BV-2 cells were treated with different concentrations of a pharmacological inhibitor for IκB kinase (IKK), BAY 11-7082, in the presence of 1 mg/mL HX106N for 24 h. Whole cell lysates were prepared and analyzed to measure the protein level of HO-1 by Western blot analysis. The expression of HO-1 protein was highly increased in the cells treated with HX106N, whereas treatment with BAY 11-7082 decreased the expression by 43% and 70% at 2.5 μM and 5 μM, respectively (Figure 44A). The increased RNA level of HO-1 was also reduced by 2.5 μM of BAY 11-7082 to 62% (data not shown). To confirm the above data, siRNA specific for IKKα (siIKKα) was transfected to BV-2 cells. The cells were treated with 1 mg/mL HX106N for 6 h, and total proteins were

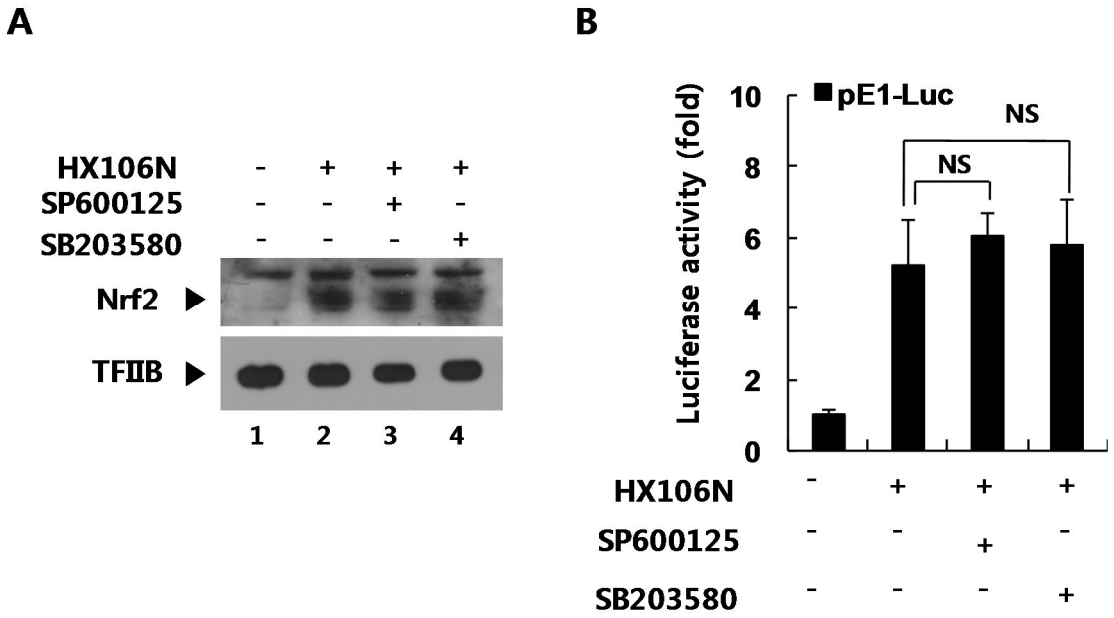

Figure 43. Effects of chemical JNK and p38 MAPK inhibitors on HX106N-mediated activation of Nrf2. (A) BV-2 cells were treated with 20 μM SP600125 or SB203580 in the presence of 1 mg/mL HX106N. After 6 h, nuclear proteins were extracted to measure the level of Nrf2 by Western blot analysis. TFIIB was used as a loading control for nuclear extracts. (B) Cells transfected with pE1-Luc were treated with 1 mg/mL HX106N and 20 μM of SP600125 or SB203580. After 9 h, cell lysates were prepared and subjected to a luciferase assay. The values are presented as the means ± SD of triplicate samples from one of three independent experiments. NS = non-significant compared to the HX106N-treated group.

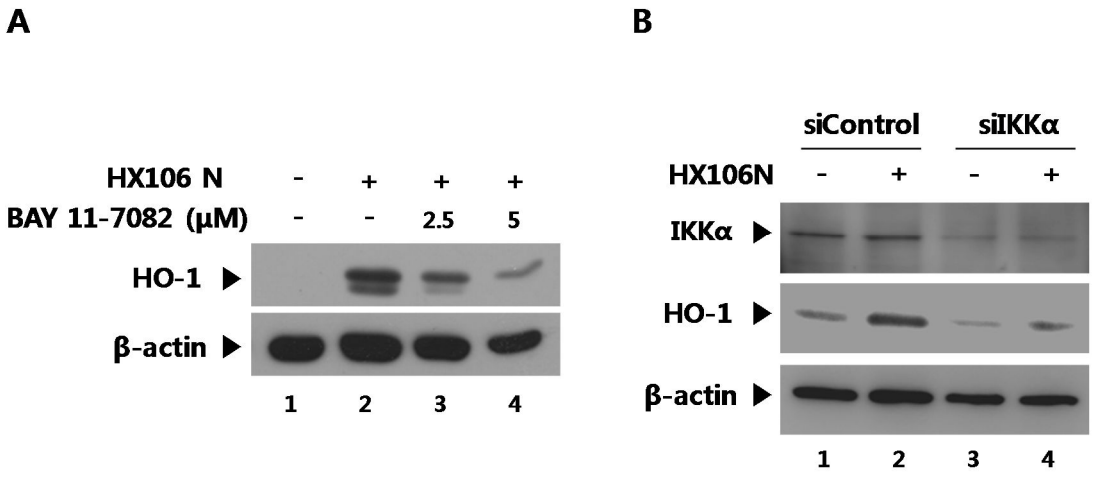

Figure 44. Roles of NF-κB in HX106N-mediated induction of HO-1. (A) BV-2 cells were treated with 1 mg/mL HX106N and 2.5 or 5 μM BAY 11-7802, an IKK inhibitor, for 24 h. Whole cell lysates were harvested and subjected to Western blot analysis for the detection of HO-1 and β-actin. β-actin was used as a loading control. (B) The siRNAs specific for IKKα and IKKβ were transfected to BV-2 cells, and the cells were treated with 1 mg/mL HX106N. After 6h, whole proteins were prepared and the protein level of IKKα, HO-1 and β-actin was measured by Western blot hybridization.

extracted to measure the levels of IKKα and HO-1 using Western blot analysis. As shown in Figure 44B, the protein level of IKKα was greatly reduced by siIKKα transfection. In these siIKKα-transfected cells, HX106N-mediated HO-1 induction was decreased by 54%, as compared to siControl-transfected cells (Figure 44B). These results demonstrated that the activation of NF-κB might contribute to HX106N-mediated HO-1 expression.

Effects of HX106N on the NF-κB pathway

To examine the effect of HX106N on the NF-κB signaling pathway, BV-2 cells were treated with 1 mg/mL HX106N, and total proteins were prepared at various time points for the detection of total and phosphorylated forms of IKK and IκB. As shown in Figure 45A, IKK phosphorylation was detected 15 min after HX106N treatment and returned to the basal level within 3 h. Consistent with the above results, a significant decrease in the level of IκB was observed between 15 min and 30 min of treatment with HX106N (Figure 45A).

The effect of HX106N on NF-κB activation was assessed by measuring the nuclear accumulation of the NF-κB p65 subunit. Nuclear extracts were prepared from BV-2 cells treated with 1 mg/mL HX106N for the indicated time periods in Figure 44B and subjected to Western blot analysis using an antibody specific for p65. The nuclear level of p65 was very low in the untreated cells but was strongly increased at all time points (1-6 h) (Figure 45B).

To confirm these observations with a gel retardation assay using an NF-κB oligonucleotide probe, BV-2 cells were treated with 1 mg/mL HX106N for 3 h, and the nuclear protein was extracted, followed by EMSA. The level of DNA-protein complex was very low in untreated cells but was dramatically increased by treatment with

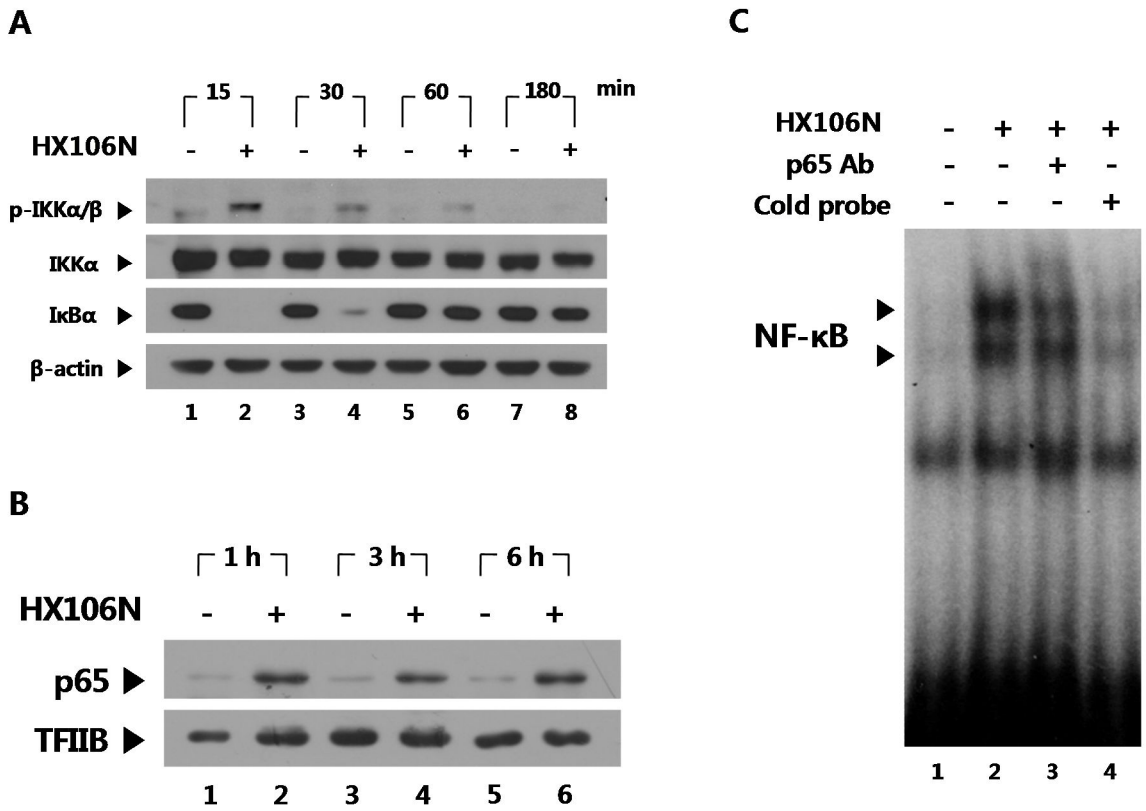

Figure 45. Effects of HX106N on the NF-κB signaling pathway. (A) The total protein was prepared from BV-2 cells treated with 1 mg/mL HX106N at the indicated time points. The level of phospho-IKKα/β, IKKα, IκBα, and β-actin was measured by Western blot analysis. (B) Cells were treated with 1 mg/mL HX106N for the indicated time periods, and nuclear proteins were extracted to determine the level of p65 and TFIIB by Western blot analysis. TFIIB was used as a loading control for the nuclear extracts. (C) Cells were treated with 1 mg/mL HX106N for 3 h. Nuclear extracts were prepared, and EMSA was conducted using a [^{32}P]-labeled NF-κB oligonucleotide as a probe. To perform the supershift/interference assays, an antibody specific for p65 was preincubated with the nuclear extracts for 30 min before adding the probe.

HX106N (Figure 45C). In the supershift/interference assay, addition of an antibody against p65 diminished the upper complex, indicating that the band was indeed the p65 subunit bound to the NF-κB oligonucleotide (Figure 45C). These results suggested that HX106N induced the activation of NF-κB.

Effects of chemical inhibitors of JNK and p38 MAPKs on HX106N-mediated activation of NF-κB

To test whether JNK and p38 MAPK were involved in HX106N-mediated NF-κB activation, BV-2 cells were treated with 20 μM SP600125 or SB203580 in the presence of 1 mg/mL HX106N. Six hours later, nuclear proteins were prepared, and Western blot analysis was performed to determine the level of p65. Treatment with both inhibitors had little effects on the HX106N-induced nuclear accumulation of p65 (Figure 46A).

It was also investigated whether SP600125 or SB203580 inhibitors has any effect on NF-κB-mediated transcriptional activity. BV-2 cells were transfected with a luciferase plasmid containing five copies of an NF-κB response element (pNF-κB-Luc), and treated with each inhibitor in the presence of 1 mg/mL HX106N for 9 h. The level of luciferase activity was elevated by 3.4-fold after HX106N treatment, while little changes were observed in the cells treated with SP600125 or SB203580 (Figure 46B). These data suggested that both of JNK and p38 were not associated with NF-κB activation.

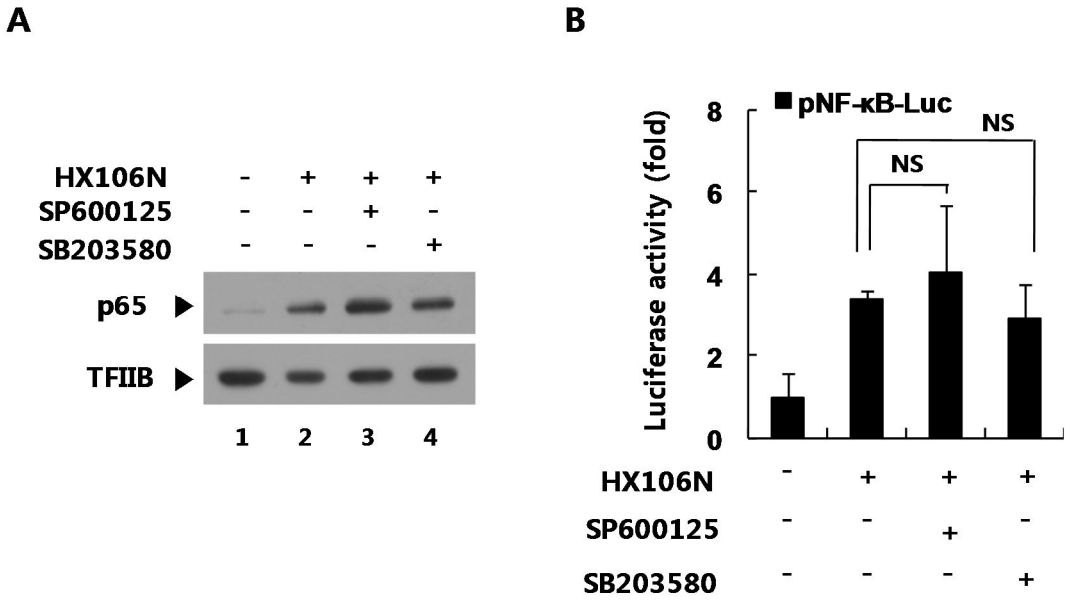

Figure 46. Effects of chemical inhibitors of JNK and p38 MAPK on HX106N-mediated activation of NF-κB. (A) BV-2 cells were treated with 20 μM SP600125 or SB203580 in the presence of 1 mg/mL HX106N for 6 h. Nuclear proteins were analyzed by Western blot analysis using specific antibodies for p65 and TFIIB. (B) Cells were transfected with a luciferase reporter plasmid containing NF-κB response element (pNF-κB-Luc). Twenty-four hours later, the cells were treated with 1 mg/mL HX106N and 20 μM of SP600125 or SB203580 for 9h, followed by a luciferase assay. The values are presented as the means ± SD of triplicate samples from one of three independent

3. Discussion

In this report, I demonstrated that HX106N reugulated the expression of HO-1 at the transcriptional level. Various cellular factors appeared to be involved in HX106N-mediated induction of the HO-1 gene, including Nrf2, NF-κB, JNK and p38 MAPK.

Nrf2 plays a crucial role in the increased expression of HO-1 by HX106N as evidenced by reduction of HO-1 induction when Nrf2-specific siRNA was used. Nrf2 is normally present in the cytoplasm in a combined form with Keap1 (Kelch-like ECH-associated protein 1) but when Nrf2 and Keap1 dissociate by various stimulations, Nrf2 translocates to the nucleus to activate the expression of a wide range of antioxidant genes (Trachootham et al., 2008, Surh et al., 2008). It was investigated which signal transduction pathway was used for activation of Nrf2, but had no success thus far. Virtually all kinases previously known to phosphorylate and activate Nrf2 did not seem to be involved in HX106N-mediated induction of HO-1 in the experiments involving the pharmacological inhibitors of MAPKs, phosphoinositide 3-kinase (PI3K), protein kinase C (PKC) and casein kinase 2 (CK2) (data not shown). Some chemopreventive agents directly oxidize or chemically modify the cysteine thiols of Keap1, leading to the dissociation of Keap1 and subsequent release of Nrf2 (Na and Surh, 2006, Dinkova-Kostova and Talalay, 2008). Therefore, it is possible that HX106N may contain compound(s) that directly modulates the Nrf2-Keap1 interaction without involving an upstream signaling pathway.

The expression of HO-1 is also reported to be regulated by NF-κB (Lu et al., 2010, Hill-Kapturczak et al., 2001, Juan et al., 2005). The activation of this transcription factor was found to be important in HX106N-mediated upregulation of HO-1, as shown in the experiments involving a pharmacological inhibitor or siRNA specific for IKK.

Since the functional NF-κB binding site has not been clearly identified in the HO-1 gene (Alam and Cook, 2007), further molecular studies to find the actual binding site for NF-κB that control HX106N-induced HO-1 gene expression would be of interest.

A variety of kinases have been identified to phosphorylate and activate transcription factors involved in regulation of HO-1 expression. It was demonstrated that JNK and p38 MAPK played a role(s) in HX106N-mediated HO-1 induction using a pharmacological inhibitor (SP600125 and SB203580) but could not find the actual transcription factor acting as their downstream mediator. It is likely that other transcription factors participate in HO-1 induction by HX106N, since the HO-1 promoter contains a variety of *cis*-acting elements, including c-AMP-responsive element (CRE), STAT and a heat shock element (Ryter et al., 2006). Both STAT3 and HSF-1 are regulated by JNK (Park and Liu, 2001, Lee et al., 2000), while the activation of CRE-binding protein by p38 MAPK was demonstrated to be involved in HO-1 expression induced by raloxifene, an estrogen receptor modulator (Lee et al., 2011). In the case of p38 MAPK, it is also possible that p38 MAPK contributes to HX106N-induced HO-1 expression without direct effect on transcription factors, because this protein is known to regulate the phosphorylation of TATA-binding protein (Carter et al., 1999).

HX106N was shown to regulate HO-1 expression probably through complex signaling pathways. In previous chapters 4 and 5, it was demonstrated that the induction of HO-1 was needed for the antioxidative activities of HX106N. In the context of the neuroprotective role(s) of HO-1, results from this study showed that HX106N might have a therapeutic potential to prevent or treat various neurodegenerative diseases.

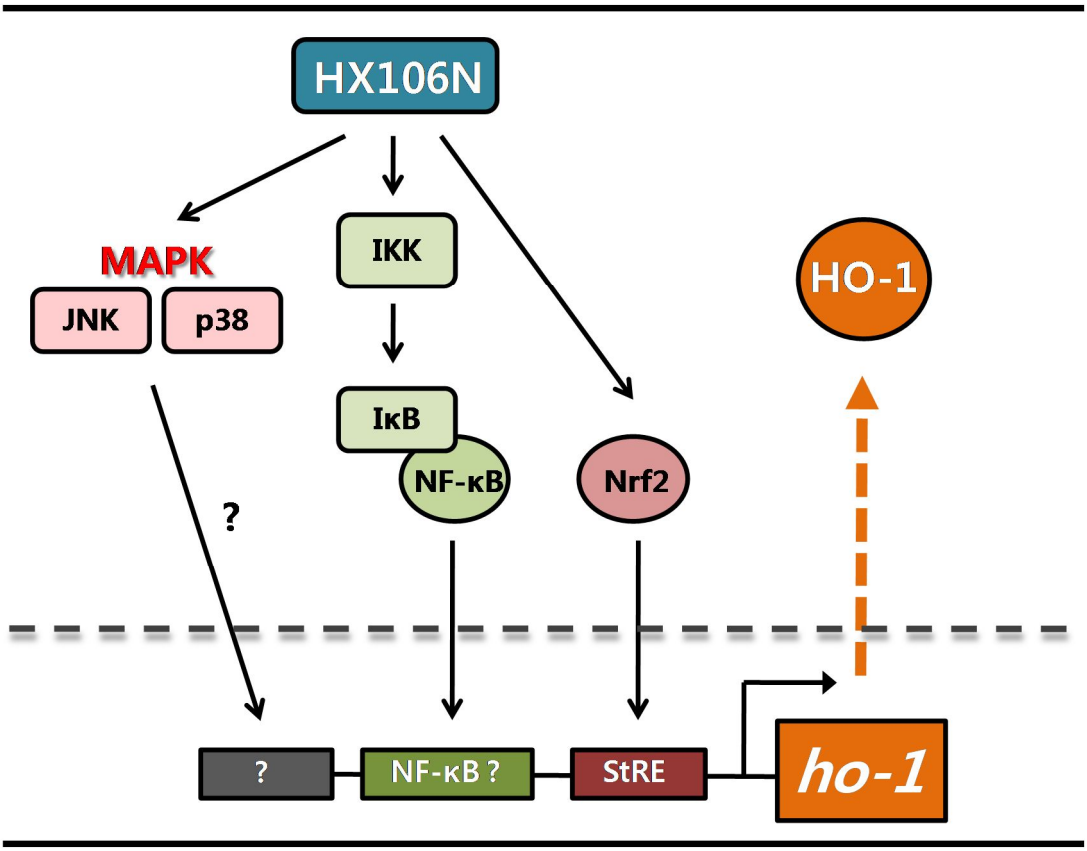

Figure 47. Schematic representation of the molecular mechanism of HX106N in this chapter. Various signaling pathways appeared to be involved in HX106N-mediated HO-1 induction. HX106N increased HO-1 expression through Nrf2-StRE pathway. Although the functional NF-κB binding site has not yet been identified in the HO-1 promoter, NF-κB pathway was shown to play a role(s) in HX106N-mediated induction of HO-1. Both JNK and p38 MAPK pathways contributed to HX106N-induced HO-1 expression through unknown mechanism(s).

CHAPTER VII

Conclusion

Dementia is characterized by loss of or decline in cognitive functions, including memory. With the rapid increase of elderly population around the world, dementia has become one of the most important burdens that society has to deal with. AD is the most common type of dementia, accounting for approximately 60-80 % of all cases. It has been believed that multiple factors are intertwined in the pathogenesis of AD, although exact mechanisms have not yet been fully elucidated. Currently available drugs for AD are known to be only symptomatic, and they do not prevent or slow down the progression of the disease (Yiannopoulou and Papageorgiou, 2013).

There are a number of documents and descriptions about the pathogenesis and treatments of dementia in TKM, and they are still being used to treat dementia patients in the healthcare system of Korea. A holistic approach that TKM is taking has advantages in treating dementia, as dementia is a chronic and complex disease caused by multiple pathological factors.

In this thesis research, I tried to develop a novel therapeutic agent for dementia, in particular for AD, on the basis of the knowledge and database from TKM. The pathologies of AD were reinterpreted in the perspective of TKM, and 4 plants targeting different pathological factors were selected to prepare a botanical formulation, named HX106N. As previously described in Chapter 3, HX106N was prepared in a reproducible manner, using newly developed bioassay systems based biological activities of HX106N. When HX106N was tested in two animal models of AD-type amnesia, a significant level of therapeutic effects was observed. Then, a series of experiments were carried out to understand the underlying mechanisms of HX106N.

In $A\beta_{25-35}$-induced amnesia animal model, oral administration of HX106N significantly improved memory impairment in both the Y-maze alternation and passive avoidance tests. In this model, memory deficits are known to be caused mainly by

oxidative stress (Alam and Cook, 2007, Hiramatsu et al., 2010). By measuring the level of TBARS, an indicator of lipid peroxidation, showed that HX106N inhibited oxidative damage in the hippocampus and cortex in $A\beta_{25-35}$-injected mice. The level of HO-1 in the hippocampus of mice was found to be maintained at a relatively high level in mice treated with HX106N, which might have contributed to the antioxidative effects of HX106N against oxidative stress induced by $A\beta_{25-35}$ injection.

Treatment with HX106N also ameliorated the cholinergic amnesia caused by injection of scopolamine, a muscarinic acetylcholine receptor antagonist, in mice. AChE activity was shown to be significantly reduced in the hippocampus and cortex of mice at one hour after oral administration of HX106N. Because cholinergic amnesia is known to be improved by preventing ACh breakdown through AChE inhibition (Hirai, 2000), the ameliorating effects of HX106N might be a result of its AChE inhibitory activity. Taken together, these data demonstrated that HX106N might improve the major pathologies associated with cognitive impairment in AD patients.

The antioxidative activities and working mechanisms of HX106N were investigated at the cellular and molecular level, using microglial and neuronal cells. HX106N effectively suppressed LPS-induced production of NO by inhibiting the expression of iNOS in BV-2 and primary microglia cells. The regulation of iNOS expression appears to occur at the post-transcriptional level, and this step needed *de novo* protein synthesis. NO production was also found to be regulated by HX106N-mediated induction of HO-1 and its enzymatic byproduct CO, particularly.

HX106N showed strong neuroprotective effects against glutamate-induced oxidative neurotoxicity in HT22 cells and primary cortical neurons. Significant decrease in ROS production was observed when cells were treated with HX106N, while the level of intracellular GSH was not affected. Although several Nrf2-dependent antioxidant

enzymes, including HO-1, NQO1 and GCLm, were increased by HX106N, they were not found to be involved in the neuroprotective effecs of HX106N. These data indicated that there might be other mechanisms responsible for its neuroprotective effects. For example, HX106N might directly scavenge ROS or act on the downstream signaling of GSH depletion.

Multiple signaling pathways were found to be involved in HX106N-mediated expression of HO-1. HX106N regulated the expression of HO-1 at the transcriptional level, probably using the StRE present in the HO-1 promoter. Data from siRNA knockdown experiments showed that only Nrf2 played a pivotal role in HX106N-activated induction of HO-1, although HX106N could activate both Nrf2 and AP-1, well-known transcription factors needed for HO-1 gene expression through StRE.

HX106N also activated NF-κB signaling pathway. Although a functional binding site for NF-κB in the HO-1 promoter has not yet been identified (Alam and Cook, 2007), NF-κB was found to be involved in HX106N-induced HO-1 expression. These results indicated that NF-κB might regulate HO-1 expression through interaction with other transcription regulators rather than directly binding to a canonical NF-κB binding site.

Data from the experiments using pharmacological inhibitors showed that JNK and p38 played a role(s) in HO-1 induction by HX106N. However they did not acted as upstream kinases of Nrf2 and NF-κB, suggesting a possible involvement of other transcription factors.

In this thesis research, I suggested that the anti-amnesic and antioxidative effects of HX106N and its underlying molecular mechanisms. Although the active compound(s) in HX106N remains to be identified, I was able to make HX106N with consistent activities using the cell-based bioassay systems. Acute or repeated-dose toxicity studies

in rats and dogs, have not shown any toxic effects of HX106N (unpublished data). Taken together, these results demonstrated that HX106N might be a potential starting point for developing appropriate therapeutic agents for various neurodegenerative diseases, including AD. Recently, an 8-week randomized, double-blind, placebo-controlled human trial of HX106N involving 75 individuals with subjective memory complaints, has been completed by clinical investigators. A significant improvement in working memory performance, the primary outcome of this study, was observed at 8 weeks after oral administration of HX106N. Based on these results, HX106N was applied to Korea FDA for the status of new health claim nutraceutical that can improve memory functions. I am now trying to concentrate bioacitivities of HX106N and further identify its active compound(s) with an aim at developing HX106N as a drug. I hope that my thesis contributes not only to the development of interesting therapeutic agents for improving cognitive functions but also to show the power of using TKM knowledge and database for the development of new and innovative therapeutics.

Figure 48. Hypothesis for the possible action mechanism of HX106N. HX106N showed great therapeutic potential for AD, through its antioxidative and anti-amnesic effects. HX106N suppressed the production of NO by controlling the level of iNOS RNA in microglia cells. NO production was also regulated by HX106N-mediated induction of HO-1. In neuronal cells, HX106N exerted neuroprotective activities against glutamate-induced oxidative neurotoxicity. In addition, HX106N had significant inhibitory effects on AChE activity. This diverse array of mechanisms of HX106N might contribute to the therapeutic effects of HX106N in senile dementia, like AD.

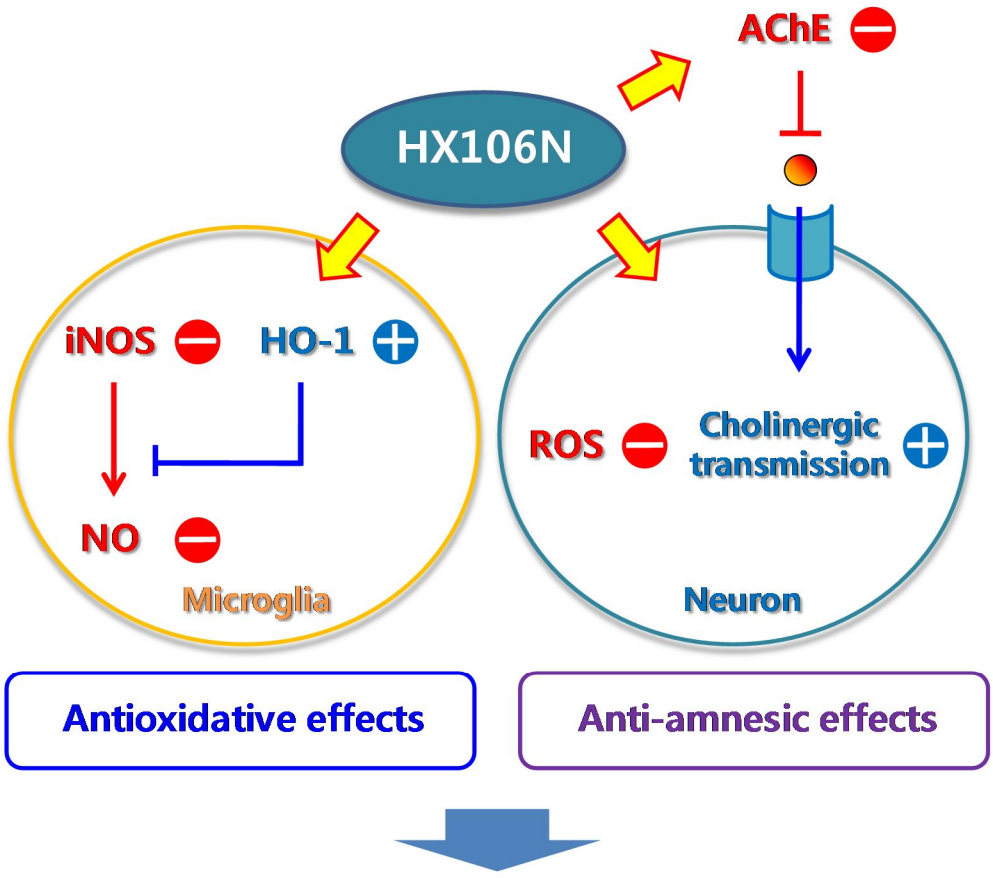
AChE
HX106N
iNOS
HO-1
NO
Microglia
ROS
Cholinergic transmission
Neuron
Antioxidative effects
Anti-amnesic effects
Therapeutic effects on senile dementia
(Alzheimer's disease)

REFERENCES

1. Assoc A. Alzheimer's Association Report 2011 Alzheimer's disease facts and figures. *Alzheimers & Dementia*. 2011;**7**:208-44.
2. Cho MJ, Lee JY, Kim BS, Lee HW, Sohn JH. Prevalence of the major mental disorders among the Korean elderly. *J Korean Med Sci*. 2011;**26**:1-10.
3. Petersen RC. Mild cognitive impairment: transition between aging and Alzheimer's disease. *Neurologia*. 2000;**15**:93-101.
4. Tanzi RE. Alzheimer's disease and related dementias: the road to intervention. *Exp Gerontol*. 2000;**35**:433-7.
5. Hebert LE, Scherr PA, Bienias JL, Bennett DA, Evans DA. State-specific projections through 2025 of Alzheimer disease prevalence. *Neurology*. 2004;**62**:1645.
6. Kim KW, Park JH, Kim MH, Kim MD, Kim BJ, Kim SK, Kim JL, Moon SW, Bae JN, Woo JI, Ryu SH, Yoon JC, Lee NJ, Lee DY, Lee DW, Lee SB, Lee JJ, Lee JY, Lee CU, Chang SM, Jhoo JH, Cho MJ. A nationwide survey on the prevalence of dementia and mild cognitive impairment in South Korea. *J Alzheimers Dis*. 2011;**23**:281-91.
7. Thies W, Bleiler L, Assoc As. 2013 Alzheimer's disease facts and figures Alzheimer's Association. *Alzheimers & Dementia*. 2013;**9**:208-45.
8. Grossman H, Bergmann C, Parker S. Dementia: a brief review. *Mt Sinai J Med*. 2006;**73**:985-92.
9. Mattson MP. Pathways towards and away from Alzheimer's disease. *Nature*. 2004;**430**:631-9.
10. Korczyn AD. Why have we failed to cure Alzheimer's disease? *J Alzheimers Dis*. 2012;**29**:275-82.
11. Liu J, Wang LN, Tian JZ. Recognition of dementia in ancient China. *Neurobiol*

Aging. 2012;**33**:2948 e11-3.

12. Hardy J, Allsop D. Amyloid deposition as the central event in the aetiology of Alzheimer's disease. *Trends Pharmacol Sci*. 1991;**12**:383-8.

13. Schubert D, Behl C, Lesley R, Brack A, Dargusch R, Sagara Y, Kimura H. Amyloid peptides are toxic via a common oxidative mechanism. *Proc Natl Acad Sci U S A*. 1995;**92**:1989-93.

14. Akiyama H, Barger S, Barnum S, Bradt B, Bauer J, Cole GM, Cooper NR, Eikelenboom P, Emmerling M, Fiebich BL, Finch CE, Frautschy S, Griffin WS, Hampel H, Hull M, Landreth G, Lue L, Mrak R, Mackenzie IR, McGeer PL, O'Banion MK, Pachter J, Pasinetti G, Plata-Salaman C, Rogers J, Rydel R, Shen Y, Streit W, Strohmeyer R, Tooyoma I, Van Muiswinkel FL, Veerhuis R, Walker D, Webster S, Wegrzyniak B, Wenk G, Wyss-Coray T. Inflammation and Alzheimer's disease. *Neurobiol Aging*. 2000;**21**:383-421.

15. Mattson MP, Cheng B, Davis D, Bryant K, Lieberburg I, Rydel RE. beta-Amyloid peptides destabilize calcium homeostasis and render human cortical neurons vulnerable to excitotoxicity. *J Neurosci*. 1992;**12**:376-89.

16. Hooper NM, Turner AJ. The search for alpha-secretase and its potential as a therapeutic approach to Alzheimer s disease. *Curr Med Chem*. 2002;**9**:1107-19.

17. Sinha S, Lieberburg I. Cellular mechanisms of beta-amyloid production and secretion. *Proc Natl Acad Sci U S A*. 1999;**96**:11049-53.

18. Hardy J. Amyloid, the presenilins and Alzheimer's disease. *Trends Neurosci*. 1997;**20**:154-9.

19. Haass C, Lemere CA, Capell A, Citron M, Seubert P, Schenk D, Lannfelt L, Selkoe DJ. The Swedish mutation causes early-onset Alzheimer's disease by beta-secretase cleavage within the secretory pathway. *Nat Med*. 1995;**1**:1291-6.

20. Mandelkow EM, Stamer K, Vogel R, Thies E, Mandelkow E. Clogging of axons by tau, inhibition of axonal traffic and starvation of synapses. *Neurobiol Aging*. 2003;**24**:1079-85.

21. Busciglio J, Lorenzo A, Yeh J, Yankner BA. beta-amyloid fibrils induce tau phosphorylation and loss of microtubule binding. *Neuron*. 1995;**14**:879-88.

22. Calhoun ME, Wiederhold KH, Abramowski D, Phinney AL, Probst A, Sturchler-Pierrat C, Staufenbiel M, Sommer B, Jucker M. Neuron loss in APP transgenic mice. *Nature*. 1998;**395**:755-6.

23. Francis PT, Palmer AM, Snape M, Wilcock GK. The cholinergic hypothesis of Alzheimer's disease: a review of progress. *J Neurol Neurosurg Psychiatry*. 1999;**66**:137-47.

24. Terry AV, Jr., Buccafusco JJ. The cholinergic hypothesis of age and Alzheimer's disease-related cognitive deficits: recent challenges and their implications for novel drug development. *J Pharmacol Exp Ther*. 2003;**306**:821-7.

25. Markesbery WR. The role of oxidative stress in Alzheimer disease. *Arch Neurol*. 1999;**56**:1449-52.

26. Wyss-Coray T, Rogers J. Inflammation in Alzheimer disease-a brief review of the basic science and clinical literature. *Cold Spring Harb Perspect Med*. 2012;**2**:a006346.

27. Liu B, Hong JS. Role of microglia in inflammation-mediated neurodegenerative diseases: mechanisms and strategies for therapeutic intervention. *J Pharmacol Exp Ther*. 2003;**304**:1-7.

28. Rogers J, Luber-Narod J, Styren SD, Civin WH. Expression of immune system-associated antigens by cells of the human central nervous system: relationship to the pathology of Alzheimer's disease. *Neurobiol Aging*. 1988;**9**:339-49.

29. Butterfield DA, Pocernich CB. The glutamatergic system and Alzheimer's disease: therapeutic implications. *CNS Drugs*. 2003;**17**:641-52.

30. Sattler R, Tymianski M. Molecular mechanisms of glutamate receptor-mediated excitotoxic neuronal cell death. *Mol Neurobiol*. 2001;**24**:107-29.

31. Schubert D, Piasecki D. Oxidative glutamate toxicity can be a component of the excitotoxicity cascade. *J Neurosci*. 2001;**21**:7455-62.

32. Murphy TH, Schnaar RL, Coyle JT. Immature cortical neurons are uniquely sensitive to glutamate toxicity by inhibition of cystine uptake. *Faseb J*. 1990;**4**:1624-33.

33. Costantini LC, Barr LJ, Vogel JL, Henderson ST. Hypometabolism as a therapeutic target in Alzheimer's disease. *BMC Neurosci*. 2008;**9 Suppl 2**:S16.

34. Landau SM, Harvey D, Madison CM, Koeppe RA, Reiman EM, Foster NL, Weiner MW, Jagust WJ. Associations between cognitive, functional, and FDG-PET measures of decline in AD and MCI. *Neurobiol Aging*. 2011;**32**:1207-18.

35. Rogers SL, Farlow MR, Doody RS, Mohs R, Friedhoff LT. A 24-week, double-blind, placebo-controlled trial of donepezil in patients with Alzheimer's disease. Donepezil Study Group. *Neurology*. 1998;**50**:136-45.

36. Rosler M, Anand R, Cicin-Sain A, Gauthier S, Agid Y, Dal-Bianco P, Stahelin HB, Hartman R, Gharabawi M. Efficacy and safety of rivastigmine in patients with Alzheimer's disease: international randomised controlled trial. *BMJ*. 1999;**318**:633-8.

37. Tariot PN, Solomon PR, Morris JC, Kershaw P, Lilienfeld S, Ding C. A 5-month, randomized, placebo-controlled trial of galantamine in AD. The Galantamine USA-10 Study Group. *Neurology*. 2000;**54**:2269-76.

38. Alfirevic A, Mills T, Carr D, Barratt BJ, Jawaid A, Sherwood J, Smith JC,

Tugwood J, Hartkoorn R, Owen A, Park KB, Pirmohamed M. Tacrine-induced liver damage: an analysis of 19 candidate genes. *Pharmacogenet Genomics*. 2007;**17**:1091-100.

39. Kihara T, Shimohama S, Sawada H, Kimura J, Kume T, Kochiyama H, Maeda T, Akaike A. Nicotinic receptor stimulation protects neurons against beta-amyloid toxicity. *Ann Neurol*. 1997;**42**:159-63.

40. Zamani MR, Allen YS, Owen GP, Gray JA. Nicotine modulates the neurotoxic effect of beta-amyloid protein(25-35)) in hippocampal cultures. *Neuroreport*. 1997;**8**:513-7.

41. Meunier J, Ieni J, Maurice T. The anti-amnesic and neuroprotective effects of donepezil against amyloid beta25-35 peptide-induced toxicity in mice involve an interaction with the sigma1 receptor. *Br J Pharmacol*. 2006;**149**:998-1012.

42. McShane R, Areosa Sastre A, Minakaran N. Memantine for dementia. *Cochrane Database Syst Rev*. 2006:CD003154.

43. Reisberg B, Doody R, Stoffler A, Schmitt F, Ferris S, Mobius HJ. Memantine in moderate-to-severe Alzheimer's disease. *N Engl J Med*. 2003;**348**:1333-41.

44. Yiannopoulou KG, Papageorgiou SG. Current and future treatments for Alzheimer's disease. *Ther Adv Neurol Disord*. 2013;**6**:19-33.

45. Schneider LS, Mangialasche F, Andreasen N, Feldman H, Giacobini E, Jones R, Mantua V, Mecocci P, Pani L, Winblad B, Kivipelto M. Clinical trials and late-stage drug development for Alzheimer's disease: an appraisal from 1984 to 2014. *J Intern Med*. 2014;**275**:251-83.

46. Hey J, Koelsch G, Bilcer G, Jacobs A, Tolar M, Tang J, Ghosh A, Hsu H, editors. Single dose administration of the β-secretase inhibitor CTS21166 (ASP1702) reduces plasma Aβ40 in human subjects. International Conference on

Alzheimer's Disease (ICAD), Chicago, IL; 2008.

47. Imbimbo BP, Giardina GA. gamma-secretase inhibitors and modulators for the treatment of Alzheimer's disease: disappointments and hopes. *Curr Top Med Chem*. 2011;**11**:1555-70.

48. Schenk D, Barbour R, Dunn W, Gordon G, Grajeda H, Guido T, Hu K, Huang J, Johnson-Wood K, Khan K, Kholodenko D, Lee M, Liao Z, Lieberburg I, Motter R, Mutter L, Soriano F, Shopp G, Vasquez N, Vandevert C, Walker S, Wogulis M, Yednock T, Games D, Seubert P. Immunization with amyloid-beta attenuates Alzheimer-disease-like pathology in the PDAPP mouse. *Nature*. 1999;**400**:173-7.

49. Janus C, Pearson J, McLaurin J, Mathews PM, Jiang Y, Schmidt SD, Chishti MA, Horne P, Heslin D, French J, Mount HT, Nixon RA, Mercken M, Bergeron C, Fraser PE, St George-Hyslop P, Westaway D. A beta peptide immunization reduces behavioural impairment and plaques in a model of Alzheimer's disease. *Nature*. 2000;**408**:979-82.

50. Salloway S, Sperling R, Fox NC, Blennow K, Klunk W, Raskind M, Sabbagh M, Honig LS, Porsteinsson AP, Ferris S, Reichert M, Ketter N, Nejadnik B, Guenzler V, Miloslavsky M, Wang D, Lu Y, Lull J, Tudor IC, Liu E, Grundman M, Yuen E, Black R, Brashear HR. Two phase 3 trials of bapineuzumab in mild-to-moderate Alzheimer's disease. *N Engl J Med*. 2014;**370**:322-33.

51. Doody RS, Thomas RG, Farlow M, Iwatsubo T, Vellas B, Joffe S, Kieburtz K, Raman R, Sun X, Aisen PS, Siemers E, Liu-Seifert H, Mohs R. Phase 3 trials of solanezumab for mild-to-moderate Alzheimer's disease. *N Engl J Med*. 2014;**370**:311-21.

52. Park SJ, Park DH, Kim DH, Lee S, Yoon BH, Jung WY, Lee KT, Cheong JH, Ryu JH. The memory-enhancing effects of Euphoria longan fruit extract in mice.

J Ethnopharmacol. 2010;**128**:160-5.

53. Hur J, Lee P, Moon E, Kang I, Kim SH, Oh MS, Kim SY. Neurite outgrowth induced by spicatoside A, a steroidal saponin, via the tyrosine kinase A receptor pathway. *Eur J Pharmacol*. 2009;**620**:9-15.

54. Zhao GR, Xiang ZJ, Ye TX, Yuan YJ, Guo ZX. Antioxidant activities of Salvia miltiorrhiza and Panax notoginseng. *Food Chem*. 2006;**99**:767-74.

55. Kim JS, Narula AS, Jobin C. Salvia miltiorrhiza water-soluble extract, but not its constituent salvianolic acid B, abrogates LPS-induced NF-kappa B signalling in intestinal epithelial cells. *Clin Exp Immunol*. 2005;**141**:288-97.

56. Kim HJ, Moon KD, Oh SY, Kim SP, Lee SR. Ether fraction of methanol extracts of Gastrodia elata, a traditional medicinal herb, protects against kainic acid-induced neuronal damage in the mouse hippocampus. *Neurosci Lett*. 2001;**314**:65-8.

57. Kosasa T, Kuriya Y, Matsui K, Yamanishi Y. Effect of donepezil hydrochloride (E2020) on basal concentration of extracellular acetylcholine in the hippocampus of rats. *Eur J Pharmacol*. 1999;**380**:101-7.

58. Maurice T, Lockhart BP, Privat A. Amnesia induced in mice by centrally administered beta-amyloid peptides involves cholinergic dysfunction. *Brain Res*. 1996;**706**:181-93.

59. Johnson KA, Minoshima S, Bohnen NI, Donohoe KJ, Foster NL, Herscovitch P, Karlawish JH, Rowe CC, Carrillo MC, Hartley DM, Hedrick S, Pappas V, Thies WH. Appropriate Use Criteria for Amyloid PET: A Report of the Amyloid Imaging Task Force, the Society of Nuclear Medicine and Molecular Imaging, and the Alzheimer's Association. *Journal of Nuclear Medicine*. 2013;**54**:476-90.

60. Saura J, Tusell JM, Serratosa J. High-yield isolation of murine microglia by mild

trypsinization. *Glia*. 2003;**44**:183-9.

61. Koh K, Cha Y, Kim S, Kim J. tBHQ inhibits LPS-induced microglial activation via Nrf2-mediated suppression of p38 phosphorylation. *Biochem Biophys Res Commun*. 2009;**380**:449-53.

62. Xie QW, Whisnant R, Nathan C. Promoter of the mouse gene encoding calcium-independent nitric oxide synthase confers inducibility by interferon gamma and bacterial lipopolysaccharide. *J Exp Med*. 1993;**177**:1779-84.

63. Juurlink BH, Schultke E, Hertz L. Glutathione release and catabolism during energy substrate restriction in astrocytes. *Brain Res*. 1996;**710**:229-33.

64. Kweon MN, Fujihashi K, VanCott JL, Higuchi K, Yamamoto M, McGhee JR, Kiyono H. Lack of orally induced systemic unresponsiveness in IFN-gamma knockout mice. *J Immunol*. 1998;**160**:1687-93.

65. Zhong XK, Li DC, Jiang JG. Identification and quality control of Chinese medicine based on the fingerprint techniques. *Curr Med Chem*. 2009;**16**:3064-75.

66. Kim D, Kim SH, Park EJ, Kang CY, Cho SH, Kim S. Anti-allergic effects of PG102, a water-soluble extract prepared from Actinidia arguta, in a murine ovalbumin-induced asthma model. *Clin Exp Allergy*. 2009;**39**:280-9.

67. Choi J, Kim SH, Kim S. Suppressive effects of PG201, an antiarthritic botanical formulation, on lipopolysaccharide-induced inflammatory mediators in Raw264.7 cells. *Exp Biol Med (Maywood)*. 2012;**237**:499-508.

68. Kim D, Choi J, Kim MJ, Kim SH, Cho SH, Kim S. Reconstitution of anti-allergic activities of PG102 derived from Actinidia arguta by combining synthetic chemical compounds. *Exp Biol Med (Maywood)*. 2013;**238**:631-40.

69. Lee J, Kim D, Choi J, Choi H, Ryu JH, Jeong J, Park EJ, Kim SH, Kim S. Dehydrodiconiferyl alcohol isolated from Cucurbita moschata shows anti-

adipogenic and anti-lipogenic effects in 3T3-L1 cells and primary mouse embryonic fibroblasts. *J Biol Chem*. 2012;**287**:8839-51.

70. Brown GC, Bal-Price A. Inflammatory neurodegeneration mediated by nitric oxide, glutamate, and mitochondria. *Mol Neurobiol*. 2003;**27**:325-55.

71. Coyle JT, Puttfarcken P. Oxidative stress, glutamate, and neurodegenerative disorders. *Science*. 1993;**262**:689-95.

72. Hirai S. Alzheimer disease: current therapy and future therapeutic strategies. *Alzheimer Dis Assoc Disord*. 2000;**14 Suppl 1**:S11-7.

73. Tanzi RE, Bertram L. Twenty years of the Alzheimer's disease amyloid hypothesis: a genetic perspective. *Cell*. 2005;**120**:545-55.

74. Walsh DM, Selkoe DJ. Deciphering the molecular basis of memory failure in Alzheimer's disease. *Neuron*. 2004;**44**:181-93.

75. Butterfield DA, Castegna A, Lauderback CM, Drake J. Evidence that amyloid beta-peptide-induced lipid peroxidation and its sequelae in Alzheimer's disease brain contribute to neuronal death. *Neurobiol Aging*. 2002;**23**:655-64.

76. Rogers J, Webster S, Lue LF, Brachova L, Civin WH, Emmerling M, Shivers B, Walker D, McGeer P. Inflammation and Alzheimer's disease pathogenesis. *Neurobiol Aging*. 1996;**17**:681-6.

77. Tuppo EE, Arias HR. The role of inflammation in Alzheimer's disease. *Int J Biochem Cell Biol*. 2005;**37**:289-305.

78. Block ML, Zecca L, Hong JS. Microglia-mediated neurotoxicity: uncovering the molecular mechanisms. *Nat Rev Neurosci*. 2007;**8**:57-69.

79. Medeiros R, Prediger RD, Passos GF, Pandolfo P, Duarte FS, Franco JL, Dafre AL, Di Giunta G, Figueiredo CP, Takahashi RN, Campos MM, Calixto JB. Connecting TNF-alpha signaling pathways to iNOS expression in a mouse

model of Alzheimer's disease: relevance for the behavioral and synaptic deficits induced by amyloid beta protein. *J Neurosci*. 2007;**27**:5394-404.

80. Wilkinson BL, Landreth GE. The microglial NADPH oxidase complex as a source of oxidative stress in Alzheimer's disease. *J Neuroinflammation*. 2006;**3**:30.

81. Jomova K, Vondrakova D, Lawson M, Valko M. Metals, oxidative stress and neurodegenerative disorders. *Mol Cell Biochem*. 2010;**345**:91-104.

82. Gandhi S, Abramov AY. Mechanism of oxidative stress in neurodegeneration. *Oxid Med Cell Longev*. 2012;**2012**:428010.

83. Sarter M, Parikh V. Choline transporters, cholinergic transmission and cognition. *Nat Rev Neurosci*. 2005;**6**:48-56.

84. Benzi G, Moretti A. Is there a rationale for the use of acetylcholinesterase inhibitors in the therapy of Alzheimer's disease? *Eur J Pharmacol*. 1998;**346**:1-13.

85. Yamada K, Nabeshima T. Animal models of Alzheimer's disease and evaluation of anti-dementia drugs. *Pharmacol Ther*. 2000;**88**:93-113.

86. Lockhart BP, Benicourt C, Junien JL, Privat A. Inhibitors of free radical formation fail to attenuate direct beta-amyloid25-35 peptide-mediated neurotoxicity in rat hippocampal cultures. *J Neurosci Res*. 1994;**39**:494-505.

87. Maurice T, Lockhart BP, Privat A. Amnesia induced in mice by centrally administered beta-amyloid peptides involves cholinergic dysfunction. *Brain Res*. 1996;**706**:181-93.

88. Hardy J, Selkoe DJ. The amyloid hypothesis of Alzheimer's disease: progress and problems on the road to therapeutics. *Science*. 2002;**297**:353-6.

89. Sze CI, Troncoso JC, Kawas C, Mouton P, Price DL, Martin LJ. Loss of the

presynaptic vesicle protein synaptophysin in hippocampus correlates with cognitive decline in Alzheimer disease. *J Neuropathol Exp Neurol*. 1997;**56**:933-44.

90. Minogue AM, Schmid AW, Fogarty MP, Moore AC, Campbell VA, Herron CE, Lynch MA. Activation of the c-Jun N-terminal kinase signaling cascade mediates the effect of amyloid-beta on long term potentiation and cell death in hippocampus: a role for interleukin-1beta? *J Biol Chem*. 2003;**278**:27971-80.

91. Wang Q, Wu J, Rowan MJ, Anwyl R. Beta-amyloid inhibition of long-term potentiation is mediated via tumor necrosis factor. *Eur J Neurosci*. 2005;**22**:2827-32.

92. Ryter SW, Alam J, Choi AM. Heme oxygenase-1/carbon monoxide: from basic science to therapeutic applications. *Physiol Rev*. 2006;**86**:583-650.

93. Klinkenberg I, Blokland A. The validity of scopolamine as a pharmacological model for cognitive impairment: a review of animal behavioral studies. *Neurosci Biobehav Rev*. 2010;**34**:1307-50.

94. Schipper HM, Cisse S, Stopa EG. Expression of heme oxygenase-1 in the senescent and Alzheimer-diseased brain. *Ann Neurol*. 1995;**37**:758-68.

95. Chen K, Gunter K, Maines MD. Neurons overexpressing heme oxygenase-1 resist oxidative stress-mediated cell death. *J Neurochem*. 2000;**75**:304-13.

96. Le WD, Xie WJ, Appel SH. Protective role of heme oxygenase-1 in oxidative stress-induced neuronal injury. *J Neurosci Res*. 1999;**56**:652-8.

97. Mukherjee PK, Kumar V, Mal M, Houghton PJ. Acetylcholinesterase inhibitors from plants. *Phytomedicine*. 2007;**14**:289-300.

98. Tran MH, Yamada K, Nabeshima T. Amyloid beta-peptide induces cholinergic dysfunction and cognitive deficits: a minireview. *Peptides*. 2002;**23**:1271-83.

99. Park J, Lee C. The encyclopedia of medicinal plants. *Shinilbooks, Seoul*. 2000:363-4.

100. Kang B, Ko E, No S, Park Y, Seo B, Seo Y. Herbology2000.

101. Uttara B, Singh AV, Zamboni P, Mahajan RT. Oxidative stress and neurodegenerative diseases: a review of upstream and downstream antioxidant therapeutic options. *Curr Neuropharmacol*. 2009;**7**:65-74.

102. Tan S, Schubert D, Maher P. Oxytosis: A novel form of programmed cell death. *Curr Top Med Chem*. 2001;**1**:497-506.

103. Murphy TH, Miyamoto M, Sastre A, Schnaar RL, Coyle JT. Glutamate toxicity in a neuronal cell line involves inhibition of cystine transport leading to oxidative stress. *Neuron*. 1989;**2**:1547-58.

104. Ho YS, Magnenat JL, Gargano M, Cao J. The nature of antioxidant defense mechanisms: a lesson from transgenic studies. *Environ Health Perspect*. 1998;**106 Suppl 5**:1219-28.

105. Stocker R, Yamamoto Y, Mcdonagh AF, Glazer AN, Ames BN. Bilirubin Is an Antioxidant of Possible Physiological Importance. *Science*. 1987;**235**:1043-6.

106. Dore S, Takahashi M, Ferris CD, Zakhary R, Hester LD, Guastella D, Snyder SH. Bilirubin, formed by activation of heme oxygenase-2, protects neurons against oxidative stress injury (vol 96, pg 2445, 1999). *P Natl Acad Sci USA*. 1999;**96**:10944-.

107. Otterbein LE, Bach FH, Alam J, Soares M, Lu HT, Wysk M, Davis RJ, Flavell RA, Choi AMK. Carbon monoxide has anti-inflammatory effects involving the mitogen-activated protein kinase pathway. *Nat Med*. 2000;**6**:422-8.

108. Balla G, Jacob HS, Balla J, Rosenberg M, Nath K, Apple F, Eaton JW, Vercellotti GM. Ferritin: a cytoprotective antioxidant strategem of endothelium.

J Biol Chem. 1992;**267**:18148-53.

109. Choi J, Lee J, Kim SH, Kim J, Kim S. PG201 downregulates the production of nitrite by upregulating heme oxygenase-1 expression through the control of phosphatidylinositol 3-kinase and NF-E2-related factor 2. *Nitric Oxide*. 2013;**33**:42-55.

110. Panahian N, Yoshiura M, Maines MD. Overexpression of heme oxygenase-1 is neuroprotective in a model of permanent middle cerebral artery occlusion in transgenic mice. *J Neurochem*. 1999;**72**:1187-203.

111. Le W, Xie W, Appel SH. Protective role of heme oxygenase-1 in oxidative stress-induced neuronal injury. *J Neurosci Res*. 1999;**56**:652-8.

112. Aktan F. iNOS-mediated nitric oxide production and its regulation. *Life Sci*. 2004;**75**:639-53.

113. Korhonen R, Kankaanranta H, Lahti A, Lahde M, Knowles RG, Moilanen E. Bi-directional effects of the elevation of intracellular calcium on the expression of inducible nitric oxide synthase in J774 macrophages exposed to low and to high concentrations of endotoxin. *Biochem J*. 2001;**354**:351-8.

114. Vodovotz Y, Bogdan C, Paik J, Xie QW, Nathan C. Mechanisms of suppression of macrophage nitric oxide release by transforming growth factor beta. *J Exp Med*. 1993;**178**:605-13.

115. Geng Y, Lotz M. Increased intracellular Ca2+ selectively suppresses IL-1-induced NO production by reducing iNOS mRNA stability. *J Cell Biol*. 1995;**129**:1651-7.

116. Tsoyi K, Kim HJ, Shin JS, Kim DH, Cho HJ, Lee SS, Ahn SK, Yun-Choi HS, Lee JH, Seo HG, Chang KC. HO-1 and JAK-2/STAT-1 signals are involved in preferential inhibition of iNOS over COX-2 gene expression by newly

synthesized tetrahydroisoquinoline alkaloid, CKD712, in cells activated with lipopolysacchride. *Cell Signal*. 2008;**20**:1839-47.

117. Vareille M, Rannou F, Thelier N, Glasser AL, de Sablet T, Martin C, Gobert AP. Heme oxygenase-1 is a critical regulator of nitric oxide production in enterohemorrhagic Escherichia coli-infected human enterocytes. *J Immunol*. 2008;**180**:5720-6.

118. Sawle P, Foresti R, Mann BE, Johnson TR, Green CJ, Motterlini R. Carbon monoxide-releasing molecules (CO-RMs) attenuate the inflammatory response elicited by lipopolysaccharide in RAW264.7 murine macrophages. *Brit J Pharmacol*. 2005;**145**:800-10.

119. White KA, Marletta MA. Nitric-Oxide Synthase Is a Cytochrome-P-450 Type Hemoprotein. *Biochemistry-Us*. 1992;**31**:6627-31.

120. Rossler OG, Bauer I, Chung HY, Thiel G. Glutamate-induced cell death of immortalized murine hippocampal neurons: neuroprotective activity of heme oxygenase-1, heat shock protein 70, and sodium selenite. *Neurosci Lett*. 2004;**362**:253-7.

121. Son Y, Byun SJ, Pae HO. Involvement of heme oxygenase-1 expression in neuroprotection by piceatannol, a natural analog and a metabolite of resveratrol, against glutamate-mediated oxidative injury in HT22 neuronal cells. *Amino Acids*. 2013;**45**:393-401.

122. Calkins MJ, Johnson DA, Townsend JA, Vargas MR, Dowell JA, Williamson TP, Kraft AD, Lee JM, Li J, Johnson JA. The Nrf2/ARE pathway as a potential therapeutic target in neurodegenerative disease. *Antioxid Redox Signal*. 2009;**11**:497-508.

123. Galea E, Reis DJ, Feinstein DL. Cloning and expression of inducible nitric oxide

synthase from rat astrocytes. *J Neurosci Res*. 1994;**37**:406-14.

124. Geller DA, Lowenstein CJ, Shapiro RA, Nussler AK, Di Silvio M, Wang SC, Nakayama DK, Simmons RL, Snyder SH, Billiar TR. Molecular cloning and expression of inducible nitric oxide synthase from human hepatocytes. *Proc Natl Acad Sci U S A*. 1993;**90**:3491-5.

125. Lyons CR, Orloff GJ, Cunningham JM. Molecular cloning and functional expression of an inducible nitric oxide synthase from a murine macrophage cell line. *J Biol Chem*. 1992;**267**:6370-4.

126. Caput D, Beutler B, Hartog K, Thayer R, Brown-Shimer S, Cerami A. Identification of a common nucleotide sequence in the 3'-untranslated region of mRNA molecules specifying inflammatory mediators. *Proc Natl Acad Sci U S A*. 1986;**83**:1670-4.

127. Brennan CM, Steitz JA. HuR and mRNA stability. *Cell Mol Life Sci*. 2001;**58**:266-77.

128. Rodriguez-Pascual F, Hausding M, Ihrig-Biedert I, Furneaux H, Levy AP, Forstermann U, Kleinert H. Complex contribution of the 3'-untranslated region to the expressional regulation of the human inducible nitric-oxide synthase gene. Involvement of the RNA-binding protein HuR. *J Biol Chem*. 2000;**275**:26040-9.

129. Pautz A, Linker K, Altenhofer S, Heil S, Schmidt N, Art J, Knauer S, Stauber R, Sadri N, Pont A, Schneider RJ, Kleinert H. Similar regulation of human inducible nitric-oxide synthase expression by different isoforms of the RNA-binding protein AUF1. *J Biol Chem*. 2009;**284**:2755-66.

130. Dean JL, Wait R, Mahtani KR, Sully G, Clark AR, Saklatvala J. The 3' untranslated region of tumor necrosis factor alpha mRNA is a target of the mRNA-stabilizing factor HuR. *Mol Cell Biol*. 2001;**21**:721-30.

131. Paschoud S, Dogar AM, Kuntz C, Grisoni-Neupert B, Richman L, Kuhn LC. Destabilization of interleukin-6 mRNA requires a putative RNA stem-loop structure, an AU-rich element, and the RNA-binding protein AUF1. *Mol Cell Biol*. 2006;**26**:8228-41.

132. Fukui M, Song JH, Choi J, Choi HJ, Zhu BT. Mechanism of glutamate-induced neurotoxicity in HT22 mouse hippocampal cells. *Eur J Pharmacol*. 2009;**617**:1-11.

133. Li Y, Maher P, Schubert D. A role for 12-lipoxygenase in nerve cell death caused by glutathione depletion. *Neuron*. 1997;**19**:453-63.

134. Li Y, Maher P, Schubert D. Requirement for cGMP in nerve cell death caused by glutathione depletion. *J Cell Biol*. 1997;**139**:1317-24.

135. Davis JB, Maher P. Protein kinase C activation inhibits glutamate-induced cytotoxicity in a neuronal cell line. *Brain Res*. 1994;**652**:169-73.

136. Alam J, Stewart D, Touchard C, Boinapally S, Choi AM, Cook JL. Nrf2, a Cap'n'Collar transcription factor, regulates induction of the heme oxygenase-1 gene. *J Biol Chem*. 1999;**274**:26071-8.

137. Alam J, Cook JL. Transcriptional regulation of the heme oxygenase-1 gene via the stress response element pathway. *Curr Pharm Design*. 2003;**9**:2499-511.

138. Alam J, Den Z. Distal AP-1 binding sites mediate basal level enhancement and TPA induction of the mouse heme oxygenase-1 gene. *J Biol Chem*. 1992;**267**:21894-900.

139. Alam J, Cook JL. How many transcription factors does it take to turn on the heme oxygenase-1 gene? *Am J Resp Cell Mol*. 2007;**36**:166-74.

140. Lu DY, Tsao YY, Leung YM, Su KP. Docosahexaenoic Acid Suppresses Neuroinflammatory Responses and Induces Heme Oxygenase-1 Expression in

BV-2 Microglia: Implications of Antidepressant Effects for Omega-3 Fatty Acids. *Neuropsychopharmacol*. 2010;**35**:2238-48.

141. Hill-Kapturczak N, V T, Liu FY, Nick HS, Agarwal A. Mechanism of heme oxygenase-1 gene induction by curcumin in human renal proximal tubule cells. *Am J Physiol-Renal*. 2001;**281**:F851-F9.

142. Juan SH, Cheng TH, Lin HC, Chu YL, Lee WS. Mechanism of concentration-dependent induction of heme oxygenase-1 by resveratrol in human aortic smooth muscle cells. *Biochem Pharmacol*. 2005;**69**:41-8.

143. Alam J, Cai J, Smith A. Isolation and characterization of the mouse heme oxygenase-1 gene. Distal 5' sequences are required for induction by heme or heavy metals. *J Biol Chem*. 1994;**269**:1001-9.

144. Alam J, Camhi S, Choi AM. Identification of a second region upstream of the mouse heme oxygenase-1 gene that functions as a basal level and inducer-dependent transcription enhancer. *J Biol Chem*. 1995;**270**:11977-84.

145. Balogun E, Hoque M, Gong P, Killeen E, Green CJ, Foresti R, Alam J, Motterlini R. Curcumin activates the haem oxygenase-1 gene via regulation of Nrf2 and the antioxidant-responsive element. *Biochem J*. 2003;**371**:887-95.

146. Camhi SL, Alam J, Otterbein L, Sylvester SL, Choi AM. Induction of heme oxygenase-1 gene expression by lipopolysaccharide is mediated by AP-1 activation. *Am J Respir Cell Mol Biol*. 1995;**13**:387-98.

147. Drechsler Y, Dolganiuc A, Norkina O, Romics L, Li W, Kodys K, Bach FH, Mandrekar P, Szabo G. Heme oxygenase-1 mediates the anti-inflammatory effects of acute alcohol on IL-10 induction involving p38 MAPK activation in monocytes. *J Immunol*. 2006;**177**:2592-600.

148. Immenschuh S, Ramadori G. Gene regulation of heme oxygenase-1 as a

therapeutic target. *Biochem Pharmacol*. 2000;**60**:1121-8.

149. Ryter SW, Xi S, Hartsfield CL, Choi AM. Mitogen activated protein kinase (MAPK) pathway regulates heme oxygenase-1 gene expression by hypoxia in vascular cells. *Antioxid Redox Signal*. 2002;**4**:587-92.

150. Trachootham D, Lu W, Ogasawara MA, Nilsa RD, Huang P. Redox regulation of cell survival. *Antioxid Redox Signal*. 2008;**10**:1343-74.

151. Surh YJ, Kundu JK, Na HK. Nrf2 as a Master Redox Switch in Turning on the Cellular Signaling Involved in the Induction of Cytoprotective Genes by Some Chemopreventive Phytochemicals. *Planta Med*. 2008;**74**:1526-39.

152. Na HK, Surh YJ. Transcriptional regulation via cysteine thiol modification: A novel molecular strategy for chemoprevention and cytoprotection. *Mol Carcinogen*. 2006;**45**:368-80.

153. Dinkova-Kostova AT, Talalay P. Direct and indirect antioxidant properties of inducers of cytoprotective proteins. *Mol Nutr Food Res*. 2008;**52**:S128-S38.

154. Park J, Liu AY. JNK phosphorylates the HSF1 transcriptional activation domain: role of JNK in the regulation of the heat shock response. *J Cell Biochem*. 2001;**82**:326-38.

155. Lee PJ, Camhi SL, Chin BY, Alam J, Choi AM. AP-1 and STAT mediate hyperoxia-induced gene transcription of heme oxygenase-1. *Am J Physiol Lung Cell Mol Physiol*. 2000;**279**:L175-82.

156. Lee SA, Kim EY, Jeon WK, Woo CH, Choe J, Han S, Kim BC. The inhibitory effect of raloxifene on lipopolysaccharide-induced nitric oxide production in RAW264.7 cells is mediated through a ROS/p38 MAPK/CREB pathway to the up-regulation of heme oxygenase-1 independent of estrogen receptor. *Biochimie*. 2011;**93**:168-74.

157. Carter AB, Knudtson KL, Monick MM, Hunninghake GW. The p38 mitogen-activated protein kinase is required for NF-kappaB-dependent gene expression. The role of TATA-binding protein (TBP). *J Biol Chem*. 1999;**274**:30858-63.

158. Hiramatsu M, Takiguchi O, Nishiyama A, Mori H. Cilostazol prevents amyloid beta peptide(25-35)-induced memory impairment and oxidative stress in mice. *Br J Pharmacol*. 2010;**161**:1899-912.

국문 초록

치매(痴呆)는 기억력 및 전반적인 인지기능이 일상생활에 지장을 줄 정도로 감퇴된 상태를 뜻한다. 대부분의 노인성 치매의 원인질환으로 알려진 알츠하이머 치매(Alzheimer's disease, 이하 AD)는 세계적으로 노인 인구의 폭발적인 증가와 함께 그 환자가 증가하여, 심각한 사회적 및 경제적 문제를 일으키는 요인으로 대두되고 있다. 현재 4가지의 치료제가 미국 FDA의 승인을 받아 사용되고 있지만 AD 환자의 인지기능을 일시적으로 개선시켜 줄 수 있을 뿐 병을 예방하거나 진행을 막지 못하는 것으로 알려져 있다. 다양한 병리적 요인들이 복잡하게 얽혀서 AD의 발병에 영향을 주는 것으로 알려져 있기 때문에 한 가지의 특정한 병태 혹은 타겟 분자에 작용하는 약물은 AD의 예방 및 치료에 한계가 있다 할 수 있다.

이 학위 논문 연구에서는 한의학적 지식 및 데이터에 기반하여 AD와 같은 노인성 치매를 개선시킬 수 있는 식물 소재의 개발 가능성을 탐색하였다. 한의학 고서들에 기재되어 있는 치매의 병태와 증상은 현대의 AD와 매우 유사하며, 크게 노화와 관련된 퇴행성 병태와 어혈(瘀血), 담음(痰飮) 등과 같은 병리적 물질이 누적되어 나타나는 병태 두 가지로 나뉘어진다. 이 연구를 통해 이러한 병태를 개선시킬 수 있는 식물로 알려진 용안육(*Dimocarpus longan*), 맥문동(*Liriope platyphylla)*, 단삼(*Salvia miltiorrhiza)*, 천마(*Gastrodia elata*)를 조합하여 HX106N이라고 하는 식

물 혼합 소재를 만들었다. 가장 먼저 수행한 실험은 두 가지의 건망증 동물모델을 이용한 기억력 개선 효과 평가였는데, HX106N은 뚜렷하게 건망증을 개선시켰다 (하기 참조). 그러나 그 효과를 나타내는 활성 성분이 무엇인지 알 지 못했기 때문에 일관된 활성을 가지는 HX106N을 얻기 위해서는 그 활성을 측정할 수 있는 방법이 필요했다. 이를 위해 3가지 생물학적 지표에 대한 효과를 측정할 수 있는 bioassay system을 개발하였다. BV-2 세포주에서 NO(nitric oxide) 생산에 미치는 효과와 HT22 세포주에서 글루타메이트(glutamate)에 의한 세포 사멸에 대한 영향, 그리고 뇌 균질액에서 아세틸콜린에스터라제(acetylcholnesterase; AChE) 활성에 미치는 효과가 그 것이다. 다른 시간대에 새로 구입된 식물 원료를 사용하여 HX106N을 만들 때에는 항상 bioassay를 수행하였고, 3개 지표 모두에서 표준 HX106N 배치의 IC_{50} 값의 ± 20% 오차 범위 내에 들어오는 배치만을 선택하여 실험에 사용하였다.

$A\beta_{25-35}$ peptide를 뇌 내에 주입함으로써 기억력 감퇴를 유발한 생쥐 모델을 이용한 Y자 미로 및 수동 회피 검사 모두에서 HX106N을 경구 투여한 경우 기억력이 통계적으로 유의미하게 개선되는 것을 확인하였다. 이 모델에서는 생쥐의 해마와 대뇌피질 조직에서 지질 산화의 표지자인 TBARS(thiobarbituric acid-reactive substances)의 양이 현저하게 감소된 것을 관찰할 수 있었다. 비선택적 무스카린 수용체 길항제인 스코폴라민(scopolamine)으로 유도한 콜린성 건망증(cholinergic amnesia) 모델에서도 Y자 미로 및 수동 회피 검사를 수행한 결과 HX106N가 건망증을 개선

하는 것을 관찰하였다. HX106N을 투약 후 생쥐의 해마와 대뇌피질 부위의 AChE의 활성을 측정한 결과 통계적으로 유의미하게 이 효소의 활성이 감소되었다.

그 작용 기전을 연구하고자 소교세포 및 신경세포 기원의 세포들에서 HX106N의 효과를 조사하였다. 생쥐 소교세포주인 BV-2 세포와 일차 소교세포에서 HX106N은 두 가지 기전을 통해 NO 생성을 조절하였다. 첫째 iNOS RNA의 안정성을 조절하여 iNOS 발현을 억제하였고, 두번째로는 HO-1(heme oxygenase-1) 발현을 증가시켜 CO(carbon monoxide)를 생성함으로써 NO 생성을 감소시켰다. 생쥐 태자에서 분리하여 배양한 일차 신경 세포와 생쥐 해마 신경 세포주인 HT22 세포에서는 HX106N가 글루타메이트에 의해 발생하는 신경 세포의 사멸과 활성산소종(reactive oxygen species; ROS)의 생산을 현저하게 감소시켰다. 이러한 결과들은 HX106N이 다양한 기전을 통해 산화 스트레스를 조절한다는 것을 보여준다.

다음으로 HX106N이 HO-1의 발현을 조절하는 기전을 분자 수준에서 연구하였다. HX106N은 Nrf2(Nuclear factor E2-related factor 2)와 NF-κB를 활성화 시켜서 HO-1의 발현을 RNA 수준에서 증가시켰다. MAPKs (mitogen-activated protein kinases)에 대한 저해제를 이용한 실험을 통해 JNK(Janus N-terminal kinase)와 p38 MAPK가 HX106N이 HO-1의 발현을 조절하는 과정에 개입함을 발견하였다. 이러한 결과들을 통해 HX106N이 최소 두 가지 이상의 시그널 전달경로를 통해 HO-1의 발현을 증가시킨다는 것을 알 수 있었다.

이 학위 논문을 통해 HX106N이 질환 모델에서 기억력을 개선시킬 수 있는 생물학적 활성을 가지고 있음을 발견하였는바, HX106N은 AD와 같은 노인성 치매 치료제 개발에 있어서 매우 유용한 시작점이 될 수 있을 것으로 사료된다.

중심어: HX106N, 한의학, 치매, 알츠하이머병, 신경퇴행성질환, amyloid β. 스코폴라민, 산화 스트레스, heme oxygenase-1

학번: 2008-20368